



Magnetosphere and Plasma Science with the Jupiter Icy Moons Explorer

A. Masters¹ · R. Modolo² · E. Roussos³ · N. Krupp³ · O. Witasse⁴ · C. Vallat⁵ · B. Cecconi⁶ · N.J.T. Edberg⁷ · Y. Futaana⁸ · M. Galand¹ · D. Heyner⁹ · M. Holmberg¹⁰ · H. Huybrighs^{10,11,12} · X. Jia¹³ · K. Khurana¹⁴ · L. Lamy^{6,15} · L. Roth¹⁶ · A. Sulaiman¹⁷ · P. Tortora¹⁸ · S. Barabash⁸ · L. Bruzzone¹⁹ · M.K. Dougherty¹ · R. Gladstone^{20,21} · L.I. Gurvits^{22,23} · P. Hartogh³ · H. Hussmann²⁴ · L. Iess²⁵ · F. Poulet²⁶ · J.-E. Wahlund⁷ · D.J. Andrews⁷ · C.S. Arridge²⁷ · F. Bagenal²⁸ · C. Baskevitch^{2,6} · J. Bergman⁷ · T.M. Bocanegra²⁹ · P. Brandt³⁰ · E.J. Bunce³¹ · G. Clark³⁰ · A.J. Coates^{32,33} · E. Galanti³⁴ · A. Galli³⁵ · D. Grodent³⁶ · G. Jones^{32,33} · Y. Kasaba³⁷ · Y. Kaspi³⁴ · Y. Katoh³⁵ · N. Kaweeyanun³⁸ · Y. Khotyaintsev⁷ · T. Kimura³⁹ · P. Kollmann³⁰ · D. Mitchell³⁰ · A. Moirano^{40,36} · G. Molera Calvés⁴¹ · M. Morooka⁷ · I.C.F. Müller-Wodarg¹ · C. Muñoz⁵ · A. Mura⁴⁰ · M. Pätzold⁴² · M. Pinto⁴ · C. Plainaki^{43,40} · K.D. Retherford^{20,21} · A. Retinò⁴⁴ · H. Rothkaehl⁴⁵ · O. Santolík^{46,47} · J. Saur⁴⁸ · G. Stenberg Wieser⁸ · F. Tsuchiya³⁷ · M. Volwerk⁴⁹ · A. Vorburger³⁵ · P. Wurz³⁵ · M. Zannoni¹⁸

Received: 4 July 2024 / Accepted: 12 February 2025 / Published online: 3 March 2025
© The Author(s) 2025

Abstract

The Jupiter Icy Moons Explorer (*JUICE*) is a European Space Agency mission to explore Jupiter and its three icy Galilean moons: Europa, Ganymede, and Callisto. Numerous *JUICE* investigations concern the magnetised space environments containing low-density populations of charged particles that surround each of these bodies. In the case of both Jupiter and Ganymede, the magnetic field generated internally produces a surrounding volume of space known as a magnetosphere. All these regions are natural laboratories where we can test and further our understanding of how such systems work, and improved knowledge of the environments around the moons of interest is important for probing sub-surface oceans that may be habitable. Here we review the magnetosphere and plasma science that will be enabled by *JUICE* from arrival at Jupiter in July 2031. We focus on the specific topics where the mission will push forward the boundaries of our understanding through a combination of the spacecraft trajectory through the system and the measurements that will be made by its suite of scientific instruments. Advances during the initial orbits around Jupiter will include construction of a comprehensive picture of the poorly understood region of Jupiter's magnetosphere where rigid plasma rotation with the planet breaks down, and new perspectives on how Jupiter's magnetosphere interacts with both Europa and Callisto. The later orbits around Ganymede will dramatically improve knowledge of this moon's smaller magnetosphere embedded within the larger magnetosphere of Jupiter. We conclude by outlining the high-level operational strategy that will support this broad science return.

Keywords Jupiter · Ganymede · Europa · Callisto · Magnetospheres · Space plasmas

1 Introduction

Space is filled with very low-density populations of charged particles, known as space plasmas. Although generally invisible to the naked eye, these environments can contain a tremendous amount of energy and momentum. Under these tenuous conditions, parcels of plasma and the magnetic field that permeates them become effectively frozen to each other, with wide-ranging consequences for the dynamics of such environments. In the Solar System, a plasma known as the solar wind flows away from the Sun in all directions, dragging the solar magnetic field into space and interacting with all the planets. Some of these planets, like the Earth, have their own magnetic field generated by a dynamo action in their interior, creating magnetospheres that are cavities in the solar wind flow. A fraction of the energy flowing within these dynamic magnetised volumes drives interaction with the planet itself, and any moons that are orbiting within the planetary magnetosphere. Such moons are of great scientific interest in their own right.

The Jupiter Icy Moons Explorer (*JUICE*) is the first large-class mission in the European Space Agency (ESA) Cosmic Vision 2015–2025 programme (Grasset et al. 2013). Following successful launch in April 2023, the spacecraft is now carrying out an interplanetary cruise to Jupiter, scheduled to arrive at the largest planet in the Solar System in July 2031. *JUICE* will then spend more than four years in the planetary system, first in orbit around Jupiter itself and then in orbit around Jupiter's largest moon Ganymede. The combination of spacecraft trajectory and measurements enabled by its payload of scientific instruments will revolutionise our understanding of the Jupiter system, including the planet's Galilean moons Europa, Ganymede, and Callisto.

Jupiter possesses the strongest magnetic field of any planet in the Solar System, carving out the largest solar system magnetosphere within the solar wind flow. Much of our understanding of Jovian magnetospheric physics is based on observations made by spacecraft that have flown past Jupiter (*Pioneer 10*, *Pioneer 11*, *Voyager 1*, *Voyager 2*, *Ulysses*, *Cassini-Huygens*, and *New Horizons*) and the two spacecraft to have already executed orbits around Jupiter: The past (1989–2003) *Galileo* mission and the ongoing *Juno* mission (Dessler 1983; Clarke et al. 2004; Khurana et al. 2004; Kivelson et al. 2004a; Krupp et al. 2004a; Thomas et al. 2004; Saur et al. 2004; Bagenal et al. 2017a; Bolton et al. 2017). Inside this system the magnetosphere is electrodynamically coupled to each of the many Jovian moons. In particular, complex interactions exist at Europa and Callisto, and Ganymede's interaction is unique (Kivelson 2004b) (see the review by Jia et al. 2010a). This is because Ganymede is the only moon in the Solar System known to produce its own magnetic field, carving out a mini-magnetosphere within the Jovian magnetosphere, which has a far larger spatial scale. In the case of all three moons, a tenuous layer of ionized exosphere (an ionosphere) plays an important role in mediating the interaction.

The Jupiter system therefore contains numerous natural space plasma laboratories in which we can test our understanding of how these systems work, and occasionally also the fundamentals of space plasma physics. These tenuous regimes cannot be re-created in Earth-based laboratories, and so direct exploration with missions like *Galileo*, *Juno*, and now *JUICE*, are needed for progress. Figure 1 shows a high-level illustration that covers much of the magnetosphere and plasma science in the Jupiter system that is relevant for *JUICE*, which will be described in more detail in later sections. Progress in understanding the moon-magnetosphere interaction at each of Europa, Ganymede, and Callisto is essential for assessing the habitability of any sub-surface oceans of liquid water, which is a key driver of the *JUICE* mission (Grasset et al. 2013).

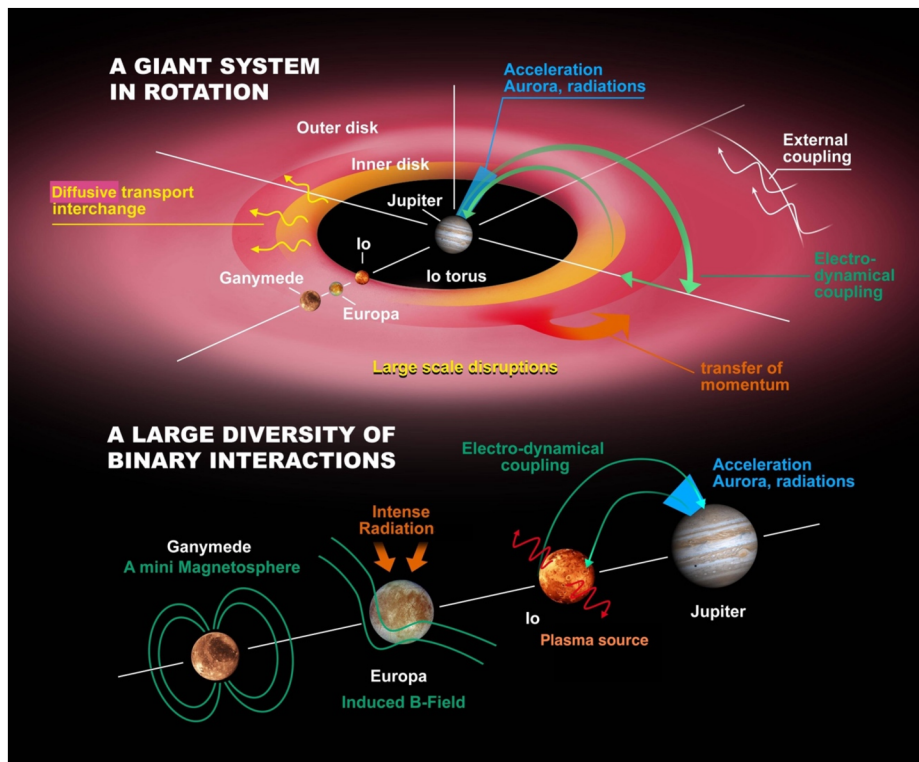


Fig. 1 High-level illustration of magnetosphere and plasma science topics in the Jupiter system that are relevant for JUICE. Credit: ESA

This paper is part of a special issue following the launch of *JUICE*. Other publications in the issue focus on topics such as the overall mission design (Witasse et al. 2025, this collection), spacecraft design (Erd et al., in preparation, this collection), ground segmentation (Altobelli et al., in preparation, this collection), trajectory design (Boutonnet et al. 2024, this collection), and each scientific instrument. Our focus is the magnetosphere and plasma science areas where the mission will allow new advances following arrival at Jupiter. This topic is the subject of one of the mission's four science Working Groups (WGs), from which the majority of the present authorship is drawn. As a general guide, plasma populations that will be studied by *JUICE* fall within our primary scope. The aim of this article is not to present a comprehensive introduction and review of all the key physics on this topic, which is the subject of a number of excellent past reviews (e.g., see relevant chapters of Bagenal et al. 2004), instead we use the *JUICE* mission as a guide to reviewing specific sub-topics, with a focus on how *JUICE* will push forward present understanding in each case.

The *JUICE* mission has six objectives, concerning Ganymede, Europa, Callisto, Jupiter's atmosphere, Jupiter's magnetosphere, and Jupiter's satellite and ring system (Witasse et al. 2025, this collection). Magnetosphere and plasma science features in all six mission objectives, as shown in Table 1. In this reduced version of the full Science Requirements Matrix we only present the investigations that are the most relevant for magnetosphere and plasma science, showing how these have originated from science objectives, which in turn stem from the six mission objectives. Table 1 also illustrates how overlap between WG papers

Table 1 Reduced JUICE Science Requirements Matrix based on selecting the investigations that are the most relevant for magnetosphere and plasma science (Witasse et al. 2025, this collection). Investigations not marked with asterisks are only covered by the content of this paper, investigations marked with one asterisk are covered partly here and partly in the paper by the internal structure, subsurface and geophysics of giant icy moons WG (Van Hoolst 2024, this collection), investigations marked with two asterisks are covered partly here and partly in the paper by the surfaces and exospheres of satellites, dust and rings WG (Tosi et al. 2024, this collection), and investigations marked with three asterisks are only covered in the paper by the Jupiter WG (Fletcher et al. 2023)

Mission objective	Science objective	Investigation
Characterise Ganymede as a planetary object and possible habitat	<p>Characterise the extent of the ocean and its relation to the deeper interior.</p> <p>Characterise the local environment and its interaction with the Jovian magnetosphere.</p>	<p>GA.2: Characterise the space plasma environment to determine the magnetic induction response from the ocean.</p> <p>GC.1: Globally characterise Ganymede's intrinsic and induced magnetic fields, with implications for the deep interior.*</p> <p>GC.2: Characterise the particle population within Ganymede's magnetosphere and its interaction with Jupiter's magnetosphere.</p> <p>GC.3: Investigate the generation of Ganymede's aurorae</p> <p>GC.4: Determine the sources and sinks of the ionosphere and exosphere.**</p>
Explore Europa's recently active zones	Study the active processes	EC.1: Study the interaction between the local environment and the Europa torus, and the effects of radiation on surface chemistry, and sputtering processes.**
Study Callisto as a remnant of the early Jovian system	Characterise the outer shells, including the ocean.	<p>CA.2: Characterise the space plasma environment to determine the magnetic induction response from Callisto's ocean.**</p> <p>CB.3: Characterize the ionosphere and exosphere of Callisto.**</p>
Characterise the Jovian atmosphere	Characterise the atmospheric dynamics and circulation.	<p>JA.4: Investigate auroral structure and energy transport mechanisms at high latitudes.***</p> <p>JA.5: Understand the interrelationships between the ionosphere and thermosphere.***</p>
Characterise the Jovian magnetosphere	Characterise the magnetosphere as a fast magnetic rotator.	<p>MA.1: Understand the structure and stress balance of Jupiter's magnetosphere.</p> <p>MA.2: Investigate the plasma processes, sources, sinks, composition and transport (including transport of magnetic flux) in the magnetosphere and characterize their variability in space and time.</p>

Table 1 (Continued)

Mission objective	Science objective	Investigation
	Characterise the magnetosphere as a giant accelerator.	<p>MA.3: Characterize the large-scale coupling processes between the magnetosphere, ionosphere and thermosphere, including footprints of the Jovian moons.</p> <p>MA.4: Characterize the magnetospheric response to solar wind variability and planetary rotation effects.</p> <p>MB.1: Detail the particle acceleration processes.</p> <p>MB.2: Study the loss processes of charged energetic particles.</p> <p>MB.3: Measure the time evolving electron synchrotron emissions.</p>
	Understand the moons as sources and sinks of magnetospheric plasma.	<p>MC.1: Study the pickup and charge exchange processes in the Jupiter system plasma and neutral tori.</p> <p>MC.2: Study the interactions between Jupiter's magnetosphere and Io, Europa, Ganymede, and Callisto.</p> <p>MC.3: Study the interactions between Jupiter's magnetosphere and small satellites.</p>
Study the Jovian satellite and ring system	Remote observations of Io	SA.2: Study of pick-up & charge-exchange processes in plasma/neutral tori.**

is handled. Most of the investigations listed are only covered in the present article, some are covered in two different WG papers, and three are only covered in other WG papers. A point deserving special note concerns overlap with the surfaces and exospheres of satellites, dust and rings WG (Tosi et al. 2024, this collection). In contrast with the general guide to our scope, we cover populations of neutral particles on the scale of Jupiter's magnetosphere where these are relevant for understanding the Jovian magnetosphere (i.e., we cover moon neutral tori). We do not cover the neutral environments local to each Galilean moon, which fall within the remit of this sister WG.

Each investigation drives requirements that have led to the payload of instruments currently on the spacecraft. Table 2 summarises the measurement capabilities that will allow magnetosphere and plasma science once the spacecraft arrives at Jupiter. This overall capability is provided by specific scientific experiments: The Magnetometer (J-MAG) (Dougherty et al., in preparation, this collection), Particle Environment Package (PEP) (Barabash et al, in preparation, this collection), Radio and Plasma Wave Investigation (RPWI) (Wahlund et al. 2025), Ultraviolet Imaging Spectrograph (UVS) (Retherford et al. 2025, in preparation, this collection), Gravity & Geophysics of Jupiter and Galilean Moons (3GM) (Iess et al. 2025, this collection), Planetary Radio Interferometry and Doppler Experiment (PRIDE) (Gurvits et al. 2023, this collection), and the RADiation hard Electron Monitor (RADEM) (Hadjas et al., in preparation, this collection). Most of these are *in situ* measurements, but remote sensing will also be a valuable tool. We refer the reader to the

Table 2 Summary of the JUICE instruments and measurement capabilities that are relevant for magnetosphere and plasma science

Instrument	Relevant Measurements
Magnetometer (J-MAG)	Magnetic field, DC to 64 Hz.
Particle Environment Package (PEP)	Electrons, 1 eV to 1 MeV.
	Ions, 1 eV to 5 MeV.
	Thermal neutrals and ions 1-1000 atomic mass units.
	Energetic Neutral Atoms (ENAs), 10 eV to 300 keV.
Radio and Plasma Wave Investigation (RPWI)	Electric field vector, DC to 1.4 MHz.
	Electric field vector (radio), 80 kHz to 45 MHz.
	Magnetic field vector, 0.1 Hz to 20 kHz.
	Plasma density, 10^{-4} to 10^5 cm^{-3} .
Ultraviolet Imaging Spectrograph (UVS)	Ultraviolet photons, 51 to 204 nm.
Gravity & Geophysics of Jupiter and Galilean Moons (3GM)	Radio occultation, Ka-band, 32.5 to 34 GHz (communication radio line carrier frequency).
Planetary Radio Interferometry and Doppler Experiment (PRIDE)	Phase scintillations of electromagnetic waves emitted by the spacecraft at 8.4 GHz (communication radio line carrier frequency) on the interplanetary plasma and in the immediate vicinity of Jupiter and its moons, including radio occultations. Total electron content along the communication line, spacecraft to ground-based radio telescope.
RADiation hard Electron Monitor (RADEM)	Electrons, 0.3 MeV to 40 MeV.
	Ions, 0.1 MeV to 250 MeV.

cited articles in this journal for further information about each experiment, including technical detail. In the interests of making this paper accessible to a broad readership, in the following sections we avoid referring to individual instruments, relying on Table 2 as a reference for the reader to understand the spacecraft's relevant capabilities. Section 6 is an exception, as it concerns spacecraft operations once in the Jupiter system.

This paper is comprised of sections that deal with the different *JUICE* magnetosphere and plasma science themes, presented in chronological order based on when we expect the first science return. Each section begins with an overview of the relevant portion of the spacecraft trajectory (Boutonnet et al. 2024, this collection). In Sect. 2 we review the advances in Jovian magnetospheric science that *JUICE* will enable, including how plasma is transported and accelerated. In Sects. 3 and 4 we review the expected advances concerning the local electrodynamic interaction between the Jovian magnetosphere and both Europa and Callisto, respectively. In Sect. 5 we outline major progress expected in understanding the magnetosphere of Ganymede, based on many months spent in orbit. In Sect. 6 we provide an overview of the observational strategy that will maximise the magnetosphere and plasma science return, from the final approach to Jupiter until the end of the mission. Finally, in Sect. 7 we conclude, and discuss the path forwards towards Jupiter orbit insertion in 2031.

2 Magnetosphere of Jupiter

Jupiter has by far the largest and most complex magnetosphere in the Solar System, illustrated in Fig. 2 (see Dessler (1983) and relevant chapters of Bagenal et al. 2004). A major

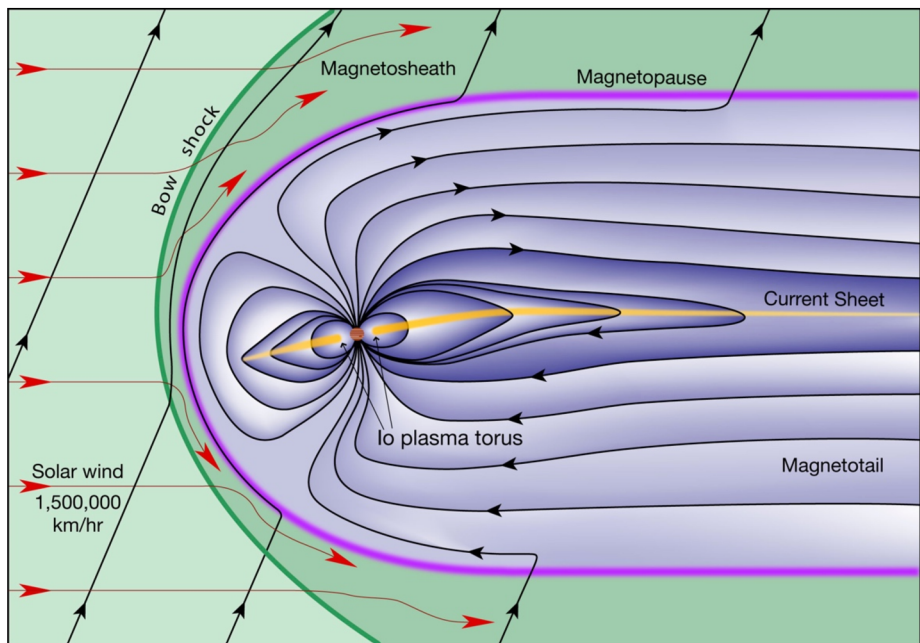


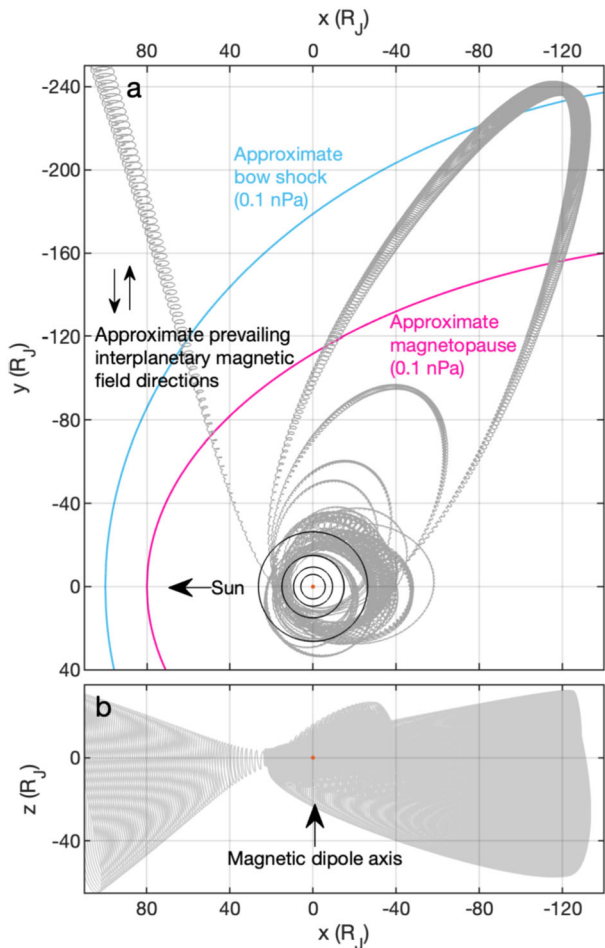
Fig. 2 Schematic illustrating the structure of Jupiter’s magnetosphere. False colour has been applied to different regions of the magnetised plasma environment. Credit: Fran Bagenal & Steve Bartlett

role is played by the innermost Galilean moon, Io, which is the most volcanically active body in the solar system. Io has an atmosphere of SO_2 from which about $\sim 1 \text{ ton s}^{-1}$ of neutral material is ejected from Io (Roth et al. 2025). The neutral material is then rapidly dissociated and ionized by the surrounding plasma, accelerated to corotate with Jupiter’s ~ 10 -hour spin period, to form a dense plasma torus (Bagenal and Dols 2020). The heavy ions, comprising various charge states of sulphur and oxygen (Clark et al. 2016, 2020; Bagenal et al. 2017b; Allen et al. 2019; Kim et al. 2020) are subsequently heated as they are transported radially out through the magnetosphere (Bagenal and Delamere 2011). The dominant heavy ion constituents of Jupiter’s magnetosphere play a key role in its dynamics due to their density and pressure contributions (Mauk et al. 2004).

Jupiter’s strong magnetic field together with its fast rotation rate coupled to this particularly active moon controls the structure and dynamics of its magnetosphere, with the solar wind playing a still-to-be-determined role. The coupling among all these elements changes in space, time and over a variety of time scales. The *JUICE* trajectory and its scientific payload will provide a new view of the structure of the Jovian magnetosphere, as well as its dynamical variations, information which can later propagate into predictive models of the moon environments. In particular, *JUICE* will show how the combination of a strong dynamo, fast rotation and internal plasma sources shape a magnetosphere and in which ways these aspects convert the Jovian system into a very efficient particle accelerator.

Referring to the *JUICE* investigations presented in Table 1, this section concerns all investigations stemming from the mission objective “Characterise the Jovian magnetosphere”, as well as the Io investigations stemming from the mission objective “Study the Jovian satellite and ring system”. Note that the scope of this section includes plasma and neutral

Fig. 3 The JUICE spacecraft trajectory during the Jupiter orbital tour, prior to Ganymede orbit insertion. See the text for a definition of the units and coordinate system used. (a) Trajectory projected onto the xy plane. Approximate positions of Jupiter's bow shock and magnetopause cross-sections are shown, which are highly sensitive to solar wind dynamic pressure (Joy et al. 2002). The approximate prevailing orientations of the interplanetary magnetic field at Jupiter's orbit are shown as black arrows. The approximate orbits of the four Galilean moons are shown as black circles, with the smallest circle approximating Io's orbit in this coordinate system ($5.9 R_J$), the next largest approximating Europa's orbit ($9.4 R_J$), the next largest approximating Ganymede's orbit ($15.0 R_J$), and the largest approximating Callisto's orbit ($26.3 R_J$). (b) Trajectory projected onto the xz plane. In both panels Jupiter is the filled orange circle centred on the origin



tori associated with moons, but more local moon-magnetosphere interactions are covered in Sect. 3.2 (Europa), Sect. 4.2 (Callisto), and Sects. 5.1 to 5.3 inclusive (Ganymede).

The trajectory of the *JUICE* spacecraft from approach to Jupiter until Ganymede orbit insertion is shown in Fig. 3 (Boutonnet et al. 2024, this collection). The coordinate system used has its origin at Jupiter's barycentre and uses spatial units of Jupiter radii (R_J ; $1 R_J = 71,492$ km). The z -axis is aligned with Jupiter's centred magnetic dipole axis (Connerney et al. 2022), the x -axis defines an xz plane that contains the vector pointing to the Sun from the origin, and the y -axis completes the right-handed cartesian set. This system has been chosen because it captures magnetospheric regions close to the planet (within $\sim 40 R_J$) by virtue of how the z -axis is defined, while also indicating the approximate direction to the Sun (positive x -axis) and the approximate direction of Jupiter's orbital motion (negative y -axis). The $\sim 10^\circ$ tilt between Jupiter's magnetic dipole and rotation axes means that the spacecraft trajectory appears to wobble over a period of ~ 10 hours when viewed in this system. Note that the utility of this system is less outside $\sim 40 R_J$, because physics beyond just the magnetic dipole equator rigidly tied to the planet start to control the structure of the system to a greater extent.

An important concept for defining magnetospheric regions is the M-shell, which we rely on frequently in this article. These are surfaces defined by magnetic field lines crossing the equator at the same distance, with an identifying number that can be turned into this distance by multiplying by 1 R_J . We use a combination of *Juno*-era models of Jupiter's internal magnetic field model (Connerney et al. 2022) and magnetodisk current sheet (Connerney et al. 2020), implemented via code released and reported in order to serve the magnetospheres of the outer planets community (Wilson et al. 2023). The current sheet model accounts for the radial distension of Jupiter's magnetic field observed outside Io's orbit, illustrated in Fig. 2. Note that this inclusion of the effect of Jupiter's magnetodisk current sheet makes Jovian M-shells different from the traditional L-shell introduced in the context of the Earth and often applied to other planets.

How JUICE will advance knowledge in this area: The spacecraft orbit within the plasma sheet and in the mid-to-high-latitude magnetosphere, together with excellent local time coverage, will bridge gaps in coverage following the *Galileo* and *Juno* missions. The extended duration of both low and high-latitude phases will offer deeper insights into the dynamical variability ranges of the magnetosphere, since several regions will be visited on multiple instances, enabled by *JUICE*'s extensive measurement capabilities. Orbit-to-orbit revisit times range from 10 days to about a month, whereas time differences between inbound-outbound crossings of similar magnetospheric ranges will allow us to probe down to a few days. *JUICE* will offer novel opportunities for continuous monitoring of the magnetosphere, with sufficient resolution to resolve a range of timescales. More detail is given in the following sub-sections.

2.1 Mapping Magnetospheric Structure and Monitoring Dynamics

2.1.1 Solar Wind Interaction and the Outer Magnetosphere

JUICE will approach Jupiter from the post-dawn local time sector (see Fig. 3a), in a trajectory roughly aligned with the Parker spiral that describes the dominant magnetic field orientations in the solar wind. This may occasionally mean that *JUICE* becomes magnetically connected to Jupiter's magnetosphere. This geometry is ideal for monitoring charged particle populations that escape from Jupiter along the interplanetary magnetic field (IMF), such as relativistic electrons (Teegarden et al. 1974; Simpson et al. 1993; Heber et al. 2007; Hospodarsky et al. 2017) or ~ 10 to ~ 100 -keV ions (Marhavilas et al. 2001; Krimigis et al. 2002). During similar entry to the Jupiter system (McComas et al. 2017; Wilson et al. 2018), the *Juno* spacecraft encountered a hot flow anomaly upstream of Jupiter's bow shock (Valek et al. 2017), and so *JUICE* may also observe evidence of this transient phenomenon.

The spectra of these populations, particularly of the relativistic electrons, appear to be regulated both by the solar wind (IMF orientation, solar wind velocity) at solar rotation time scales (weeks) and planetary rotation (Morioka and Tsuchiya 1996; Tsuchiya et al. 1999). Krupp et al. (2002, 2004b) report even shorter periods (e.g. 40 minutes) in the modulation of escaping electrons, periods that have also been identified throughout the Jovian outer magnetosphere and the aurora (Simpson et al. 1992; Gladstone et al. 2002; Dunn et al. 2017; Manners and Masters 2020). These observations hint that there is a strong coupling of the outer magnetosphere with the solar wind, that is still poorly understood. The same applies for the source region and release processes of the escaping particle populations. *JUICE* will be capable of monitoring these populations for long periods, in parallel with *in situ* sampling of the solar wind and remote sensing observations of the magnetosphere in the ultraviolet (UV), infrared (IR) and in Energetic Neutral Atoms (ENAs) (e.g., Mauk et al. 2002; Steffl

et al. 2006), offering a global perspective of the magnetospheric state and adding another dimension for interpreting the particle escape episodes.

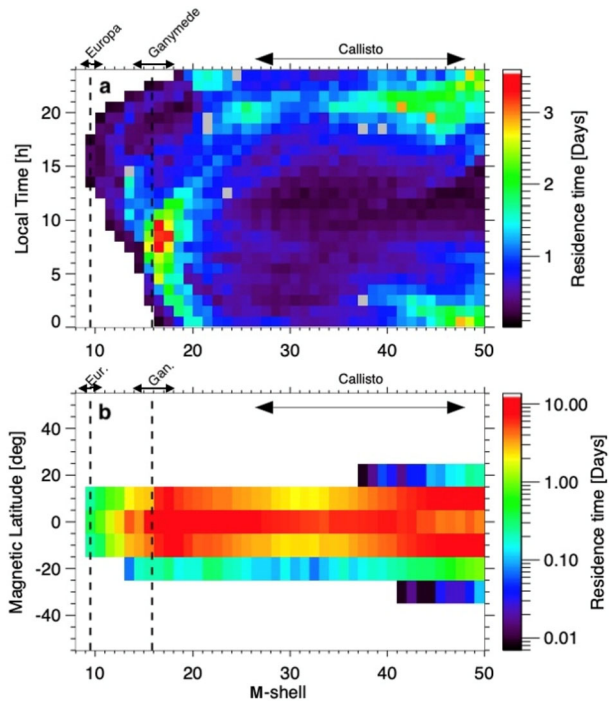
JUICE will also have the unique opportunity to measure the extended nebulae of Jupiter: A disk-shaped neutral cloud extending more than 400 R_J from the planet, only identified through remote sensing so far (Mendillo et al. 1990). This cloud is believed to contain sodium atoms, sourced and neutralised in the Io torus, spreading outwards with energies of about 400 eV (De Becker et al. 2023). *JUICE* will be able to search for *in situ* evidence of this disk of neutrals, and any correlation with Io volcanism could also be investigated during approach via remote sensing.

Furthermore, approach to Jupiter and the period surrounding the first orbital apoapsis point following Jupiter orbit insertion will offer opportunities for simultaneous *in situ* solar wind monitoring and remote monitoring of the magnetosphere. Past studies indicate that a dawn-dusk asymmetry in extreme UV emissions from the plasma torus associated with the moon Io (see Sect. 2.3) is indicative of a dawn-to-dusk electric field in Jupiter's magnetosphere (Barbosa and Kivelson 1983). Propagated solar wind conditions hint that this electric field is regulated by the solar wind dynamic pressure (Murakami et al. 2016) which in turn affects other elements of the magnetosphere, such as the electron radiation belts (Han et al. 2018). *JUICE* observations during approach will not suffer from the large uncertainty associated with solar wind propagations, allowing us to look for local time asymmetry, as predicted by several theoretical models (Goertz and Ip 1984).

Long-term monitoring campaigns may reveal the links between the inner and the outer Jovian magnetosphere: Kimura et al. (2018), Tsuchiya et al. (2018), Yoshioka et al. (2018), and Tao et al. (2021), using Earth-based observations of electron heating episodes and auroral UV emission bursts, found that variations in the internal plasma supply through Io's volcanism modifies the large-scale plasma circulation throughout the magnetosphere. Remote sensing carried out by *JUICE* that includes ENA imaging (see Sect. 2.4), the latter offering a novel insight into suprathermal ion populations, could provide key information on how such episodes evolve across different magnetospheric regions and particle populations.

The residence of *JUICE* in the outer magnetosphere will be short compared to the mission duration. Arrival is expected to be around solar minimum, with solar wind dynamic pressures most likely around 0.1 nPa (Joy et al. 2002), which means that there is high confidence that only during approach and the apojove of the first *JUICE* orbit will there be an opportunity to study the magnetospheric boundaries (bow shock and magnetopause), which will lie beyond $\sim 140 R_J$ from the planet at the relevant local times (see Fig. 3a) (Joy et al. 2002). We expect the spacecraft to cross the bow shock and magnetopause boundaries ~ 1 –2 weeks before the first closest approach to Jupiter (Jupiter orbit insertion), and we have high confidence that ~ 2 –4 weeks after this event the spacecraft will cross boundaries again and make at least one excursion into the solar wind during the Jupiter tour. The exact timing of boundary crossings cannot be predicted accurately because of the highly unpredictable and variable solar wind dynamic pressure conditions (e.g. Joy et al. 2002). Magnetopause crossings will allow us to search for evidence of key energy transport processes (Ebert et al. 2017; Masters 2017; Montgomery et al. 2022), and any pre-dawn crossings would allow us to study a region just inside the magnetosphere where Vasyliūnas (1983) proposed that a plasma cycle, similar to the Earth's Dungey cycle, forms an X-line of plasmoid disconnections (Krupp et al. 1998, 2001a,b; Vogt et al. 2014, 2020); however, some analyses of Jupiter magnetospheric data indicate that such an X-line may not develop frequently (e.g., Bagenal et al. 2017b). The low inclination of the *JUICE* orbits that would cross the magnetopause, compared to the fast north-south crossings of *Juno*, plus the better time resolution of *in situ*

Fig. 4 Residence time of JUICE as a function of M-shell during the Jupiter orbital tour, prior to Ganymede orbit insertion. (a) Residence time as a function of M-shell and magnetic local time. (a) Residence time as a function of M-shell and magnetic latitude. In both panels the M-shells of three Galilean moons are marked based on the same field model. Since Callisto is located in the magnetodisk region, its magnetic distance can significantly change as Jupiter rotates, whereas for the other two moons this range is smaller



measurements compared to *Galileo* and the possibility of remotely monitoring the global magnetospheric response may further contribute to our understanding of plasma circulation at Jupiter (Kronberg et al. 2007; Louarn et al. 2014; Kimura et al. 2018).

2.1.2 Plasma Sheet and Mid-Latitude Magnetosphere

After the initial orbits, *JUICE* will remain inside $65 R_J$ until the end of the mission. Figure 4 shows the spacecraft residence time as a function of M-shell, covering the orbits of Europa, Ganymede, and Callisto. Outside the orbits of the Galilean moons ($>30 R_J$), the dipolar magnetic field is distorted by both the outward moving plasma and a sheet of current in the equator of about 100 million amperes (Khurana and Schwarzl 2005) (see Fig. 2 and Sect. 2.2), forming radially distended field lines near the equatorial plane (Achilleos et al. 2015), similar to the cross-tail current at the Earth, but with approximate axial symmetry. The equatorial magnetosphere ultimately assumes a flattened pancake-like structure, known as the magnetodisk (see Fig. 2). Such stretching of the field lines facilitates magnetic reconnection and plays an important role in the magnetospheric dynamics as magnetic energy is converted to particle energy through impulsive events that stream both tailward and planetward.

JUICE will be able to observe the aftermath of magnetotail reconnection events through the detection of planetward flows, signatures of transient particle acceleration, or distinctive magnetic signatures (Vogt et al. 2014; Yao et al. 2019; Yuan et al. 2021). This may explain Jovian dawn auroral storms, of which transient variability was continuously monitored with the *Hisaki* satellite (Kimura et al. 2015, 2017). Bonfond et al. (2021) compared the transient dawn auroral storms to terrestrial substorms, supporting the idea that mass and energy do not

circulate smoothly, but accumulate until the magnetosphere collapses, generating substorm-like auroral responses. Recent *Juno* observations indicate the plasma sheet is dense, with weak associated wave intensity, but that the dawn-dusk asymmetric plasma sheet boundary layer is more tenuous and has larger wave activity, observations that could map boundary layer origin to transient reconnection (Zhang et al. 2020). This is an area where further *JUICE* observations will be valuable.

Many types of plasma instabilities may occur in the magnetodisk, such as ballooning instability or cross-field current instability (Bonfond et al. 2021; Guo et al. 2021). These instabilities can lead to a disruption of the azimuthal currents in the middle magnetosphere and dipolarisation of the magnetic field lines that would be progressively swept away from the nightside by planetary rotation. The *Cassini* spacecraft observed small-scale reconnection occurring throughout the magnetodisk of Saturn (Guo et al. 2018), a process that may regulate the shedding of mass and energy from the planet's magnetosphere, in addition to nightside reconnection. The potential to search for signatures of instabilities and small-scale reconnection at Jupiter also exists for *JUICE*, thanks to its extensive survey of the Jovian magnetodisk.

The middle magnetosphere that is the subject of this section includes the region where rigid corotation of plasma with Jupiter breaks down. This corotation breakdown region is the subject of Sect. 2.2, which includes discussion of the role of corotation enforcement currents in driving Jupiter's auroral emissions.

2.1.3 Inner Magnetosphere and Radiation Belts

We define the outer boundary of the inner magnetosphere at an equatorial distance of $\sim 30 R_J$ in the vicinity of the orbit of the outer Galilean moon, Callisto. Coincidentally, it is outside that distance where the magnetodisk plane hinges (Khurana 1997), whereas inside the planetward rise of >1 MeV (relativistic) radiation belt electron fluxes becomes steeper (Kollmann et al. 2018), and the trapping of energetic protons and heavier ions is more stable (Birmingham 1982; Selesnick et al. 2001). *JUICE* measurements of plasma moments, energetic particle spectra, ion composition, angular distributions, electromagnetic wave spectra and their spatial dependencies will be key for understanding a variety of features in the inner magnetodisk.

Estimates of the radial profile of magnetic flux tube content may define whether the magnetosphere is conducive to processes like centrifugal interchange. The latter could drive planetward injections and energisation of particles to radiation belt energies, as observed at Saturn (Mitchell et al. 2015). While most injections are observed in the range $10 < L < 20$ (Mauk et al. 1999; Dumont et al. 2014), it is unclear if centrifugal interchange is their driver, given the shallow flux tube content negative gradient with M-shell reported by Bagenal et al. (2016). These authors used re-processed *Galileo* plasma data to demonstrate that the ion temperature increases at M-shells beyond Europa's orbit, contrary to the expected adiabatic cooling. The presence of a heating source is thus implied, linked to a combination of turbulence, diffusive transport, and advective flows (Ng et al. 2018, 2022).

Radial transport is especially important for charged particle acceleration in the radiation belts, while conserving the first two adiabatic invariants of motion. Analysis of *Galileo* energetic particle measurements and *Juno* data suggest this process may be responsible for accelerating electrons into the range of several to tens of MeV, at least out to the orbit of Ganymede (Kollmann et al. 2018; Ma et al. 2021), and may drive dynamics (Hao et al. 2020), but these measurements lack the energy resolution to conclude with certainty. With a combination of measurements *JUICE* will measure electrons all the way from a few keV

to ~ 40 MeV, as well as protons up to ~ 250 MeV. This is the first-time proton measurements above 10 MeV will be made over long periods of time in the Jovian system (Hajdas 2025, this collection). This extension of the energy range above the $\lesssim 1$ MeV range provided by past spacecraft (e.g. Shen et al. 2022) is particularly important in the inner magnetosphere for quantitatively understanding surface weathering and exosphere generation at the Galilean moons (e.g. Teolis et al. 2017) (see Sects. 3 to 5).

JUICE will be able to search for signatures of the various acceleration processes by characterising the spectral shape at MeV energies and observe dynamics, particularly during times of sudden “storm” enhancements (Yuan et al. 2021). The multiple crossings of the Galilean moon M-shells will also offer the opportunity to detect microsignatures (regions of absorbed energetic electrons), the profile of which can be used to quantitatively assess radial transport (e.g. Roussos et al. 2016). Moreover, *JUICE* will search for external sources of energetic particles that have been identified in other planets such as Cosmic Ray Albedo Neutron Decay (Roussos et al. 2022).

Competing with adiabatic heating is electron energisation by strong electromagnetic whistler mode waves, which can accelerate electrons to relativistic energies of several MeV on timescales of tens of days, comparable to the time needed for electron transport across the region $6 < L < 12$ (Horne et al. 2005; Shprits et al. 2012; Woodfield et al. 2014). These intense waves, especially whistler mode chorus emissions, have been observed by the *Galileo* and *Juno* spacecraft along the anticipated regions that *JUICE* will sample in the Jovian magnetosphere (Menietti et al. 2008, 2016, 2021a, 2021b, Li et al. 2020), in a close relationship with anisotropic electron distributions at energies of tens of keV (Katoh et al. 2011). However, these measurements do not provide us with crucial parameters of these wave particle interactions; polarisation and propagation properties of electromagnetic waves are still unknown. *JUICE* will be able to close this knowledge gap by providing three-dimensional (3D) measurements of fluctuating magnetic and electric fields at frequencies up to 20 kHz, and precise characterisation of the background magnetic field and energetic electrons. Anisotropic distributions generated by moon-magnetosphere interactions may also lead to enhanced chorus wave activity that may also drive extreme acceleration of electrons near Ganymede or Europa (Shprits et al. 2012), hints of which may have been observed at the latter moon by *Juno* (Allegrini et al. 2020). Direct measurements by *Juno* at Europa (Kurth et al. 2023) and Ganymede (Kurth et al. 2022) clearly show presence of whistler-mode chorus, captured by one electric and one magnetic antenna. *JUICE*'s 3D measurements during the extended period spent near Ganymede will be particularly interesting in this respect.

Besides acceleration, particle loss is also an important process that regulates radiation belt populations. Theory and modelling studies suggest that interactions with electromagnetic ion cyclotron (EMIC) waves play significant roles in the loss processes of energetic ions (Mauk 2014, 2022), radiation belt protons (Nénon et al. 2018), and possibly radiation belt electrons as observed in the terrestrial magnetosphere. *Galileo* measurements reveal enhancements of EMIC waves around icy satellites (Volwerk et al. 2001, 2013). High-latitude observations by *Juno* suggest one of the major loss processes for energetic ions near and outward of Ganymede's orbit is scattering into Jupiter's loss cone (Mauk et al. 2022). While *Juno*'s high-latitude orbit is ideal to resolve the loss cone and directly measure the result of the scattering, it does not cover the equatorial plane well, which is where the scattering may predominantly occur. *JUICE* can contribute to the investigation of the distribution of EMIC waves in the equatorial plane of the Jovian magnetosphere and their roles they play in determining the observed intensity as well as the dynamics of energetic ions (Yao et al. 2021). *JUICE* will also be capable of directly measuring energy exchange between energetic ions and waves (Katoh et al. 2018).

2.2 The Corotation Breakdown Region

Having now reviewed the global magnetosphere of Jupiter relevant for *JUICE*, this section is dedicated to discussion of the corotation breakdown region. This region deserves special attention here because of a combination of its importance for understanding how the system works and the expectation that *JUICE* measurements in the region will lead to a step-change in our understanding.

2.2.1 Concept and Consequences

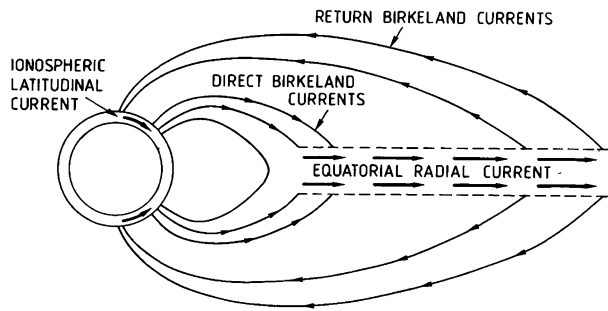
A combination of strong magnetic, mechanical and thermal stresses is responsible for the large size of Jupiter's magnetosphere. The hot plasma that dominates the plasma pressure has a temperature exceeding 20 keV outside of Io's torus. The ratio of plasma pressure to magnetic pressure (the plasma β) exceeds unity beyond a radial distance of 30 R_J (Kane et al. 1995; Mauk et al. 2004) inflating the magnetosphere. The cooler plasma that dominates the plasma number density experiences strong outward centrifugal force that further inflates the magnetosphere. The magnetospheric plasma consists of various charge states of S and O ions, protons and electrons and is originated principally from Io's torus with minor contributions from a neutral torus at Europa, the solar wind, and the planetary ionosphere (Bagenal and Sullivan 1981; Belcher et al. 1980; Hill 1983; Martin et al. 2020). It is estimated that Io's plasma torus slowly diffuses and convects radially outward (Hill 1976; Southwood and Kivelson 1987, 1989), while the magnetic flux is returned to the inner magnetosphere in narrow channels that are devoid of cold plasma (e.g., Kivelson et al. 1997).

The plasma is known to be close to corotation with Jupiter up to a radial distance of 20 R_J , but falls substantially below corotation further out (Kane et al. 1995; Krupp et al. 2001a). A strong dawn/dusk asymmetry in the flow velocity is also observed with plasma closer to corotation in the dawn sector but lagging substantially below it in the dusk sector (Krupp et al. 2001b). As the plasma moves outward, it expands to fill a larger volume and is therefore expected to get cooler if the expansion process is adiabatic. However, the thermal plasma is seen to increase in temperature from 30 eV in Io's torus to ~ 1 keV in the outer magnetosphere suggesting the need for a source of local heating (Bagenal and Delamere 2011).

As magnetospheric plasma moves radially outward in Jupiter's magnetosphere while conserving its angular momentum, its angular velocity falls with radial distance. The resulting viscous drag between the ions and neutrals on the same flux tube in the upper atmosphere of Jupiter exerts a torque on the ionospheric plasma that is transmitted to the magnetosphere via field-aligned (Birkeland) currents (Hill 1979; Vasyliūnas 1983). In the equatorial plane, the electric current becomes radial in direction and applies a Lorentz force ($\mathbf{J} \times \mathbf{B}$) in the azimuthal direction (see Fig. 5) to keep plasma in corotation. This long-distance interaction between the ionospheric and magnetospheric plasmas results in a net transfer of angular momentum from Jupiter's atmosphere into the Jovian magnetosphere, with limits on the transfer of angular momentum from the upper atmosphere of Jupiter explaining the sub-corotation beyond $\sim 20 R_J$ (Hill 1979; Huang and Hill 1989). It is important to note that while the large-scale picture of currents shown in Fig. 5 is present, and leads to the angular momentum transport discussed here, the current system is considerably more structured when viewed on smaller scales, particularly close to the planet (e.g. Mauk et al. 2020a,b).

As the angular momentum of a parcel of corotational plasma increases proportional to the square of its radial distance from Jupiter, corotation must break down where the ionosphere, through the viscous torque applied by the ionosphere on the outflowing plasma, is not able to

Fig. 5 The configuration of the field lines (thin black lines) and the electric currents (thin and thick arrows) that reinforce corotation in Jupiter's magnetosphere. Reproduced from Vasyliūnas (1983)



impart sufficient angular momentum to the magnetosphere (Hill 1979). Hill (1979) showed that the ion-neutral collisions in the ionosphere exert a rotational torque on the plasma which increases with the L-shell value of the field lines, defined in the classic sense using only the dipole field of the planet (i.e., differing from M-shells), and is proportional to the height-integrated Pedersen conductance of the ionosphere. The limitation in momentum transfer may be local to the ionospheric layer because of its finite conductivity.

However, an even stronger restraint on the angular momentum transfer from the ionosphere is provided by the rotational slippage of the neutral atmosphere itself because of the inability of the lower atmosphere to supply the angular momentum to the upper atmosphere (Huang and Hill 1989). The rate of increase of angular momentum in the magnetosphere is proportional to the rate of outward mass transport (Hill 1979). Equating the two results yields a differential equation that introduces a corotation break-down distance L_0 which is proportional to the ionospheric conductivity and inversely proportional to the mass outflow rate. For values typical of the Jovian magnetosphere (height integrated conductance = 0.1 S and a mass outflow rate of 10^{28} amu s^{-1}), $L_0 = 64 R_J$. This calculated value of the corotation break-down is considerably higher than the observed value of 20–30 R_J . An additional constraint on the outward flow of angular momentum is required to explain the plasma velocity observations.

In the rest frame of the magnetospheric plasma, the electric field must vanish. It is normally assumed that the neutral atmosphere at ionospheric altitudes corotates rigidly with Jupiter. This may, however, not be valid because the neutrals in the ionosphere may not have sufficient angular momentum and start lagging the angular velocity of Jupiter. Because a vertical gradient in the azimuthal velocity of neutrals is resisted by the viscosity of the atmosphere, the upward (antiplanetward) transfer of angular momentum in the neutral atmosphere is controlled by the effective eddy viscosity of the upper atmosphere.

Huang and Hill (1989) show that atmospheric density and eddy viscosity alone determine the fractions of the magnetospheric corotation lag that is attributable to the slippage of the neutral atmosphere relative to Jupiter. The balance between the transfer of angular momentum to ions from the neutral-ion collision force and the upward transfer of angular momentum to the neutrals in the ionosphere from the lower atmosphere determines the angular velocity of the magnetospheric ions. They showed that the slippage of the neutrals can reduce the effective Pedersen conductivity of the ionosphere by a factor of 10 to 100, compared to the situation without slippage. This reduction in the effective conductivity of the ionosphere decreases the effective corotation breakdown distance by an additional factor of 2–3 which is consistent with the observations of plasma velocity in the magnetosphere. Indeed, Cowley and Bunce (2001) and Nichols and Cowley (2003) demonstrate that the effective height integrated conductivity required in their models (~ 0.1 S) of magneto-

sphere/ionosphere coupling is substantially lower than the expected value of 1–10 S from observations.

The strength of the corotation enforcement current system is extremely large (60–100 MA) and requires the availability of sufficient population of electrons to carry the field-aligned current at high latitudes. Two processes are known to limit the supply of electrons at high latitudes. First, in the upward current region where electrons are moving downward (planetward), they must overcome the magnetic mirror forces to precipitate in the extremely strong dipolar field of Jupiter to close the current loop. Next, in the Jovian magnetosphere, the heavy ions are confined close to the equatorial plane of the magnetosphere by the centrifugal force of the rapidly rotating plasma. An ambipolar electric field develops between ions and electrons and further restricts the high-latitude populations of electrons (Ray et al. 2009, 2010). Observations in the Earth's and Jupiter's magnetosphere have shown that in this situation, strong field-aligned potentials can develop above the ionosphere that accelerate the stably trapped thermal plasma into the loss cone and help close the current circuit (McIlwain 1960; Evans 1968; Knight 1973; Lysak 1990; Cowley and Bunce 2001; Mauk et al. 2002; Nichols and Cowley 2004).

Both remote measurements of the energies of auroral precipitating electrons from far UV spectra (Gérard et al. 2003, 2014) and local measurements of electrons in the Jovian ionosphere (Mauk et al. 2017; Clark et al. 2017, 2018) show that the precipitating electrons have characteristic energies of 100–300 keV. Ray et al. (2009, 2010) Vlasov model reproduces many of the observed features and have shown that the maximum field-aligned current density in the ionosphere is lower than that derived by the Knight (1973) analysis when the additional current choke in the high latitude region from the ambipolar electric field is included. An alternative model postulated by Saur et al. (2003, 2018) invokes magnetohydrodynamic (MHD) turbulence acceleration of electrons in the magnetosphere. Clark et al. (2018) compared the observational characteristic energies with predictions from these two models but concluded that they could not distinguish the primary drivers.

Recently, Bonfond et al. (2020) have provided several arguments against the ability of the corotation enforcement theory to explain the main aurora at Jupiter. In particular, they mention that the anticorrelation expected between particle velocities and the bend-back of the field is not observed in data. They also show that the bend-back of the field lines is the strongest in the dawn sector whereas the auroral emissions peak in the dusk sector. On the other hand, Nichols and Cowley (2022) systematically evaluated radial currents in the dawn sector from *Juno* orbits 3–7 and show that they are directly correlated to the strength of the aurora (maximum mean auroral intensity).

Measurements of energetic electrons over the main aurora obtained by the *Juno* spacecraft revealed that these electrons are often bi-directional and broadband in nature (e.g., Mauk et al. 2017, 2018). Salveter et al. (2022) performed a statistical study of auroral electron distribution functions and found that more than 90% of these are indeed broadband and bidirectional, while mono-energetic uni-directional electrons occur less than 10% of the time. A steady-state current system in combination with an acceleration through a steady state voltage drop (Knight 1973), however, does not seem to be consistent with the predominantly observed distribution function of Jupiter's auroral ovals as the Knight-relationship predicts uni-directional monoenergetic beams. The broad-band bi-directional nature of the auroral electron beams rather suggests that stochastic acceleration possibly related to fluctuating fields and AC electric currents plays a dominant role (e.g., Saur et al. 2018; Damiano et al. 2019; Lysak and Song 2020).

2.2.2 Expected Advances Enabled by JUICE

One objective targeted by *JUICE* will be the determination of the mass outflow rate in Jupiter's magnetosphere. The plasma production rate in Io's torus must equal the plasma loss through mass outflow. It assumes that other sources of loss in Jupiter's magnetosphere are of secondary importance but in the other hand losses into the atmosphere of Jupiter and into the Jovian neutral atom nebula through charge exchange of ions with neutrals have not been carefully quantified (Hill 1983). The plasma production rate can be determined through modelling of the UV emissions in Io's torus (Shemansky 1980; Delamere and Bagenal 2003) using emission spectroscopy and physical chemistry models of the torus. UV observations provide a great opportunity to monitor Io's torus remotely in several wavelengths and determine the plasma production rates. Moreover, the Io torus can also be observed via ENA imaging (Futaana et al. 2015) (see Sect. 2.4). Measurements of the bulk densities and velocities of the co-rotating magnetospheric plasma and embedded magnetic field can together provide a coherent picture of the structure of the plasma flows in the equatorial magnetosphere.

Characterisation of the magnetised plasma environment where corotation breaks down will impact the debate regarding what drives Jupiter's main auroral emission in the UV. *JUICE* will obtain plasma moments and make magnetic field and plasma wave measurements across a wide range of distances, local times, and latitudes within the magnetodisk and corotation breakdown region, of which only a fraction has been covered by past or ongoing missions. Concurrent auroral imaging will indicate how the magnetodisk is coupled to Jupiter's atmosphere (Fletcher et al. 2023), allowing an assessment of the relative importance of field-aligned potentials compared to stochastic acceleration via wave-particle interactions.

The conductivity of Jupiter's ionosphere is determined by the strength of Jupiter's magnetic field and various collision frequencies between the charged particles and neutrals. Even though, the rate of ionospheric production from UV ionisation can be evaluated quite precisely, the production of ions and electrons from electron impacts has not been yet fully quantified in Jupiter's ionosphere. Most models suggest that energetic particle precipitation dominates over UV ionisation in both heating the atmosphere and creating and maintaining the population of electrons in the auroral region (Strobel 1983). Radio occultation measurements, combined to the long dwell time of *JUICE* in Jupiter's vicinity, its several high latitude orbits, will yield many measurements of electron density profiles of Jupiter's ionosphere.

Moreover, *JUICE* will spend a large fraction of its time measuring local field and plasma properties in the region (10–30 R_J), the outer part of which is connected to the auroral oval. By comparing local populations with remote sensing observations of Jupiter's auroral zones, we expect significant progress in understanding how the conductivity of the Jovian ionosphere is modified by plasma precipitation. In situ fields and particles measurements will be essential to further understanding of the magnetospheric energy input to the ionosphere.

One of the key unanswered questions for corotation breakdown is the rate of slippage of neutrals in the ionosphere. The upward transfer of angular momentum is facilitated by eddy diffusion processes in Jupiter's ionosphere. It has been speculated that the eddy diffusion coefficient in the auroral zone is at least a factor of 10 higher than that observed in the equatorial regions of Jupiter's atmosphere (Huang and Hill 1989). Tantalizing, though very limited observation of He 584Å airglow made by the *Cassini* UV spectrometer is indeed consistent with elevated eddy diffusion by a factor of 4–20 (Parkinson et al. 2006). By studying the emissions, thanks to ultraviolet remote sensing capabilities to observe He

airglow, under various levels of polar cap activities and plasma conditions in the magnetosphere, *JUICE* will finally help us understand how the angular momentum is transported upwards into the ionosphere of Jupiter and then transmitted into the magnetosphere.

2.3 Neutral and Plasma Tori of Moons

As introduced at the beginning of this section, Jupiter's most active moon, Io, is a significant source of neutral particles, forming a neutral torus and an associated plasma torus formed through ionisation inside Jupiter's magnetosphere (see the reviews by Thomas et al. 2004 and Bagenal and Dols 2020) (Bagenal et al. 1997). Plasma is created at a rate of ~ 100 to $\sim 300 \text{ kg s}^{-1}$. Europa is also known to be a source of neutral particles, forming its own tori at larger distances from the planet. This section specifically deals with these dynamic structures, and how *JUICE* will advance our understanding in these areas. A key factor in the formation of the neutral and plasma clouds due to Io and Europa is the $\sim 10^\circ$ offset between Jupiter's rotation and magnetic dipole axes (e.g. Connerney et al. 2022). An important concept is the centrifugal equator, introduced by Hill et al. (1974), which is defined by the points along magnetic flux tubes that are farthest from Jupiter's spin axis, applying from 5 to 30 R_J (Phipps and Bagenal 2021). The centrifugal equator is tilted by $\sim 6.4^\circ$ with respect to the rotational equator ($\sim 2/3$ of the magnetic dipole tilt) evolving to the dipole tilt as the current sheet strengthens beyond $\sim 12 R_J$.

2.3.1 Io Neutral Torus and Plasma Torus

Intense volcanic activity produces a cloud of SO_2 along Io's orbital path. Clouds of atomic sulphur, sulphur molecules, sulphur dioxide, oxygen, chlorine, sodium, potassium and sodium chloride dust rotate around Jupiter along the planet's equatorial plane at a tangential velocity of $\sim 17.33 \text{ km s}^{-1}$. At Io's orbital distance the speed of rigid corotation with Jupiter is $\sim 74.23 \text{ km s}^{-1}$, and so a flow of charged particles tied to Jupiter's magnetic field is incident on the wide neutral cloud of material around Io. Through collisions with electrons, neutrals are ionised, giving rise to plasma (Phipps and Withers 2017).

A combination of *in situ* and remote observations by past missions to Jupiter has told us much about the Io plasma torus, allowing mapping of its spatial extent, distance from Jupiter, and how far it extends above and below the centrifugal equator. Radio occultation measurements have quantified the total electron content of the torus, allowing reconstruction of the 3-D electron density distribution (Warwick et al. 1979a, 1979b; Bird et al. 1992). Energy is emitted from the plasma torus in the form of UV photons (Sandel et al. 1979; Hall et al. 1995), the energy source of these emissions is important to determine, as well as how fast the energy is emitted. The power sources are of two categories: The neutral cloud theory where power is provided by the pick-up of ionised oxygen or sulphur (Broadfoot et al. 1979; Barbosa 1994), and power due to the inward transport of hotter plasma from the plasma sheet (Smith et al. 1988; Herbert and Sandel 2000). These sources have long cooling times, however from observed emissions it was concluded that the cooling time should be short, possibly as short as two hours (Dessler and Sandel 1992, 1993).

Physical chemistry models of the Io plasma torus have been extended from a cubic centimetre in the centre of the torus (Delamere and Bagenal 2003; Shemansky 1988) to radial profiles (Barbosa 1994; Delamere et al. 2005; Nerney et al. 2017; Nerney and Bagenal 2020; Yoshioka et al. 2014, 2017) and azimuthal variations (Steffl et al. 2008; Tsuchiya et al. 2019) as well as temporal variations apparently driven by volcanic outbursts on Io (Delamere et al. 2004; Kimura et al. 2018; Tsuchiya et al. 2018; Yoshioka et al. 2018). Volwerk (1997)

showed that indeed a 2-hour cooling time agrees with the observations, through a lack of correlation between the brightness of the two ansae of the plasma torus.

Bagenal and Sullivan (1981) analysed measurements made by *Voyager 1* and put forward a model of the Io plasma torus, divided into three different zones based on temperature and major ion species: the cold torus, the ribbon and the warm torus. The innermost zone, centred at 5.2 R_J from Jupiter's barycentre, is the cold torus. Electron density decreases with increasing distance away from the centrifugal equatorial plane, with an e-folding length of 0.1 R_J (the scale height of the cold torus). Peak cold torus density is at $\sim 5.23 R_J$, with the high-density region extending from 4.9 to 5.5 R_J , with a characteristic density of ~ 1000 electrons cm^{-3} . The composition of the cold torus is mainly S^+ ions, with a lower abundance of O^+ . The mid-zone is the ribbon, a narrow region that extends from 5.5 to 5.7 R_J , with a scale height of 0.6 R_J and higher densities of ~ 3000 electrons cm^{-3} . This area of the plasma torus is dominated by O^+ ions, with a smaller abundance of S^+ . Finally, the outermost zone is the warm torus, extending from 5.7 to 8.0 R_J and with a scale height of $\sim 1 R_J$. This is the thickest region with the largest variety of ion species despite an electron density of ~ 2000 electrons cm^{-3} which is lower than in the ribbon. The warm torus mainly consists of S^{2+} and O^+ ions, with traces of O^{2+} , S^+ , and S^{3+} .

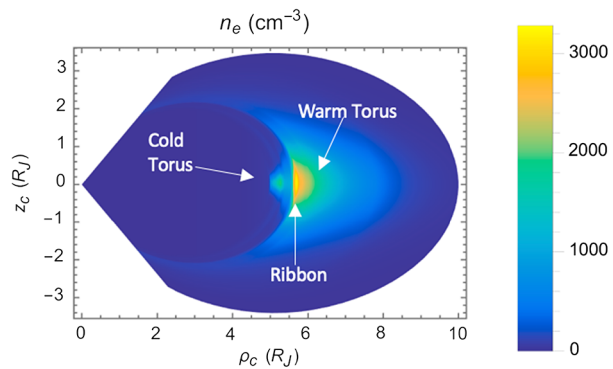
In the model described above, the plasma torus structure is a function of the distance from Jupiter and the distance away from the centrifugal equator. In reality, the plasma torus varies with the longitude of the System III reference frame (which corotates with Jupiter), due to time-dependent asymmetries in the magnetic field and temporal variations in the production of material by Io's volcanoes (see below). Temporal and longitudinal variations of the Io plasma torus have been identified in both *Cassini* data (Steffl 2004a,b; Steffl et al. 2006, 2008) and by the more recent *Hisaki* mission (Murakami et al. 2016; Yoshikawa et al. 2017; Tsuchiya et al. 2018; Yoshioka et al. 2018; Koga et al. 2019; Tsuchiya et al. 2019). In addition, UV observations by the two *Voyager* spacecraft and ground-based measurements suggest that the ribbon feature shows strong, asymmetric longitudinal variability (Volwerk 2018).

The almost polar orbits of the *Juno* spacecraft and perijoves at $\sim 1.05 R_J$ have most recently provided a new perspective on the Io plasma torus through radio occultations. At each perijove there is a path delay in the radio signal that is proportional to the total electron content along the signal path, and the unique orbital geometry allows constraint of the vertical extension of the torus within a single longitudinal sector on each perijove. Phipps and Withers (2017) developed a simplified Io plasma torus model in which each region (cold and the warm torus plus the ribbon) is modelled by a double-Gaussian function, allowing fitting of the radio occultation data from the earliest occultations by *Juno* (Phipps et al. 2018, 2019, 2020, 2021). A further refinement of the Phipps and Withers (2017) model has now been reported by Moirano et al. (2021). These authors were able to improve the axisymmetric model by including both the longitudinal and the temporal periodicities and successfully fitting to 15 of the first 25 Io plasma torus radio occultations by *Juno*. Also in the *Juno* era, modelling work has been reported by Nerney and Bagenal (2020) that combines UV observations and a physical chemistry framework to shed light on the hot electron component of the plasma torus. Figure 6 shows a result of this modelling, indicating the expected, detailed torus structure.

2.3.2 Europa Neutral and Plasma Torus

Because plasma processes in Jupiter's magnetosphere will also cause erosion of Europa's surface and escape of atoms and molecules (Plainaki et al. 2018) a neutral cloud and an

Fig. 6 The modelled electron number density distribution in a cross-section of the Io plasma torus. z_c is vertical distance away from the centrifugal equator (positive z_c is north of this surface) and ρ_c is perpendicular distance from Jupiter's barycentre along the centrifugal equator. Taken from Nerney (2023)



associated plasma torus can be expected in the vicinity of Europa's orbit ($9.4 R_J$), much like the structures at Io's orbit around $5.9 R_J$. ENAs originating from the neutral torus were observed by *Cassini* (Mauk et al. 2003; Smith et al. 2019). The measured ENA intensities allowed the authors to constrain the torus geometry and estimate the neutral densities, although the more detailed geometry and chemical composition of the torus remain to be constrained. Also, the Sulphur-to-Oxygen composition ratio decreases beyond Io's orbit, consistent with a Eurogenic plasma source (as Europa's atmosphere is primarily composed of Oxygen). Both Europa's exosphere (see Tosi et al. 2024, this collection) and this neutral torus are the products of surface or sub-surface release processes from the icy surface of this moon (Vorburger and Wurz 2018; Plainaki et al. 2018). These processes include sublimation, desorption, micrometeoroid impact vaporisation and sputtering caused by plasma and energetic particles from the Jovian magnetosphere (Galli et al. 2022).

Europa's neutral gas torus has an estimated density of $20\text{--}40 \text{ cm}^{-3}$ (Lagg et al. 2003); for comparison, the neutral clouds of SO_2 and O at Io's orbit are on the order $50\text{--}100 \text{ cm}^{-3}$ each (Bagenal and Dols 2020). The chemical composition of Europa's neutral torus is expected to be mostly H_2 with minor H, O_2 , and O contributions (Smyth and Marconi 2006; Smith et al. 2019). Modelled distributions of H_2 and H are shown in Fig. 7. Comparisons between the *Cassini* ENA images (Mauk et al. 2003) and modelling of ENA emission processes estimate the total neutral torus content at around $(0.6 \pm 0.25) \times 10^{34}$ molecules/atoms (Mauk et al. 2004). This torus is estimated to be supplied by a source with a strength of 2×10^{27} molecules s^{-1} , which, assuming a primarily water-group composition, is in the range of $10\text{--}100 \text{ kg s}^{-1}$ (Schreier et al. 1993). This makes Europa's contribution comparable to that of Enceladus at Saturn. Recently, Szalay et al. (2024a) estimated that $4.5 \pm 2.4 \times 10^{26} \text{ H}_2/\text{s}$ (requiring, due to radiolysis, $13 \pm 7 \text{ kg/s}$ of H_2O ice to be dissociated) are available to potentially be lost to the torus.

Estimates of the vertical thickness of the neutral gas torus have been made using charged particle data from *Galileo* to measure the energetic proton depletion, constraining the neutral cloud scale-height to be $1\text{--}2 R_J$, likely closer to $1 R_J$ (Kollmann et al. 2016), similar to the estimated scale-height of the Io torus. Simulations of Europa's neutral torus by Smith et al. (2019) demonstrate that the azimuthal distribution of gas is far different to that of Iogenic matter, with oxygen and sulphur remaining relatively local to Europa in local time (Bagenal and Dols 2020). *Hubble Space Telescope* (HST) UV observations put additional constraints on the distribution of neutral oxygen and hydrogen component sources (Roth et al. 2023).

The Io and Europa plasma tori are often described as well-defined structures, but in fact they overlap to some extent (Bagenal and Dols 2020). The outer edge of the warm Io plasma

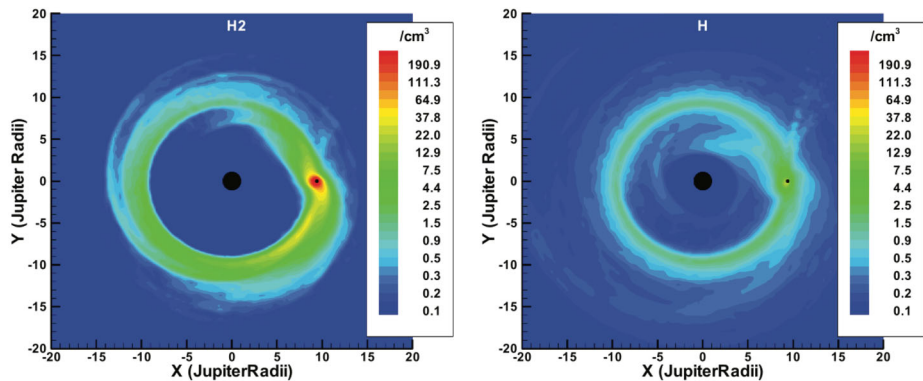


Fig. 7 Europa-generated H_2 (left panels) and H (right panels) model particle distributions. Panels display densities (cm^{-3}) as in the xy plane (the negative y-axis points toward the Sun and perpendicular to Jupiter's rotational axis - the z-axis, with the x-axis completing the right-handed orthogonal set) in Jovian radii (R_J). Adapted from Smith et al. 2019 with permission from the Astrophysical Journal

torus extends past Europa's orbit and merges with the equatorial plasma sheet in the magnetosphere. Consequently, any Europa plasma torus can be considered embedded within the Io torus. Attempts to model the Europa plasma torus by using *Voyager* data suggest that only about 12% of the plasma in the vicinity of Europa originated from the moon itself, and the rest is radially transported outward from Io's orbit (Schreier et al. 1993). A rich composition of species in the Europa plasma torus has been inferred using ion cyclotron wave observations made near Europa's wake. These species include SO_2^+ , K^+ , Cl^+ , Cl^- , O_2^+ and Na^+ (Volwerk et al. 2001). H_2^+ , O^+ , O^{++} , O_2^+ originating from Europa were directly measured in the plasma sheet by *Juno/JADE* (Szalay et al. 2022, 2024b). The properties of the Europa plasma torus are summarised in Table 5 of Bagenal and Dols (2020). The electron density is estimated at around 160 electrons cm^{-3} , which is about 5–10% of the density at Io's orbit and within the warm Io torus. Recently, Kurth et al. (2023) also measured the electron density during *Juno's* Europa flyby to be $\sim 100 \text{ cm}^{-3}$ upstream for that single epoch. The modelling work by Schreier et al. (1993) suggests that the large radial diffusion coefficient generated by outward-migrating Iogenic plasma inhibits the growth-rate of the Europa plasma torus. There is evidence of only a few percent increase in plasma density at Europa's orbit (De-la-mere et al. 2005), and the main contribution is the increase in ion temperature provided by fresh pickup ions at around 650 eV for O^+ .

2.3.3 Expected Advances Enabled by JUICE

JUICE will further our understanding of both the Io and Europa neutral tori, particularly through remote measurements. The spacecraft has the capability to take images in ENAs, generating 2-D images of both these neutral tori. Because ENAs are the product of charge exchanges between local ions and neutral atoms, ENA images will constrain the neutral density of H_2 (and possibly other neutral species) in the neutral tori, given our knowledge of ion densities and ion energies. More information is given in Sect. 2.4 below, where ENA imaging with *JUICE* is discussed in detail. Note that this technique will also allow us to search for neutral tori associated with Ganymede and Callisto that are yet to be identified (Mauk et al. 2003).

For the Europa neutral and plasma tori, *in situ* measurements will also be valuable. *JUICE* will measure the chemical composition of this moon's neutral torus during the few

occasions when the spacecraft comes within $9.4 \pm 1.5 R_J$ of Jupiter, within the estimated width of the Europa neutral torus (Smyth and Marconi 2006; Smith et al. 2019). Combining these *in situ* measurements with the ENA images taken at larger distances will constrain the geometry of the Europa neutral torus far beyond what has previously been possible. These occasions when *JUICE* is inside the Europa neutral torus are also valuable opportunities to simultaneously sample Europa's associated plasma torus. In situ plasma measurements will determine ion distributions both near and far from Europa within this torus, revealing the driving force behind the ion sputter process. Bringing together the new information about both neutral and ion densities will shed light on the surface composition of Europa, and the relative importance of the various release processes of particles from Europa's surface. As for the remote sensing discussed above, *in situ* measurements will also be used to search for neutral and plasma tori around Ganymede and Callisto. *JUICE* trajectories that cross plasma wake and interaction regions at Callisto will allow the determination of the atmospheric loss rates in the form of pick-up ions (Galli et al. 2022). Similarly, during the Ganymede orbital phase it will be possible to estimate the loss of the exospheric neutral density through in situ particle measurements.

Radio occultations will be an especially powerful tool for both the Io and Europa plasma tori. When *JUICE* is in occultation with the Io and Europa plasma tori, as seen from the Earth, the radio carrier frequencies suffer a phase shift due to the radio wave propagation in the torus plasma. This is seen in the receiver as a slight frequency shift. This frequency shift is proportional to the temporal change of the total electron content with respect to the measurement time. The total electron content is the integrated electron density, along the line-of-sight of the radio ray path from the spacecraft to Earth. Using two coherent downlink frequencies, the recorded frequencies can be differenced and integrated to derive the total electron content as a direct observable. These observations will allow the development of an electron density model from the torus at the time of the sounding, extending the validity and consistency of the current models (e.g. Bird et al. 1992; Phipps and Withers 2017; Moirano et al. 2021).

Although the Io plasma torus mixed model presented in (Moirano et al. 2021) shows residuals in the least-square fit of the path delays which are about 40% better than previous models, there is still much to be investigated in terms of longitudinal and temporal variability of the Io plasma torus. Most of *Juno*'s radio occultations were (and will be) carried out during the polar orbits at Jupiter, thus the torus sections probed by *Juno* all have very similar characteristics. Furthermore, the characteristic periodicity of 430 days in the plasma torus reported in Moirano et al. (2021) is somewhat close to the periodicity of Io's Loki Patera volcano as recently published in De Kleer et al. 2019. There is no clear correlation between the volcanism on Io and the response of the plasma torus to the mass transport from the volcanoes into the neutral torus. These questions may be better addressed by theoretical work on the local interaction of Io with its plasma torus, and new observations by *JUICE* that will monitor the level of volcanic activity.

2.4 Magnetospheric Science Enabled by Energetic Neutral Atom Imaging

Energetic neutral atoms (ENAs) are produced from energetic ions charge exchanging with a neutral gas or a plasma, and thus allow us to remotely investigate magnetospheric plasma structures and dynamics, and the interaction within plasma and neutral environments (e.g., atmospheres, exospheres, neutral and plasma tori, and surfaces) (Roelof et al. 1985; Gruntman 1997; Wurz et al. 2000; Futaana et al. 2011; Brandt 2021). When ions are neutralised their original charge state is lost and they propagate along straight trajectories decoupled

from magnetic and electric fields. Conventionally, the energy range of ENAs refers to energies above the gravitational escape energy, so that their trajectories can be considered straight. Therefore, by detecting the direction of ENAs, remote images of the interaction between energetic ions, plasma and neutral gas can be reconstructed. This enables imaging of ion populations responsible for ENA creation (i.e., the plasmas where the neutralisation occurs). Special consideration of gravitationally affected trajectories has to be taken in the circumstances where the ENAs have energies that are close to the gravitational escape, such as those produced in the Io Plasma Torus. ENAs are also produced when energetic ions directly impact a surface, such as the regolith surface of the Moon or the icy surface of Ganymede (Wieser et al. 2009, 2020; Futaana et al. 2012; Pontoni et al. 2022; Szabo et al. 2024). However, this topic falls outside the scope of the present paper. We refer the reader to Tosi et al. (2024, this collection) elsewhere in this special issue for a detailed discussion of this topic.

The only dedicated instrument capable of ENA imaging operated near Jupiter's magnetosphere so far is the Ion and Neutral Camera (INCA) on the *Cassini* spacecraft. During *Cassini*'s Jupiter encounter, high energy ENAs (>30 keV) were imaged by INCA (Krimigis et al. 2002; Mauk et al. 2003, 2004). Publications presenting analyses of these measurements concluded that the ENAs originated from part of the combined Io-Europa tori. Upon arrival at Saturn, INCA on *Cassini* successfully visualised the dynamic plasma environment of Saturn's magnetosphere, capturing impulsive injections, the solar wind influence, and moon-magnetosphere interactions. Combining ENA imaging with *in situ* observations of fields and charged particle led to significant progress in Saturnian magnetospheric science.

In the Jupiter environment, several other instruments have "serendipitously" measured high-energy ENAs. Kirsch et al. (1981) reported the first signal of ENAs from Jupiter due to charge exchange of the magnetospheric ions and neutral tori (Cheng 1980). These measurements were made by examining "background" counts in the Low Energy Charged Particle instrument on *Voyager* 1. More recently, the *Juno* spacecraft's Jupiter Energetic particle Detector Instrument was used to investigate ENAs >50 keV (Mauk et al. 2020b), distinguishing for the first time the ENA emissions coming from Io, Europa, and Jupiter uniquely. On the other hand, no lower-energy (10 eV to keV) ENA measurements have ever been made at the outer planets.

JUICE will be the first Jupiter mission with dedicated ENA imaging capability, part of the PEP instrument (Barabash et al., in preparation, this collection), with the relevant sensors based on the successful cameras flown on *Chandrayaan* (Barabash et al. 2009), *Cassini* (Krimigis et al. 2004) and IMAGE (Mitchell et al. 2000). Global imaging of the magnetosphere in ENAs will be possible, with resolution of ENAs from the Europa neutral and Io plasma tori being particularly valuable for Jupiter magnetospheric science (see Sect. 2.3.1). An example of predicted intensities of Oxygen ENAs based on simulations are shown in Fig. 8. As was the case with *Cassini* at Saturn, we once again expect powerful combinations of ENA imaging and *in situ* measurements made by several *JUICE* instruments.

Many plasma populations interact to accelerate and heat plasma in Jupiter's magnetosphere, with populations and processes including the corotating plasma driven by fast planetary rotation, magnetic reconnection occurring within the associated radially distended magnetic field structure (Krupp et al. 2004b), inward diffusion resulting from interchange instabilities, and wave-particle interactions. ENA imaging, in general, provides the global morphology of these plasma populations and processes operating in the Jovian environment. In particular, ENA imaging with *JUICE* will help us to understand the relationships between small and large-scale plasma injections (Achilleos et al. 2015). *JUICE* will determine the spatial distribution and temporal variability of these injections. Further comparison

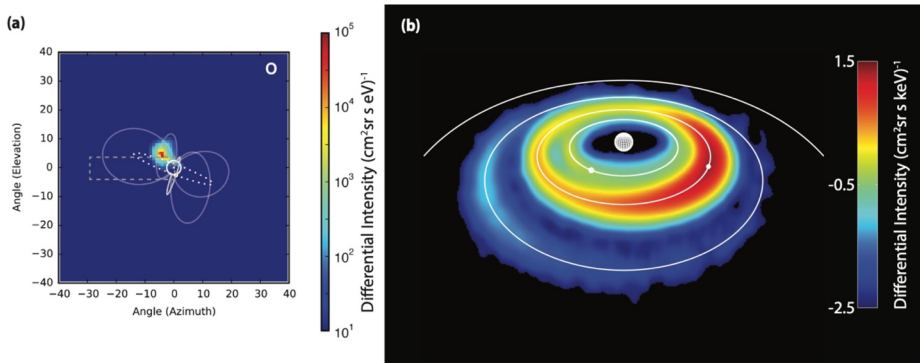


Fig. 8 (a) Simulations of the predicted intensities of Oxygen ENAs originating from charge exchange between the Oxygen plasma and neutrals in the torus peaking around 460 eV due to the corotational velocity of the plasma. Adapted from (Futaana et al. 2015). (b) Simulations of 40 keV hydrogen ENAs predominantly from charge exchange between magnetospheric energetic protons and the H₂ molecules in the Europa neutral torus (Breer et al. 2019)

with *Cassini* in the Saturn system highlights what we expect with *JUICE*, where periodic injection events in Saturn's magnetosphere have been observed in ENA image sequences (Mitchell et al. 2005, 2009; Paranicas et al. 2005; Brandt et al. 2008, 2010) with high correlation with both Saturn Kilometric Radiation and Narrowband Emissions (Wing et al. 2020). At Jupiter, *Galileo* has observed quasiperiodic injection events with a ~ 3 -day period (Krupp et al. 1998; Kronberg et al. 2007) suggesting a direct causal link to the periodicities observed in Jupiter's decametric radio emissions (Louarn et al. 2015). A further area where ENA imaging will play a key role is the response of Jupiter's magnetosphere to changes in the solar wind, particularly the impact of sudden changes in dynamic pressure associated with coronal mass ejections (Kita et al. 2019). Global magnetospheric ion variations caused by such instances will be reflected in ENA imaging data returned by *JUICE*.

ENA imaging will not only be relevant for Io plasma torus but also the equivalent structure associated with Europa, where the two are closely related (see Sect. 2.3). During *Cassini*'s Jupiter flyby, imaging of high energy (>30 keV) ENAs suggested that 50–80 keV ENAs were originating from the Europa's orbit (Krimigis et al. 2002; Mauk et al. 2003). More recently, Mauk et al. (2020b) have reported azimuthally asymmetric, time-variable fluxes of ENAs from the vicinity of both Europa and Io orbit. The two plasma tori, corotating with the Jovian magnetosphere, charge exchange with the neutral tori to produce ENAs that fly approximately on azimuthal trajectories with respect to the planet when created. ENA production is one of the primary loss mechanisms of these magnetospheric ions. *JUICE* will directly quantify the rate of outward transport of Io and Europa tori plasma through ENA imaging. The temporal variations of ENAs sourced from these tori that *JUICE* will observe will be determined by a combination of the fast rotation of Jupiter's magnetosphere, the orbits of the moons, and the spacecraft motion (Futaana et al. 2015). In addition, it will be necessary to account for the drift time of the ENAs (~ 74 km s⁻¹, the corotation speed for Io plasma torus ions), which is affected by the strong Jovian gravity and the Coriolis force. This is a complex operational issue for the operation that will need to be resolved to determine the required pointing (Futaana et al. 2015).

2.5 Magnetospheric Science Enabled by Measuring Low-Frequency Radio Emissions

Similar to Sect. 2.4 on ENA imaging, the expected science gain from *JUICE* measuring low-frequency radio emissions around Jupiter motivates this dedicated section. The ground-based detection of intense, non-thermal, radio emissions from Jupiter at decametric (10–40 MHz) wavelengths in the 1950s, early interpreted as driven in the auroral regions by electron cyclotron motion close to the electron gyrofrequency, provided both the first evidence of the magnetic field of Jupiter and the first estimate of the surface magnetic field of ~ 1.4 mT (Burke and Franklin 1955). The subsequent observation of the Jovian radio spectrum at lower frequencies by space probes such as *Voyager*, *Cassini*, *Ulysses* (flybys) or *Galileo* (in orbit) yielded a detailed characterisation of the macroscopic properties of the decametric, hectometric and broad-band kilometric components (Zarka 1998; Kimura et al. 2008a,b). These are highly circularly polarised, strongly beamed, transient emissions similar to the Auroral Kilometric Radiation (AKR) at Earth, and display a remarkable periodic behaviour that has been used to define the rotational period of both Jupiter and Saturn. AKRs are known to be produced in rarefied and highly magnetised plasma by out-of-equilibrium Electron Distribution Function (EDF) of a few keV through the Cyclotron Maser Instability (Wu and Lee 1979; Treumann 2006), and to be highly correlated with terrestrial substorms (Liou et al. 2000). The emission source mechanism could be validated *in situ* thanks to the traversal of auroral radio sources by the *Juno* polar orbiter in the 2010s, which provided evidence of the prominence of loss cone EDF of a few keV as a source of free energy (e.g., Louarn et al. 2017; Louis et al. 2020; Collett et al. 2023).

The Jovian radio emissions display some remarkable properties and open up a window to understanding large-scale magnetospheric processes at Jupiter with important implications for also astrophysical observations of exoplanets and brown dwarves. The most powerful decametric emissions were early shown to be driven by the Io moon (Bigg 1964), but Europa and Ganymede have also been shown to drive fainter emissions (Louis et al. 2017; Zarka et al. 2018) and can in turn be used to probe the Jupiter/moon electrodynamic interactions. The various radio emissions not induced by moons (Marques et al. 2017) relate to planetary auroral and magnetospheric activity (e.g. Zarka and Kurth 2005), partly controlled by the solar wind (e.g., Gurnett et al. 2002; Hess et al. 2014). Their sources are located along high latitude magnetic field lines at the equatorward edge of the main auroral oval (e.g. Ladreiter et al. 1994; Imai et al. 2019; Louis et al. 2019). The radio beaming pattern is a hollow cone, which opening depends on the local plasma conditions and the cyclotron maser instability. The emission cone is aligned with the local magnetic field, with a large 70 to 80° aperture angle and a few degrees wide (e.g., Imai et al. 2008; Lamy et al. 2022) and likely flattened toward the equator (Galopeau and Boudjada 2016). A radio source is thus visible only to observers geometrically located within the thin conical sheet of the beaming pattern. The Jovian radio emissions have been successfully modelled using the ExPRES (Exoplanetary and Planetary Radio Emission Simulator) code (e.g., Hess et al. 2008; Cecconi et al. 2021; Louis et al. 2021). Within the envelope of the radio emission, fine structures can be observed as individual bursts driven at timescales of milliseconds. They are interpreted as individual electron beams traveling along magnetic field lines (e.g., Hess et al. 2007). The polarization state of the radio waves, which can be elliptical, depending on the hemisphere of origin and the radio emission mode (e.g., Goertz 1974; Lecacheux et al. 1991; Reiner et al. 1993).

Periodic emissions have clearly been observed at Jupiter by *Galileo*/PWS in hectometric and narrowband emissions (Louarn et al. 2007) that are strikingly similar to what has been observed at Saturn in Kilometric and narrowband emissions (Gurnett et al. 2002). With the surprising discovery of the changing period of SKR from *Cassini* (Gurnett et al.

2005) it soon became clear that both SKR and narrowband emissions are associated, and likely ultimately driven by large-scale energetic ion injections similar to terrestrial substorms (Mitchell et al. 2009; Achilleos et al. 2015; Wing et al. 2020). Given the similarity with Jovian emissions, these results imply that analogous processes at Jupiter may be responsible for the periodic emissions at Jupiter. Furthermore, the results open up the intriguing possibility of magnetospheric dynamics at brown dwarves, where auroral and radio periodicities have been observed (Hallinan et al. 2015).

JUICE will be the first orbiter of Jupiter able to fully characterise the Jovian kilometric to decametric radio emissions with goniopolarimetric capabilities (e.g. Cecconi and Zarka 2005; Kimura et al. 2012), based on the *Cassini*/RPWS (Gurnett et al. 2004) heritage but with innovative onboard processing capabilities allowing to better separate radio sources from each hemisphere when they are simultaneously active (Wahlund et al. 2025). *JUICE* will measure the radio wave's flux density, full polarisation state and direction of arrival, improving the *Juno*/Waves wave intensity measurements by a spinning dipole (Kurth et al. 2017). The goniopolarimetric capabilities will also be used to track Ganymede's radio emissions (Kurth et al. 1997), to characterize the ionospheric properties of the Galilean moons, using occultation of the Jovian radio sources (Cecconi et al. 2021). Furthermore, these ambient radio emissions can form the basis of passive radar measurements at these moons (Van Hoolst 2024, this collection).

2.6 The Magnetosphere Upstream of Europa, Ganymede, and Callisto

As introduced in Sect. 1, Jupiter's Galilean moons Europa, Ganymede and Callisto are major targets of the *JUICE* mission. These moons are located in the inner and middle magnetosphere of Jupiter, reviewed in Sect. 2.1, at mean radial distances of 9.4, 15.0, and 26.3 RJ from the planetary centre, respectively. This Section is dedicated to the specific state of Jupiter's magnetosphere upstream of each of these moons, namely, the particle and field environments along their orbital paths. These time-dependent conditions represent boundary conditions for the system immediately around each moon where there is a direct interaction between each moon and the surrounding magnetosphere. Note that Sects. 3.2, 4.2, and 5 all deal with these more local, moon-magnetosphere interactions, where the upstream conditions reviewed here frame each problem.

Because of their locations relative to Jupiter's magnetospheric regions, the main source of upstream plasma at each moon is the innermost moon Io. As we have seen, this means the main cold ion species upstream of all of Europa, Ganymede, and Callisto are O^+ , S^{++} and O^{++} (Bagenal et al. 1994, 2016). Recently, Kim et al. (2020) presented a method to derive the ion properties in Jupiter's plasma sheet by using Jovian Auroral Distributions Experiment Ion sensor (JADE-I) data and applying a ray tracing simulation combined with carbon foil effects. They found that O^+ and S^{++} contribute 62–69% of the iogenic ions and 50–66% of the Jovian magnetospheric ion number density. The authors proposed also that the mean relative abundance for O^+ and S^{++} is 0.37 and that the total oxygen ions to total sulfur ions (O^{n+}/S^{n+}) ratios range between 0.2 and 0.6, which is lower than the values derived from models (e.g. Delamere et al. 2005).

H^+ has also been detected but remains a minor population for particles with energies below ~ 50 keV (Mauk et al. 2004; Bodisch et al. 2017). As well as from Io, H^+ can come from Europa, Ganymede, and Callisto. A recent study by Huscher et al. (2021), focusing on the investigation of Jupiter's plasma disk from 10 to 50 R_J , based on Juno JADE and magnetometer data between March 2017 and April 2020, showed that protons comprise about 10% of the ion density in the center of the disk. In general, the plasma density shows a

considerable small-scale structure (Huscher et al. 2021) that is consistent with the cold blobs features that were seen in the Voyager plasma data (Dougherty et al. 2017). The electron distribution functions measured by *Voyager* show evidence of a thermal bulk population and a suprathermal tail at higher energies. However, the properties of these populations are not well constrained. For example, the obtained hot electron temperature varies from around 300 eV (Bagenal et al. 2016) to 1 keV (Scudder et al. 1981; Sittler and Strobel 1987).

A summary of fields and particle properties upstream of Europa, Ganymede, and Callisto are given in Table 3. Wherever appropriate a range of parameter values is given, in addition to the typical value. This time-dependence of all three upstream environments is especially important when considering each moon-magnetosphere, which will be similarly dynamic as a result. The primary origin of the time-dependence is the oscillation of Jupiter's centrifugal equator back and forth over each moon, resulting in oscillation of the plasma sheet with respect to each moon over a planetary rotation (see Sect. 2.1.2) (Phipps and Bagenal 2021). At all three relevant moons, the cold plasma density has been shown to vary with a factor of ~ 2 , ~ 5 , and ~ 10 , respectively, over a period of ~ 5 h (Kivelson 2004b; Huscher et al. 2021). In addition, the plasma in Jupiter's inner and middle magnetosphere is almost corotating with Jupiter, at azimuthal speeds of ~ 98 , ~ 150 , and ~ 200 km s $^{-1}$ at the orbital distances of Europa, Ganymede, and Callisto. Comparing these values to the moon's orbital speeds of 14, 11, and 8 km s $^{-1}$, respectively, shows that the plasma is overtaking the moons. The upstream plasma is therefore incident on the trailing hemisphere of each moon, and wake phenomena are located ahead of each moon in its orbital motion.

When a magnetized plasma flows past an obstacle, perturbations are excited and propagated through the plasma as waves, therefore it is important to determine the plasma flow speed relative to the speed of plasma waves excited by this local interaction. Indeed, if the upstream flow speed is greater than all wave speeds, then a shock wave will stand just upstream of the obstacle (c.f., the solar wind interacting with Jupiter's magnetosphere, see Sect. 2.1.1). As shown in Table 3, this is not the case for Jupiter's magnetosphere interacting with any of the three moons of interest. In all cases the upstream Alfvén speed is larger than the flow speed, and the same is true of the fast magnetosonic speed (Kivelson 2004b). Such interactions are therefore sub-Alfvénic, implying no need for a shock to form around the obstacle. This has implications for the local moon-magnetosphere interaction that includes the formation of Alfvén wings (see Sects. 3.2, 4.2, and 5).

While the sub-Alfvénic interaction may be typical at all three moons, transient super-fast-magnetosonic conditions may occur, given the extreme variability of the environment. This remains to be confirmed. This atypical scenario that would lead to shock formation is more likely to occur at Callisto (Saur et al. 2013) where the Alfvén speed is somewhat lower than the relative velocity between the moon and the magnetospheric plasma flow, but it could even happen at Europa, where a series of puzzling, shock-like signatures in the magnetic field with unknown origin have been previously detected (Jia et al. 2018).

The upstream environments of Europa, Ganymede, and Callisto also include energetic charged particles with energies ranging from a few keV/nucleon and well into the relativistic energy range (see Sect. 2.1.3). For these energies we currently lack detailed descriptions of each moon environment that would complement our understanding of lower energy particle conditions. However, radiation environment models or investigations of past flyby observations can be used to extract relevant parameters (e.g., Paranicas et al. 1999; Cooper 2001; Mauk et al. 2004; Sicard et al. 2004; Garrett et al. 2016; Paranicas et al. 2021), as discussed by Galli et al. (2022).

Common features of the energetic particle environment upstream of each moon are injection events that typically last several minutes and concern particles in the tens of keV to low

Table 3 Overview of magnetised plasma conditions upstream of Europa, Ganymede, and Callisto (Uncited row values can be derived from other rows)

Parameter (unit)	Europa (9.4 R_J)	Ganymede (15 R_J)	Callisto (26.3 R_J)
Cold electron density, n_e (cm^{-3})	⁶ 158 (63-290)	¹ 2 (0.6 - 2)	^{1,2} 0.2 (0.1-1.0)
Cold electron temperature, T_e (eV)	⁶ 20 (10-30)	⁷ 60 (30-60)	^{2,9} 100
Hot electron density, $n_{e,h}$ (cm^{-3})	⁶ 7.9 (3-16) or ^{11,7} 0.5 (0.1-3)	⁷ $\sim 0.1 n_e$ or ^{11,7} 0.5 (0.1-3)	^{11,7} 0.5 (0.1-3)
Hot electron temperature, $T_{e,h}$ (eV)	⁶ 300 (200-1200) or ^{11,7} $1e3$ (600-1200)	⁵ 300 or ^{11,7} $1e3$ (600-1200)	^{11,7} 1000 (600-1200)
Cold ion density, n_i (cm^{-3})	⁶ 158 (63-290) or ¹³ 30-200	² 0.8 (0.5 - 1.2) (H^+), 4 (1.7-6) (heavy)	⁶ 0.10 (0.01-0.5)
Cold ion temperature, T_i (eV)	⁶ 88 (48-340) or ¹ 139 (20-500) or ¹³ 30-600	² 100 (50-110) (H^+), 60 (20-100) (heavy)	^{1,2,9} 200 (100-500)
Heavy Ion, A/Z	⁵ 18.5/1.5 or ⁶ 18	^{2,3} 15.7 (15.6-15.8) or ⁸ 14	⁹ 15
Dominant ion species	⁶ $\sim 30\%$ O^+ , $\sim 13\%$ S^{++} , $\sim 7\%$ O^{++}	⁸ O^+ , S^{++}	¹² O^+
Magnetic field strength, B (nT)	⁶ 450 (423-480)	⁴ 95 (70-120)	^{5,9} 35 (4-42)
Ion thermal pressure, $P_{i,th}$ (nPa)	⁶ 2.4 (2.2-3.9)	0.05 (0.001-0.12)	0.003 (0.0002 - 0.04))
Energetic ion pressure, $P_{i,ener}$ (nPa)	⁵ 12	⁵ 3.6	⁵ 0.37
< 1 MeV ion charge states, Q (Q, R[Q])	¹⁰ Oxygen (Q= 1, 1 Q 4); Sulfur (Q= 2, 1 Q 5)		
(Cold & Hot) Electron pressure, P_e (nPa)	⁵ 3.2	0.02 (0.006 - 0.02)	0.02 (0.02 - 0.03)
Magnetic pressure, P_B (nPa)	80 (71-92)	3.6 (1.9-5.7)	0.5 (0.006-0.7)
Plasma β	0.039 (0.03-0.04)	1 (0.5-1.5)	1.3 (0.02 - 1.9)
Azimuthal plasma speed, v (km/s)	⁶ 98 (76-123)	^{2,5} 150 (130 - 170)	⁵ 200
Orbital speed, v_s (km/s)	⁵ 14	⁵ 11	⁵ 8
Alfvén speed, v_A (km/s)	⁶ 220 (153-372)	260 (156-504)	624 (32 - 2370)
Sound speed, C_S (km/s)	⁵ 92 (76-330)	240 (194-372)	511 (228 - 1640)
Ram pressure, P_{ram} (nPa)	⁵ 24 (38)	1.2 (0.4-2.3)	0.05 (0.005-0.25)

¹Bagenal and Delamere (2011) ²Dougherty et al. (2017), Bodisch et al. (2017) ³Kim et al. (2020) ⁴Connerney et al. (2018, 2020) ⁵Kivelson (2004b) ⁶Bagenal et al. (2015) ⁷Sittler and Strobel (1987) ⁸Jia and Kivelson (2021) ⁹Neubauer (1998) ¹⁰Geiss et al. (1992), Clark et al. (2016, 2020), Allen et al. (2019), ¹¹Scudder et al. (1981), ¹²Liuzzo et al. (2015), ¹³Satoh et al. (2024)

MeV range (Clark et al. 2016). During these events the suprathermal ion and electron fluxes increase significantly. How the cold plasma and magnetic fields behave during the events is not well established, but based on observations of similar events in Saturn's magnetosphere

(e.g. André et al. 2005), we may expect to see significant changes in plasma density, temperature and the magnetic field. Note that at Jupiter we expect a much lower injection rate at Callisto, compared to Europa and Ganymede (Mauk et al. 1999; Dumont et al. 2014). Extreme (but rare) radiation belt transients, with the most prominent one recorded in *Galileo*'s C22 at the orbit of Ganymede (Roussos et al. 2018; Hao et al. 2020), have also been observed. Regarding the energetic ion composition, protons, sulphur and oxygen are the most abundant species at all three moons (Mauk et al. 2004), with the relative abundance differing with the moon in question, energy and possibly also magnetic latitude. Towards the highest energies ($\gg 1$ MeV/nucleon), energetic carbon ions of solar origin are also a significant component of the heavy ion spectrum, particularly at Callisto (Cohen et al. 2001).

JUICE will explore the Jovian magnetosphere upstream of Europa, Ganymede, and Callisto, particularly comprehensively in the case of the latter two moons (see Figs. 2 and 3). As indicated by the above review of present understanding, past exploration leaves many important gaps to be filled, and the *JUICE* mission is well-positioned to close many of these. A more complete picture of each upstream magnetised plasma environment is needed, which must include constraint on the significant levels of variability if we are to understand the more local interaction between Jupiter's magnetosphere and each moon of interest. This is central to determining sputter rates from moon surfaces (see the discussion in Plainaki et al. 2020) and establishing local plasma mass budgets that will have implications for the global magnetosphere, for example. In particular, cold electron properties are poorly defined, especially below 100 eV. *JUICE* will shed light on the cold upstream plasma populations, both electrons and ions down to as low as ~ 1 eV, as well as up to relativistic energies. An indication of the problems resulting from incomplete current knowledge include the large ranges in estimated exospheric densities of each moon (Plainaki et al. 2018) (Tosi et al. 2024, this collection).

Of all three moons, Callisto's upstream conditions are particularly unclear, and so this is an area where particularly significant progress is expected thanks to *JUICE*. Callisto orbits in a location where the magnetosphere begins to transition to a thin magnetodisk-dominated configuration. This configuration means that Callisto's excursions in magnetic latitude as Jupiter rotates expose the moon to very diverse plasma environments. When Callisto's magnetic latitude maximises, field lines crossing the moon have their current-sheet centre foot-point as far as 40–60 R_J (see Fig. 3), and the current sheet thickness may be sensitive to solar wind dynamic pressure, particularly at dawn (Xu et al. 2023). This range depends on the magnetic field model used and the properties of the current sheet which may also change significantly (Vogt et al. 2019). Note that even magnetospheric plasma velocities are more uncertain, ranging from near-rigid corotation with Jupiter based on thermal plasma measurements (Bagenal et al. 2016) to much lower velocities from energetic particle data (Waldrop et al. 2015). *Juno* observations have recently improved the quality of plasma observations at Callisto's orbit (Kim et al. 2020; Huscher et al. 2021). However, the present description of Callisto's environment from a limited number of encounters may be far from being representative, leading to the need for more comprehensive observation by *JUICE*.

3 Magnetised Plasma Environment Around Europa

This section concerns the local interaction between Europa and the surrounding magnetosphere of Jupiter. Important context is provided in Sect. 2.6, which reviews the state of the magnetosphere at Europa's orbit. While in orbit around Jupiter, *JUICE* will make two close flybys of Europa, where "close" can be loosely defined as closest approach distance within

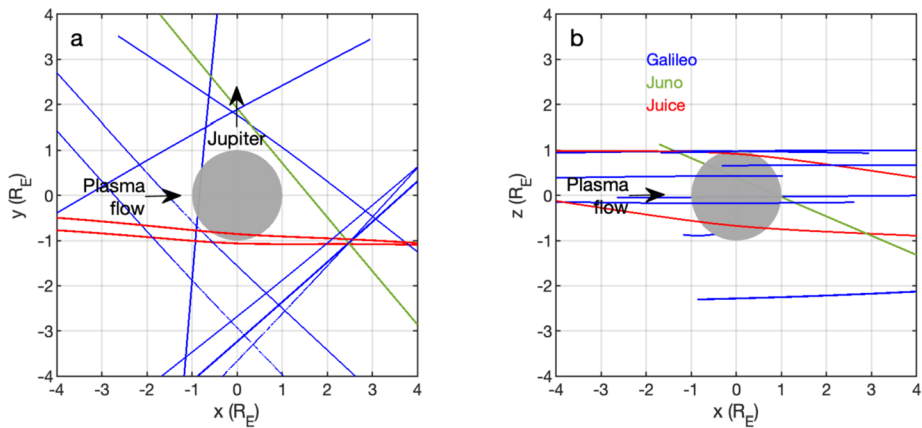


Fig. 9 Trajectories of all spacecraft flybys of Europa to date, and the predicted trajectories during the two planned flybys by JUICE. (a) Trajectories projected onto the xy plane. (b) Trajectories projected onto the xz plane. Both panels use the EphO coordinate system, Europa is shown as a grey circle, and trajectories are only shown in the $\pm 4 R_E$ range for all three spatial coordinates. Past Galileo spacecraft flybys are shown in blue, and the more recent Juno spacecraft flyby is shown in green. Future JUICE flybys are shown in red

a few Europa radii of the moon's barycentre. In this section we use spatial units of both Europa radii (R_E ; $1 R_E = 1561$ km) and km, and we often use the Europa Phi Orbital (EphO) coordinate system. The origin of this system is co-located with Europa's barycentre, the x-axis in the direction of the incident flow of Jovian magnetospheric plasma that is qualitatively co-rotating with the planet, the y-axis points towards Jupiter's barycentre, and the z-axis completes the right-handed Cartesian set.

Figure 9 shows close encounters with Europa made by the *Galileo* and *Juno* spacecraft in the past, and also the two future encounters that will be made by *JUICE*. Closest approach during the two *JUICE* flybys will be on the anti-Jupiter side of Europa, one just below (southern hemisphere) and one just above (northern hemisphere) Europa's orbital plane. For more detailed information on the flyby trajectories and their design, we refer the reader to Boutonnet et al. (in preparation, this collection).

Referring to the *JUICE* investigations presented in Table 1, this section concerns the investigation stemming from the mission objective “Explore Europa's recently active zones”, as well as the investigation MC.2 stemming from the mission objective “Characterise the Jovian magnetosphere”. Note that while Europa's exosphere is partly covered here, this topic primarily falls within the scope of Tosi et al. (2024, this collection).

How JUICE will advance knowledge in this area: As shown in Fig. 9, due to the small number of Europa flybys to date, *JUICE*'s two flybys will significantly improve sampling of the near-Europa space environment. Specifically, we will measure the environment relatively close to Europa on the anti-Jupiter side, at both high and low latitudes, as well as during passes through the extended upstream and downstream regions. *JUICE*'s fields-and-particles measurement capabilities are considerably greater than those of the past *Galileo* spacecraft, which made most of the flybys to date. Measurements around times of closest approach to Europa will sample the moon ionosphere at new combinations of angles to the upstream flow and sunward directions. The following sections present more detail on *JUICE*'s contribution in this area.

3.1 Europa's Ionosphere

This section concerns Europa's ionosphere, the ionised constituent of Europa's atmosphere. This layer around the moon interacts with the surrounding magnetosphere, and so understanding its properties is central to understanding the interaction itself. Electron impact ionisation and photoionisation of Europa's neutral atmospheric gases lead to the formation of an ionosphere. The characteristics of such an ionosphere (e.g. densities, distribution and composition) depend primarily on the plasma flow in its vicinity and the underlying neutral atmosphere. For a review of Europa's neutral atmosphere, we refer the reader to Tosi et al (2024, this collection).

Of the two ionization processes, impact ionization of O_2^+ due to magnetospheric electrons is found to be dominant with a rate of $\sim 10^{-6} \text{ s}^{-1}$ (Saur et al. 1998; Schilling et al. 2008; Rubin et al. 2015). Data-driven updates have been derived from *Juno*'s recent flyby, where intense electron beams were discovered (Allegrini et al. 2024) that can drive the impact ionization rate up to $\sim 10^{-5} \text{ s}^{-1}$ for O_2^+ in some locations (Szalay et al. 2024a). Additionally, Carberry Mogan et al. (2023) provided comprehensive model estimates for reaction rates at all the icy satellites. The electrons from the surrounding magnetospheric plasma are diverted by the electrodynamic interaction of the moon (see Sect. 3.2). A fraction, on the order of a few tens of percent of the upstream electrons, are convected into the atmosphere. In the atmosphere, the electrons are cooled through inelastic electron-neutral collisions, losing energy from upstream to downstream. The characteristics of these electron convection and cooling patterns determines the distribution and efficiency of impact ionisation. Electron-neutral collisions also lead to the generation of far-UV neutral oxygen emissions, which have been regularly imaged by the *HST* (McGrath et al. 2009; Roth et al. 2016). The observed emission patterns undergo periodic variations connected to the periodically changing plasma conditions and the emission topology and variations might be reflected in the ionosphere in a similar way.

The O_2^+ photoionisation rate is estimated to be a few 10^{-8} s^{-1} (Saur et al. 1998) and thus at least an order of magnitude lower. However, photoionisation might be an important source on the sunlit side, in the case of weak electron impact ionisation such as in the near-surface wake regions where electrons might have cooled significantly due to the interaction with the surface, or when the ambient magnetospheric plasma density is particularly low.

Controlled by the plasma velocity field, ionospheric particles are convected downstream and eventually accelerated to co-rotation speeds. This creates a narrow plasma wake as observed during the *Galileo* flyby E4 behind the moon. Recombination plays a minor role for the ionospheric loss, except in the region of the highest ionosphere densities (Saur et al. 1998; Rubin et al. 2015).

As O_2 is likely the dominant species in the global atmosphere, O_2^+ would be expected to be the dominant ion (Rubin et al. 2015; Dols et al. 2016). It's noteworthy that O_2^+ was directly measured in-situ by *Juno*, but was not found to be the dominant ion as many of the other charge states of O and S were also present at significant quantities (Szalay et al. 2024a). While the sputter-induced O_2 atmosphere is expected to be global (with some potential variations in density), asymmetries and inhomogeneities in the neutral environment might originate from plumes (Roth et al. 2014a; Blöcker et al. 2016; Jia et al. 2018; Vorburger and Wurz 2021) or a sublimated dayside H_2O atmosphere (Roth 2021; de Kleer et al. 2023). A localised plume-ionosphere was suggested to be present during the *Galileo* flyby E12 leading to a sharp peak in electron density as derived from wave measurements near the closest approach (Jia et al. 2018). Such contributions would also change the ionosphere composition with H_2O^+ possibly being the dominant ion near the subsolar point and in plume regions.

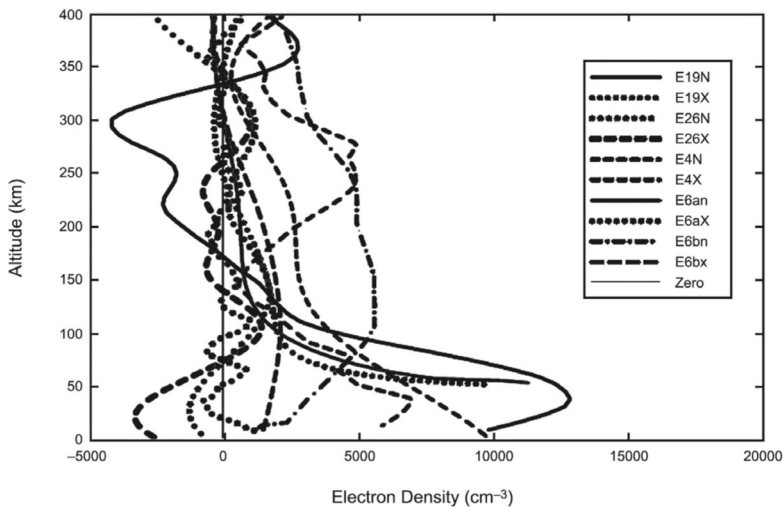


Fig. 10 Electron densities derived from Galileo radio occultation and near-occultation observations indicate a variable ionosphere at Europa (from McGrath et al. 2009)

Ionospheric electron signatures were observed during seven radio occultation measurements by the *Galileo* spacecraft (6 clear detection, 1 weak detection, see Fig. 10) and one from *Juno* (Parisi et al. 2023). Some measurements suggested peak electron densities above $\sim 10^4 \text{ cm}^{-3}$, while no ionosphere was detectable during 3 individual measurements (Kliore et al. 1997; McGrath et al. 2009). The results suggest a temporally and spatially variable ionosphere as expected from simulations. *Galileo* plasma instruments have not confirmed the electron densities derived from radio occultations (Paterson et al. 1999). A more detailed discussion of the ionosphere measurements can be found in McGrath et al. (2009). Recently, electron densities were directly measured in Europa's vicinity from *Juno*'s Waves instrument onboard *Juno* (Kurth et al. 2023; see also Sect. 2.3.2).

The presence of an ionosphere at Europa is therefore well established, and previous results indicate that it might undergo changes related to Europa's orbital period (84 hours) as well as the synodic period of the magnetospheric environment (11 hours). In addition, the ionosphere might be highly asymmetric and inhomogeneous, as it is affected by the electron flow pattern and the possibly inhomogeneous atmosphere (Oza et al. 2019; Addison et al. 2024). Three types of atmospheric observations suggest the existence of plumes at Europa's surface. Two of them used the *HST*: UV emission from the dissociation products of water (Roth et al. 2014a) and absorption by plume material imaged when Europa transited Jupiter (Sparks et al. 2017). The third type of observations was electromagnetic perturbations induced by the plume density. Indeed, *Galileo* flybys E12 and E26, whose closest approach was within 400 km, show fine structures in the magnetic field perturbations. Comparisons with an MHD model (Blöcker et al. 2016; Jia et al. 2018) and a Hybrid model (Arnold et al. 2019) show that the presence of a plume is required to explain the fine structures. In addition to field disruption, these active processes can form an additional source of neutrals and locally increase plasma density, which can locally increase the aurora brightness (Roth et al. 2014b) and cause ENA emissions (Huybrighs et al. 2020, 2021; Jia et al. 2021). If present, local plumes might lead to significant transient changes in the ionospheric density and composition (McGrath and Sparks 2017).

Europa ionosphere questions to be addressed by *JUICE* include:

- How is the three-dimensional distribution of ionospheric densities and composition changing with solar, magnetospheric, and orbital conditions?
- How does the ionosphere vary due to active processes on Europa's surface, such as sputtering or potential plumes?
- How is the ionosphere convected downstream?
- What is the fraction of dust in the ionosphere?
- How does the ionosphere influence the moon-magnetosphere interaction and thereby other measurements to determine Europa's ocean or plumes?

Measurements of plasma distributions, magnetic field, plasma waves, radio waves, and radio occultations will all be important tools that *JUICE* will use to further our understanding. Furthermore, dust impact monitoring will be possible (Wahlund et al. 2025). In situ measurements will be focused on the two Europa flybys and particularly in the period around the closest approach. Both flybys have closest approach altitudes of ~ 400 km above the surface (see Fig. 9), and so *in situ* measurements by *JUICE* will probe the uppermost ionosphere regions. Searching for evidence of plume activity will be a key consideration when the returned data are analysed. *JUICE* will measure charged particles spanning several orders of magnitude, from eV to MeV, which is expected to significantly push forward the state of the art. Data sets will be combined to identify ionospheric boundaries and place constraints on how electrically conductive the environment is, including insight into electrical currents flowing in the plasma. Magnetic field measurements will be particularly useful in studying the expected electric current closure. Global simulation will provide essential context for understanding the structure and dynamics of Europa's ionosphere.

JUICE will make radio occultation measurements of Europa's ionosphere, which are currently lacking. These will be made during both spacecraft ingress and egress. The transverse velocity of *JUICE* with respect to Europa during the radio occultations will be about 10 km s^{-1} . With this high velocity we can get a sensitivity for the electron density of $\sim 350 (1-\sigma) \text{ cm}^{-3}$, with an altitude resolution of ~ 10 km (Withers 2020). A better spatial resolution can be obtained at the cost of worsening the electron density resolution (less et al. 2025, this collection). These measurements will provide line-of-sight integrated profiles of electron column densities as a function of altitude, providing a wider picture of the ionosphere. Inversion of these profiles to retrieve number densities of electrons around the moon relies on assumptions for their spatial distribution. Another remote sensing context will be provided by ultraviolet observations of electron-excited auroral emissions from the global atmosphere. Emission line ratio diagnostics for atomic oxygen and other emissions are related to both electron density and temperature. Therefore, constraining the energy distributions in combination with other *in situ* measurements along the spacecraft trajectory will enable mapping of ionospheric bulk density enhancements globally at the time of each flyby. Note that neutral particle measurements surrounding each flyby will also provide important context (Tosi et al. 2024, this collection).

3.2 Moon-Magnetosphere Interaction at Europa

As introduced in Sect. 2, Europa is located in Jupiter's inner magnetosphere. Here, the moon interacts with magnetospheric plasma and fields, acting as both a source and sink of (neutral and charged) particles while also being connected to Jupiter's auroral region through magnetic field lines that are in contact with the moon. Furthermore, a dipole magnetic field is induced within Europa by the time-varying component of Jupiter's magnetic field resulting from the 10° tilt of the Jovian dipole with respect to the planet's rotational axis (see Van Hoolst 2024, this collection).

Europa is a body embedded in a sub-magnetosonic and sub-Alfvénic plasma flow, therefore no bow shock is present in front of the moon (see Sect. 2.6). The flow overtakes Europa with a speed of $\sim 100 \text{ km s}^{-1}$ from the trailing side. The co-rotating plasma flow is deflected around Europa, through electromagnetic interaction with Europa's ionosphere and collisions with the tenuous atmosphere. The regions near Europa where the plasma flow is perturbed, are associated with perturbations in the electromagnetic field. In front of Europa where the plasma flow is slowed down, magnetic pile-up occurs. The relative speed between the slowed-down plasma in front of Europa and the undisturbed corotating plasma results in a 'bend back' of the magnetic field. The two cylindrical regions of bend-back, extending north and south of Europa are referred to as Alfvén wings (Neubauer 1980; Goertz 1980; Kivelson et al. 2009). The characteristics of the interaction outlined in this paragraph and illustrated in Fig. 11 are strongly variable because they depend on variable magnetospheric conditions as well as variations in the particle and field environment local to Europa (Saur et al. 1998; Kabin et al. 1999; Schilling et al. 2007; Rubin et al. 2015; Blöcker et al. 2016; Dols et al. 2016; Jia et al. 2018; Arnold et al. 2019; Harris et al. 2021, 2022; Cervantes and Saur 2022; Addison et al. 2024).

Perturbations in the fields are mediated by waves; specifically, Alfvén waves carry the perturbations generated near Europa away along the Alfvén wings. The field configuration near Europa is further complicated by Europa's induced dipole, assumed to be related to the conductive subsurface ocean (Khurana et al. 1998; Neubauer 1999; Schilling et al. 2007; Van Hoolst 2024, in preparation, this collection), which shifts and shrinks the Alfvén wings, for example (Neubauer 1999; Volwerk et al. 2007). Currents flow in regions of perturbed fields, such as currents associated with the Alfvén wings or with the "J cross B" forces that contribute to the magnetic pile-up (Kivelson et al. 2009).

Perturbed fields near Europa, due to factors such as magnetic pile up, atmospheric inhomogeneities and the induced dipole, affect the motion and precipitation of thermal and energetic plasma near Europa (Paranicas et al. 2000; Breer et al. 2019; Huybrighs et al. 2023). Downstream of Europa the wake region is found. In this region deflected fields, electromagnetic waves and energetic particle depletions have been detected (Volwerk et al. 2001; Kivelson et al. 2009; Allegrini et al. 2024).

Europa acts as a source of charged and neutral particles, and has an ionosphere, as introduced in the preceding section. Beyond the ionosphere, pick-up ions around Europa have been detected by *Galileo* using past wave and ion particle measurements (Paterson et al. 1999; Volwerk et al. 2001). Besides positive ions, negative Cl⁻ ions have also been inferred, possibly originating from the subsurface salty ocean (Desai et al. 2017). More recently Juno confirmed the presence of H₂⁺ and O₂⁺ pickup ions in Europa's wake (Szalay et al. 2024a). Furthermore, Intriligator and Miller (1982), Russell et al. (1998), and Eviatar and Paranicas (2005) suggest that Europa is trailed by a plume of plasma. Plasma impinging on Europa's surface is expected to sputter neutrals from the surface (Johnson 2004; Cassidy et al. 2013; Plainaki et al. 2013, 2018; Breer et al. 2019; Addison et al. 2022), sustaining a neutral torus (see Sect. 2.3.2).

Europa also acts as a sink of particles. Plasma and energetic particles precipitate on Europa's surface, where the precipitation depends on the field configuration and variation near Europa (Saur et al. 1998; Paranicas et al. 2000, 2001, 2007; Addison et al. 2021; Davis et al. 2021; Harris et al. 2021, 2022; Nordheim et al. 2022). Furthermore, energetic ions are depleted by atmospheric charge exchange with Europa's atmosphere, plumes and torus (Lagg et al. 2003; Kollmann et al. 2016; Nénon and André 2019; Huybrighs et al. 2020, 2021; Jia et al. 2021). Also, due to finite Larmor radii, the newly created pick-up ions on the sub-Jovian side can be lost to the moon's surface, which is especially visible during the E15 flyby of Europa by the *Galileo* spacecraft (Kivelson et al. 2009).

Europa's potential water plumes are expected to form an additional source of neutrals and plasma, perturb the fields (Blöcker et al. 2016; Jia et al. 2018; Arnold et al. 2019), produce a UV emission surplus (Roth et al. 2014a), cause energetic particle dropouts and ENA emissions (Huybrighs et al. 2020, 2021; Jia et al. 2021) and cause upper hybrid resonance (UHR) emissions (Jia et al. 2018). Putative plume sources are scattered across the surface of Europa, but are mostly located on the southern hemisphere (Roth et al. 2014a; Sparks et al. 2016, 2017; Jia et al. 2018; Arnold et al. 2019; Paganini et al. 2020). Finally, Europa is coupled to the wider magnetosphere. For example, by contributing water-group pickup ions to the magnetosphere and modifying the plasma sheet composition (Szalay et al. 2022, 2024b). Furthermore, perturbed field lines near Europa (the Alfvén wings) are connected to Jupiter's auroral zone where an auroral footprint of Europa is observed (Clarke et al. 1998, 2002; Grodent et al. 2006; Allegrini et al. 2020).

While our understanding of the magnetospheric interaction of Europa has expanded over the past three decades, many unknowns remain, stemming from limitations of the Earth-based remote sensing observations and of the limited temporal and spatial resolution, as well as mass separation, of in-situ data returned by the *Galileo* mission. In particular, in-situ measurements of Europa's tenuous atmosphere and the low energy (<10 eV) component of the ionosphere using particle detector instruments will be provided by *JUICE* for the first time. Thereby key parameters in our understanding of the moon-magnetosphere interaction such as the mass, spatial and temporal distribution of the particles are left uncertain. With its expansive suite of magnetospheric instruments, consisting of particle detectors for electrons, positive and negative ions, neutrals and ENAs, magnetometer, wave instruments and UV detector, *JUICE* will be able to constrain the magnetospheric interaction at Europa in unprecedented detail. Of these, direct measurement capability of neutrals and ENAs have not featured in past missions.

JUICE will address questions such as:

- How does the magnetospheric interaction affect the particles, fields, waves and currents at Europa?
- What is the contribution of Europa as a source and sink to the particle population in Jupiter's magnetosphere?
- How does magnetospheric interaction vary over time?
- What is the effect of active processes, such as sputtering or the potential water plumes on the magnetospheric interaction?
- What can the magnetospheric interaction tell us about our knowledge of the subsurface ocean?

JUICE is scheduled to make two flybys of Europa, one nearer the southern hemisphere, one nearer the northern hemisphere (see Fig. 9). The flybys will pass from upstream to downstream and thereby also provide a unique opportunity to characterize Europa's wake. Figure 11 also provides a visual overview of the measurements that *JUICE* will make in order to address the above questions.

Fields and particle measurements made during the flybys will determine the composition of the neutral and ionized environment around Europa, including potential plumes (Huybrighs et al. 2017; Winterhalder and Huybrighs 2022; Dayton-Oxland et al. 2023). It will also be possible to monitor micrometre dust impacts on the spacecraft. We will be able to locate magnetic field and plasma boundaries and reveal the temperature and bulk velocity of different plasma populations with a high enough time resolution to investigate temporal changes in the magnetospheric interaction. *JUICE* will detect particles precipitating onto the surface, as well as those sputtered and reflected. An important contribution will be the anticipated monitoring of the dispersive Alfvén waves and related wave activity in the Alfvén

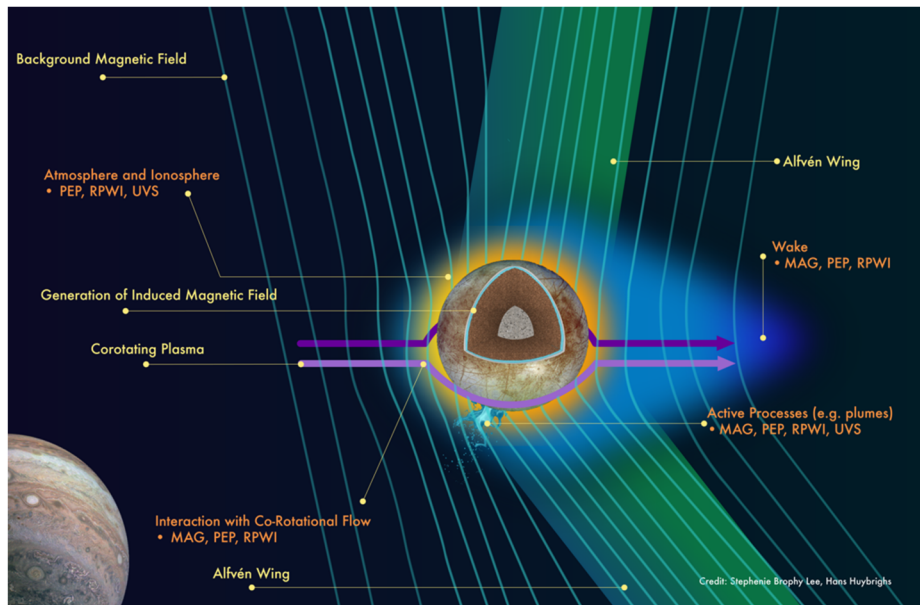


Fig. 11 Schematic illustrating Europa's interaction with the surrounding Jovian magnetosphere, and the areas where specified JUICE measurements will enable progress. Credit: Stephanie Brophy Lee, Hans Huybrighs

wings or interaction boundaries between Europa's cold ionospheric plasma and the hotter streaming magnetosphere plasma.

Furthermore, remote sensing of ultraviolet emissions will provide global maps of atomic oxygen emissions, which are to a large fraction excited by electrons from Jupiter's magnetosphere and by newly created ionospheric electrons. The emission distribution is primarily determined by the distribution of the electrons around the moon, revealing the electron flow patterns and indirectly the topology of the guiding magnetic field and its perturbations. Monitoring of UV emissions from the global O_2 atmosphere will provide a diagnostic for where magnetospheric electrons interact with the neutrals and surface. At the same time, such observations will provide important constraints for the O_2 atmosphere models proposed so far (e.g., Cervantes and Saur 2022; Plainaki et al. 2013, 2018). Observations of the aurora could potentially also be used to characterise the subsurface ocean analogous to studies at Ganymede (Saur et al. 2015; Van Hoolst 2024, this collection).

4 Magnetised Plasma Environment Around Callisto

This section concerns the local interaction between Callisto and the surrounding magnetosphere of Jupiter. Important context is provided in Sect. 2.6, which reviews the state of the magnetosphere at Callisto's orbit. While in orbit around Jupiter, *JUICE* will make 21 close flybys of Callisto, where "close" can be loosely defined as closest approach distance within a few Callisto radii of the moon's barycentre. In this section we use spatial units of both Callisto radii (R_C ; $1 R_C = 2410$ km) and km, and we often use the Callisto Phi Orbital (CphiO) coordinate system. The origin of this system is co-located with Callisto's barycentre, the

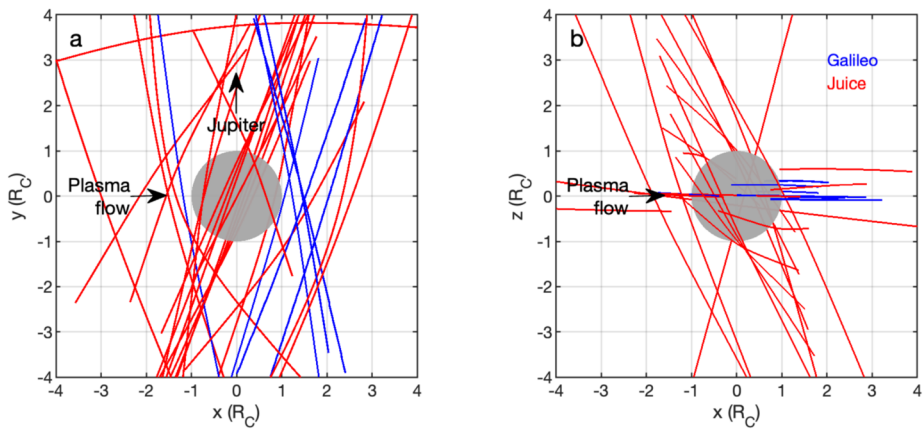


Fig. 12 Trajectories of all spacecraft flybys of Callisto to date, and the predicted trajectories during the future flybys by JUICE. (a) Trajectories projected onto the xy plane. (b) Trajectories projected onto the xz plane. Both panels use the CphiO coordinate system, Callisto is shown as a grey circle, and trajectories are only shown in the $\pm 4 R_E$ range for all three spatial coordinates. Past Galileo spacecraft flybys are shown in blue. Future JUICE flybys are shown in red

x-axis in the direction of the incident flow of Jovian magnetospheric plasma that is qualitatively co-rotating with the planet (i.e., pointing in the direction of Callisto’s orbital motion), the y-axis points towards Jupiter’s barycentre, and the z-axis completed the right-handed Cartesian set.

Figure 12 shows close encounters with Callisto made by the *Galileo* spacecraft in the past, and also the future encounters that will be made by *JUICE*. Closest approach positions across all the *JUICE* flybys will cover all major locations: upstream, downstream, the Jupiter side, and the anti-Jupiter side, and measurements during these flybys will provide coverage over a region that extends well above and well below Callisto’s orbital plane. For more detailed information on the flyby trajectories and their design, we refer the reader to Boutonnet et al. (2024, this collection).

Referring to the *JUICE* investigations presented in Table 1, this section concerns the investigation stemming from the mission objective “Study Callisto as a remnant of the early Jovian system”, as well as the investigation MC.2 stemming from the mission objective “Characterise the Jovian magnetosphere”. Note that while Callisto’s exosphere is partly covered here, this topic primarily falls within the scope of Tosi et al. (2024, this collection).

How JUICE will advance knowledge in this area: As shown in Fig. 11, *JUICE* will dramatically increase the number of close Callisto flybys with respect to the baseline provided by the past *Galileo* mission. The *JUICE* flybys will lead to comprehensive coverage of near-Callisto space in latitude, upstream-to-downstream angle, solar zenith angle, and altitude. In addition, the number and timing of flybys mean we will observe the environment at a range of Jupiter longitudes, and we will therefore sample the system under different upstream plasma states. *JUICE*’s fields-and-particles measurement capabilities are considerably greater than those of the past *Galileo* spacecraft. The following sections present more detail on *JUICE*’s contribution in this area.

4.1 Callisto's Ionosphere

This section concerns Callisto's ionosphere, the ionised constituent of Callisto's atmosphere. This layer around the moon interacts with the surrounding magnetosphere, and so understanding its properties is central to understanding the interaction itself. For a review of Callisto's neutral atmosphere, we refer the reader to Tosi et al. (2024, this collection). Similar to Europa, an ionosphere with peak densities of $\sim 10^4 \text{ cm}^{-3}$ was derived at Callisto from *Galileo* radio occultation measurements (Kliore et al. 2002), before a substantial O_2 atmosphere was detected (Cunningham et al. 2015). Detectable electron densities could be obtained during six of the eight *Galileo* opportunities, see Fig. 13. The derived densities indicate both spatial and temporal variability in the ionosphere. A substantial ionosphere was observed only when the trailing side of Callisto was sunlit, where trailing is with respect to the direction of the moon's orbital motion, i.e., where the co-rotating plasma hit the surface. *Galileo* did not observe substantial ionosphere signals when the leading side was sunlit during the C9 flyby.

Both generation processes considered for Europa – electron impact ionisation and photoionisation – can in principle contribute to ionosphere formation at Callisto (Kliore et al. 2002) but the details of the interaction suggest different roles. Callisto's neutral atmosphere is also exposed to a fast flow of magnetospheric plasma. The strength of the ambient Jovian magnetic field is, however, about two orders of magnitude lower at Callisto compared to Europa (Kivelson 2004b) leading to much higher ionospheric electric conductivity (Strobel et al. 2002). The strongly short-circuited motion electric field at these high conductivity leads to effective shielding such that $<1\%$ of the magnetospheric plasma reaches Callisto's near-surface atmosphere. Impact by magnetospheric electrons is therefore expected to be negligible compared to photoionisation. Liuzzo et al. (2019) modelled the dynamics of energetic magnetospheric electrons exposed to the highly perturbed and asymmetric plasma environment of Callisto and found that the moon's Jupiter-facing and Jupiter-averted hemispheres are partially shielded from energetic electron precipitation. Consequently, the ionisation of Callisto's atmosphere is expected to be inhomogeneous.

As the composition and density of the neutral atmosphere are only loosely constrained, the composition of the ionosphere is basically unknown. The initially detected CO_2 in the atmosphere is too dilute and likely plays a minor role for the ionosphere (Kliore et al. 2002). If the atmosphere is dominated by O_2 globally, O_2^+ will be the major ion (Liuzzo et al. 2015). A possible H_2O atmosphere on the dayside (Vorburger et al. 2015; Hartkorn et al. 2017; Carnielli et al. 2020a,b) might produce a local H_2O^+ dominated ionosphere.

Similar to the main ionisation process, the process for generating the faint atmospheric far-UV oxygen emission observed by the *HST* (Cunningham et al. 2015) is suggested to be photo-electron excitation rather than excitation by magnetospheric electrons (Hartkorn et al. 2017). However, recently optical oxygen aurora was detected when Callisto was eclipsed by Jupiter, which cannot be excited by photoelectrons, but likely by magnetospheric electrons (de Kleer et al. 2023). A scenario that can explain the variable ionospheric profiles found by *Galileo* and the auroral emission intensities might be a day-night asymmetry (Hartkorn et al. 2017) and possibly transient changes in eclipse in the atmosphere.

Galileo wave measurements revealed enhanced electron densities (about two orders of magnitude larger than the magnetospheric background density) in Callisto's wake at altitudes of $>1000 \text{ km}$ (Gurnett et al. 1997, 2000). These elevated electron densities might be connected to an ionosphere interacting with the impinging magnetospheric plasma, but the measured high densities require a denser O_2 atmosphere (Liuzzo et al. 2015, 2016) than derived from oxygen observations and radio occultations (Cunningham et al. 2015; Hartkorn

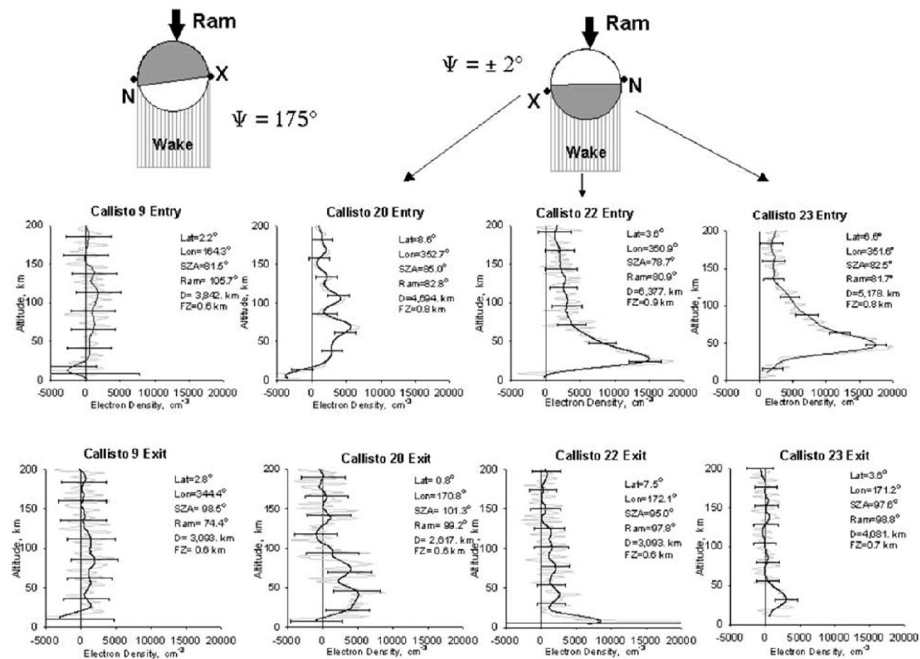


Fig. 13 Electron densities derived from Galileo radio occultation observations at Callisto (from Kliore et al. 2002)

et al. 2017). Alternatively, to a dense O₂ atmosphere, ionization of an extended H₂ atmosphere might produce these high-altitude enhanced plasma densities locally (Carberry Mogan et al. 2021, 2023; Carberry Mogan 2022).

Anisotropy of Callisto's ionospheric conductivities similar to Cowling-conductivities (Hartkorn and Saur 2017) could generate an enhancement effect on ionospheric loop currents that are driven by the time-variable Jovian magnetic field at the location of this moon. Electromagnetic induction in the ionosphere might therefore contribute to the observed induced dipole signature from Callisto (Strobel et al. 2002; Hartkorn and Saur 2017), which was first used as diagnostic for an electrically conductive subsurface water ocean (Khurana et al. 1998; Zimmer 2000; Van Hoolst 2024, this collection). Whether ionospheric induction can fully explain the signals from the *Galileo* flybys is not yet clear, and depends on the configuration of the atmosphere and ionosphere.

As for Europa, the presence of an ionosphere at Callisto is established, but detailed characteristics like composition, global distribution and time-variability are poorly understood. If Callisto's atmosphere is relatively stable and the ionosphere primarily generated by photoionisation, then any variability should be modulated by the orbital period and less by the periodically changing magnetospheric environment.

Callisto ionosphere questions to be addressed by *JUICE* include:

- How are 3D maps of ionospheric densities and composition changing with solar, magnetospheric, and orbital conditions? How pronounced is the apparent day-night asymmetry?
- How much is the ionosphere affected by the interaction with the plasma environment?
- Are the ionospheric densities high enough for a measurable or a dominant secondary magnetic field to be induced in the ionosphere?

JUICE will push forward the boundaries of our understanding in this area thanks to its 21 flybys of Callisto, with closest approach altitudes spanning ~ 200 km to several 1000's of km. As shown in Fig. 12, *JUICE* will more than double the number of flybys of Callisto ever made. Half of the *JUICE* flybys have closest approach altitudes of ~ 200 km from the surface, allowing *in situ* probing of the upper ionosphere. As indicated by the *Galileo* results, a widely extended region of enhanced plasma densities might exist, which can be well investigated by *JUICE* during the ~ 10 more distant flybys.

As for Europa (see Sect. 3.1), a combination of *in situ* and remote investigations will be carried out by *JUICE*. As before, fields and particles measurements will be combined with global modelling results. This will further our understanding of the distribution of ionospheric conductivity and how it changes with time, for example. This will feed directly into our knowledge of electric currents flowing in the plasma, which is a particularly important topic in the context of Callisto for reasons described above. Remote sensing will also be carried out, once again focused on radio occultations and observed ultraviolet emissions. For the former, the expected range of transverse spacecraft velocity with respect to Callisto during both close and distant radio occultation opportunities of $0.5\text{--}4\text{ km s}^{-1}$ leads to an electron density sensitivity in the range $400\text{--}1000\text{ cm}^{-3}$ ($1\text{-}\sigma$), with an altitude resolution ranging between 0.5 and 4 km (Withers 2020; Iess et al. 2025, this collection). For the latter, UV data will allow us to map the photoelectron-excited oxygen airglow emissions on the dayside of Callisto during all flybys. This airglow is a direct tracer for where photoionisation is happening in Callisto's atmosphere. In addition, constraints on the far-UV emissions on the nightside will enable estimates of the impact of magnetospheric electrons on the UV emissions, and thereby also on the generation of the ionosphere. Note that neutral particle measurements surrounding each flyby will also provide important context (Tosi et al. 2024, this collection).

4.2 Moon-Magnetosphere Interaction at Callisto

Callisto is immersed in Jupiter's magnetosphere at a distance of 26.9 R_J where the magnetospheric plasma is rotating with a speed of approximately 200 km s^{-1} . This is much faster than the orbital speed of Callisto (8 km s^{-1} , orbital period of 16.7 days) and Callisto's trailing hemisphere therefore becomes the ram-side of the resulting moon-magnetosphere interaction. Similar to other moon-magnetosphere interactions systems (and different from solar wind-planet interactions) the angle between the ram-side and dayside will vary with the orbital phase of Callisto around Jupiter. Furthermore, Jupiter's dipole axis is tilted with respect to the rotation axis by about 9.6° and as the magnetospheric plasma is denser toward Jupiter's magnetic equator Callisto will encounter an upstream plasma flow that is also depends on the orbital phase (Kivelson 2004b).

Callisto has a tenuous atmosphere where oxygen dominates (Cunningham et al. 2015) and carbon dioxide is also abundant (Carlson 1999). Photo-ionisation and magnetospheric particle impact ionisation lead to an ionosphere being formed (see Sect. 4.1). However, the ionosphere appears to be present only when the dayside coincides with the upstream side (Kliore et al. 2002). Since there is no internal magnetic field present at Callisto (Khurana et al. 1997), no intrinsic magnetosphere is formed (Gurnett et al. 1997). The atmosphere and ionosphere, together with the equivalent global dipole field induced by the periodic change of the magnetic field of Jupiter (due to the tilt of the dipole), becomes an effective obstacle to the incoming magnetospheric flow (Liuzzo et al. 2015). The appearance and reappearance of the ionosphere changes the characteristics of the interaction which also varies with the orbital phase around Jupiter. Callisto normally encounters a sub-sonic and sub-alfvenic flow

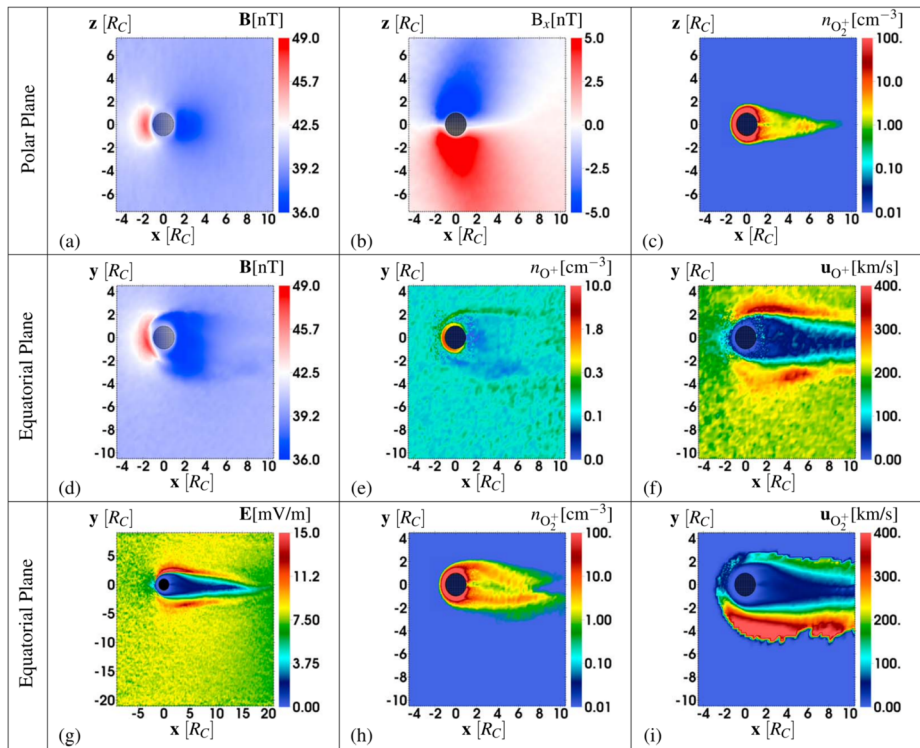


Fig. 14 Callisto's plasma environment (magnetic field, ionospheric (O_2^+) and magnetospheric (O^+) plasma density, flow velocity as well as the electric field strength) simulated for the case of when Callisto is located in the magnetospheric lobe of Jupiter. From Liuzzo et al. (2015)

of magnetospheric plasma (see Sect. 2.6) (Neubauer 1998) which implies that there will be no bow shock forming upstream of Callisto and the magnetospheric plasma slows down gradually upstream of the moon.

The interaction with the upstream plasma results in two coupled phenomena: plasma processes in the near Callisto environment such as ionospheric currents, and also Alfvén wings (Neubauer 1998, 1999), and the induction of currents in the subsurface ocean of Callisto (Van Hoolst 2024, this collection), leading to changes of the external magnetic field conditions (Khurana et al. 1998; Kivelson et al. 1999; Zimmer 2000). The Alfvén wings and the bending of the magnetic field leads to the formation of electric current loops, which go through Callisto's ionosphere and close through its conducting interior on one end, and through Jupiter's ionosphere on the other end. Note that Strobel et al. (2002) argued that UV emission measurements could be interpreted in such a way that Callisto's ionospheric conductance would be sufficient to account for the conductance otherwise required by Kivelson et al. (1999) and Zimmer (2000) to assume that induction in a subsurface ocean was present. Hartkorn and Saur (2017) furthermore argued that induction in Callisto's ionosphere as part of Callisto's plasma interaction could be so significant that it might explain the measured magnetic field data by *Galileo*, and so without the need to infer a subsurface ocean.

Simulations of the plasma environment and the interaction with the ambient plasma of Jupiter's magnetosphere have been carried out by Lindkvist et al. (2015) and Liuzzo et al. (2015) for the case of an ionosphere not present and present, respectively. Example results

are shown in Fig. 14. The gyroradius of newborn ions around Callisto is on the order of the moon's size and therefore an MHD approach does not apply and kinetic or hybrid models need to be used. One conclusion from those studies is that when Callisto is located in Jupiter's current sheet, magnetic perturbations due the plasma interaction may obscure the signatures of an induced magnetic field. Also, the simulations by Liuzzo et al. (2015) suggested that an ionosphere must be present on the downstream side to explain the high density observed with *Galileo*, and deflected Jovian plasma alone is not enough. An assessment was made by Liuzzo et al. (2018) to see how likely it is that *JUICE* will be able to observe signatures of the induction. They concluded that during some of the flybys it will be possible, but only when the plasma interaction is sufficiently weak, which in turn depends on the ambient plasma that Callisto is located in at the time of the flyby.

JUICE will contribute to the understanding of Callisto's interaction with the Jovian magnetosphere by characterising the space plasma environment and determining the magnetic induction response from Callisto's subsurface ocean (Van Hoolst 2024, this collection). All the fields and particles instruments will all be crucial for this task. Through a series of 21 close Callisto flybys, ranging in closest approach altitude from 200 km to several 1000's of km, *JUICE* will investigate this plasma environment in detail. Vector-measurements of magnetic and electric fields (DC to 3 MHz), ion and electron density, ion velocity vector, and electron temperature (which will give information on local conductivity and electric currents) as well as 3D velocity distribution functions of electrons and ions will provide new comprehensive knowledge on the physics of the moon-magnetosphere interaction.

Measurements of the plasma and field from several different flybys will provide knowledge of the general structure and dynamics of the moon-magnetosphere interaction and how that varies with Jupiter's rapid rotation phase, Callisto's orbit around Jupiter, the relative location to the Jovian magnetic equator, and the associated changes in ionisation sources. The very formation and destruction of the ionosphere, the currents systems forming, particle acceleration and plasma escape processes, for instance, will all be assessed in greater detail with *JUICE*. Furthermore, the investigation of the presence of a subsurface ocean from the magnetic field experiments will now be performed with a more detailed understanding of the external plasma conditions as compared to during the *Galileo* era. This is crucial for separating the field changes due to the subsurface ocean to those arising from external plasma effects, caused by the moon-magnetosphere interaction (Van Hoolst 2024, this collection).

5 Magnetosphere of Ganymede

This section concerns the local interaction between Ganymede and the surrounding magnetosphere of Jupiter. Once again, important context is provided in Sect. 2.6, which reviews the state of the magnetosphere at Ganymede's orbit. Unlike the interactions at Europa and Callisto reviewed in Sects. 3 and 4 respectively, the interaction at Ganymede falls in a different category because it is the only moon in the Solar System known to generate a strong (i.e., global) intrinsic magnetic field in its interior. Ganymede is a particular focus of the *JUICE* mission. After multiple flybys during the Jupiter tour, *JUICE* will become the first spacecraft to orbit Ganymede itself (Witasse et al. 2025; Boutonnet et al. 2024, both in this collection).

In this section we use spatial units of both Ganymede radii (R_G ; $1 R_G = 2634$ km) and km, and we often use the Ganymede Phi Orbital (GphiO) coordinate system. The origin of this system is co-located with Ganymede's barycentre, the x-axis in the direction of the incident flow of Jovian magnetospheric plasma that is qualitatively co-rotating with the planet (i.e.,

pointing in the direction of Ganymede's orbital motion), the y-axis points towards Jupiter's barycentre, and the z-axis completed the right-handed Cartesian set. Figure 15a shows the trajectories of past Ganymede flybys made by the *Galileo* and *Juno* spacecraft projected onto the xy plane (looking down onto Ganymede's orbital plane). The background is the output of a global MHD model of Ganymede's magnetosphere and the surrounding magnetosphere of Jupiter (Jia et al. 2008), showing the x -component of the bulk plasma velocity that reveals Ganymede's magnetospheric cavity as the region of near-stagnant flow.

Figure 15b shows the same information in the xz plane (looking along Ganymede's orbital velocity vector), with the addition of selected *JUICE* orbits from different Ganymede orbit phases. *JUICE* orbits are only shown in Fig. 15b because they are close to polar, and because of the large number of orbits that will be executed we only show selected orbits that lie close to $y = 0 R_G$. The full coverage provided by the many orbits can be visualised by rotating these selected orbits around the z -axis, providing excellent coverage of all regions of the interaction. In order, the Ganymede orbital phases will be elliptical orbits (Ganymede Elliptical Orbit, GEO), near-circular orbits at an altitude of 5000 km (Ganymede Circular Orbit 5000, GCO5000), another set of elliptical orbits (GEO), and then circular orbits at an altitude of 500 km (Ganymede Circular Orbit 500, GCO500). Figure 15b includes circular orbits at an altitude of 200 km (Ganymede Circular Orbit 200, GCO200), an agreed element of the tour not yet implemented in the baseline mission at the time of writing. For more detailed information on the flyby trajectories and their design, we refer the reader to Boutonnet et al. (Boutonnet et al. 2024, this collection).

Referring to the *JUICE* investigations presented in Table 1, this section concerns the investigation stemming from the mission objective "Characterise Ganymede as a planetary object and possible habitat", as well as the investigation MC.2 stemming from the mission objective "Characterise the Jovian magnetosphere". Note that while Ganymede's exosphere is partly covered here, this topic primarily falls within the scope of Tosi et al. (2024, this collection).

How JUICE will advance knowledge in this area: As the first spacecraft to orbit Ganymede, *JUICE* will revolutionise our knowledge of Ganymede's space environment. As shown in Fig. 15, the spacecraft trajectory while in orbit will allow us to sample different regions of the magnetosphere that have either barely, or never before been explored, with the comprehensive measurement capability of *JUICE*. These regions include the upstream environment, magnetotail and wake region, open-closed field line boundary (OCFB), closed field regions, and polar caps. The following sections present more detail on *JUICE*'s contribution in this area.

5.1 Magnetospheric Configuration

Ganymede's internal dynamo field is large enough to stand off the impinging Jovian magnetospheric plasma. Similar to those of solar system planets, its magnetic field carves out a volume in its near-space environment to form its magnetosphere. By contrast, however, Ganymede's magnetosphere is uniquely exposed to sub-magnetosonic flows resulting in a geometry that is fundamentally different to its planetary counterparts (see Sect. 2.6).

The magnetospheric cavity forms a cylinder that extends north and south of Ganymede and is tilted in the direction of the upstream flow at an angle, $\theta = \arctan v_{\text{flow}}/v_{\text{Alfvén}}$. This is in response to the disturbances arising from the external plasma, where the flow is roughly perpendicular to field direction. The disturbances propagate along the background magnetic field, above and below Ganymede at $v_{\text{Alfvén}}$. Associated with the radiating disturbances are

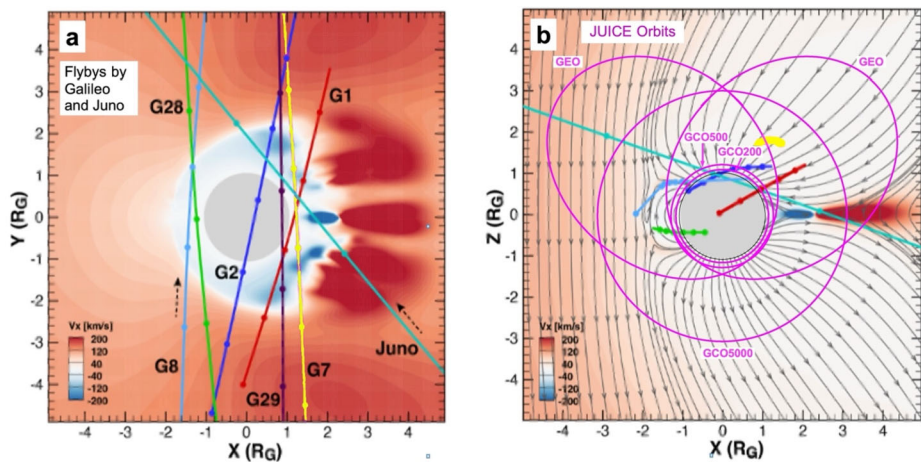


Fig. 15 Trajectories of all spacecraft flybys of Ganymede to date and selected future orbits by JUICE. (a) Trajectories projected onto the xy plane, excluding the near-polar JUICE orbits. (b) Trajectories projected onto the xz plane, including the near-polar JUICE orbits, and showing selected magnetic field lines in grey. Both panels use the GphiO coordinate system, and Ganymede is shown as a grey circle. The background in both panels is a snapshot of the x-component of bulk plasma flow, given by an MHD model (Jia et al. 2008)

field-aligned currents that couple Ganymede's magnetospheric environment to Jupiter's polar ionosphere, channelling the electrons that precipitate and lead to Ganymede's aurora footprint (Bonfond et al. 2013).

Ganymede's mini-magnetosphere was discovered by close flybys of the *Galileo* spacecraft (Kivelson et al. 1996; Gurnett et al. 1996). Various regions inside the magnetosphere were sampled, as well as the distant wake, and the ambient environment upstream of the magnetosphere (see Fig. 15). Equipped with fields and particle instruments, *Galileo* acquired quantitative constraints on Ganymede's internal magnetic moments, including contributions from the induced fields arising from a subsurface ocean, as well as the variability of the plasma and field properties in its near-space environment. The primarily dipolar internal field has an equatorial field strength of 719 nT and is tilted at 176° with respect to Ganymede's spin axis, thereby presenting a near anti-parallel magnetic shear angle at the equator against the Jovian magnetic field (Kivelson et al. 2002). This favourable magnetic configuration makes magnetic reconnection the most likely mechanism for momentum and energy exchange between Jupiter's and Ganymede's magnetospheres (see Sect. 5.2).

Ganymede's magnetosphere is subjected to periodic variations in the upstream magnetic and plasma conditions imposed by Jupiter's dipole tilt. With every oscillation of Jupiter's plasma sheet at a synodic period of 10.53 hours, Ganymede sweeps through magnetic latitudes of $\pm 9.5^\circ$. This exposes it to a large range of plasma properties along Jovian field lines, as discussed in Sect. 2.6. The two extremes are when Ganymede is (i) at the centre of the plasma sheet, where the plasma is dense and cold; and (ii) farthest from the plasma sheet, where the plasma is relatively tenuous and hot. As a result, the global configuration of Ganymede's magnetosphere changes in response to the periodic variations upstream, such as the geometry of the Alfvén wings and the associated field-aligned currents (Jia et al. 2008, 2009).

The typical flow upstream speed in Ganymede's rest frame is 140 km s^{-1} and the characteristic MHD wave speeds exhibit large temporal variability making the Alfvén and sound speeds range from $120\text{--}380 \text{ km s}^{-1}$ and $85\text{--}110 \text{ km s}^{-1}$, respectively (Kivelson 2004b).

These values indicate that the fast magnetosonic and Alfvén Mach numbers can occasionally attain unity, although this regime had not been confirmed by measurements by the *Galileo* spacecraft. Consistent with a sub-magnetosonic interaction, no bow shock has been detected upstream of Ganymede. The larger characteristic wave speeds imply that the inflowing plasma is decelerated well upstream of the magnetosphere by the action of counter-propagating compressional magnetosonic waves. Some of the inflowing plasma is diverted around the magnetosphere and reaccelerated along the flanks to freestream conditions.

The global configuration of Ganymede's magnetosphere is primarily controlled by its dynamics, i.e., how it interacts with and couples to the Jovian magnetosphere. The true picture of Ganymede's magnetosphere is time-evolving, whereby its magnetic field is episodically merging and unmerging with the Jovian field via magnetic reconnection. The overall magnetic flux is balanced presumably via reconnecting and circulating field lines analogous to the Dungey cycle. Ganymede's outermost field lines therefore undergo episodes of being either 'closed', i.e., having both footpoints connected to itself, or 'open', i.e., one footpoint connected to itself and the other far afield at Jupiter. The 'open' magnetic fields thread Ganymede's polar regions in both hemispheres create a pathway for electrons to travel to and from Jupiter, establishing the route for electrodynamic coupling.

Figure 15 illustrates the geometry of Ganymede's magnetosphere by showing the results of an MHD simulation by Jia et al. (2008). The region of near-stagnant flow defines Ganymede's magnetosphere, and the magnetic field lines shown in Fig. 15b are most useful for showing magnetospheric structure. The magnetopause standoff distance is $\sim 2 R_G$, which is largely confined by the external total pressure. Embedded within the larger cylindrical topology is a much smaller region of 'closed' magnetic field lines near the equator. The closed region is more confined in latitude at the tail side. The polar cap regions, where 'open' field lines link to Jupiter, thread a much larger range of latitudes. The boundary between the two regions, known as the OCFB, is the channel along which electrons can precipitate into Ganymede's tenuous atmosphere and form the auroras (McGrath et al. 2013).

The configuration of Ganymede's magnetosphere with respect to the plasma sheet influences the magnetospheric electron and ion circulation in the vicinity of this moon. Recent modelling work by Liuzzo et al. (2020) showed that Ganymede's trailing anti-Jovian equator receives the least flux over geologic timescales and that the trailing surface near the region near the open-closed field boundary lines the most. Recent simulations of the Jovian energetic ion precipitation to Ganymede's surface (Plainaki et al. 2015, 2022), for three distinct configurations between moon's magnetic field and Jupiter's plasma sheet (i.e., when the moon was above, inside, and below the center of the sheet), showed that the ion circulation within Ganymede's magnetosphere is strongly guided by the position of the open-closed field boundary line and the ion species and energies. Moreover, a spatially extended ion low in the anti-Jupiter low-latitude and equatorial regions above the leading hemisphere is expected. These authors also showed that the ion flux incident at 500 km altitude is not a good approximation of the surface's precipitating flux. For studying, therefore, Ganymede's surface erosion processes, the particle and field measurements at low-altitude orbits (e.g., 200 km) are fundamental. Indeed, with JUICE a detailed investigation of the Ganymede environment and its implications on the moon's surface evolution will be possible through low-altitude observations.

The observed magnetic field in Ganymede's environment is a superposition of magnetic fields from various sources. These are: (i) Jupiter's interior magnetic field, (ii) Jupiter's external magnetic field arising from its magnetospheric currents, (iii) Ganymede's interior dipolar magnetic field, (iv) Ganymede's external magnetic field arising from its magnetospheric currents, and (v) Ganymede's interior magnetic field induced from a putative subsurface salty

ocean. Carrying out the challenging task of separating out each of the contributions requires both field and particle measurements to characterise the magnetic fields induced by plasma currents, aided by the long-term sampling on a global scale afforded by *JUICE*'s orbit.

JUICE will resolve the three-dimensional structure of Ganymede's magnetosphere and assess its response to external and internal time-varying processes. The GEO orbits are designed to sample various regions of Ganymede's magnetosphere, namely the radiation belts and inner magnetosphere, the lobes and magnetotail downstream, and the Alfvén wings and OCFB in the polar magnetosphere. Determining the geometries and range of positions occupied by the boundaries are critical to understanding the large-scale magnetospheric dynamics, such as transport processes and magnetic flux circulation (See Sect. 5.2).

Routine excursions of *JUICE* into the Jovian plasma regime will place constraints on both the range of upstream conditions that Ganymede's magnetosphere is subjected to and the extent to which the magnetospheric boundaries respond accordingly. The spatial coverage enabled by GEO will be adequate to construct an empirical model of Ganymede's magnetopause, like those of planets (e.g. Joy et al. 2002; Winslow et al. 2013), characterising useful properties such as compressibility. *JUICE* will spend enough time just upstream to observe whether the flow conditions do indeed make the transition to super-Alfvénic or super-magnetosonic, and thus develop a bow shock. The expected consequence on Ganymede's magnetosphere would be an evolution from a cylindrical to a bullet-shaped structure, a unique magnetosphere in the solar system known to have this potential.

Limited coverage from the *Galileo* trajectories have made it difficult to differentiate between the dipole and quadrupole magnetic field contributions, whereby all the non-axial terms of the quadrupole moment cannot be uniquely defined. The GEO and GCO orbits will provide the first truly global coverage of Ganymede's magnetosphere from which a high-order spherical harmonic model of the internal magnetic field can be constructed. As a result, hemispheric asymmetry and small-scale anomalies will be identifiable. In the magnetospheric context, the primary utility of such a model will be magnetic field line mapping. For example, in-situ fields and particle observations of magnetic reconnection can be directly related to remote observations of the UV aurora, allowing for an end-to-end analysis of Ganymede's auroral processes. Defining Ganymede's L-shells (defined in the classic sense using only the dipole field of the planet) will be necessary for investigating the radiation belts and space weathering.

NASA's *Juno* mission recently performed a close flyby of Ganymede with a closest approach altitude of ~ 1030 km and its magnetospheric payload allowed for contemporaneous field and particle observations. However, recent results suggest that *Juno* remained on open field lines and did not sample the precipitating particles creating the aurora (e.g., Allegrini et al. 2022; Clark et al. 2022; Hansen et al. 2022; Kurth et al. 2022; Paranicas et al. 2022). Therefore, fundamental questions remain regarding the processes that form Ganymede's aurorae. In addition to Ganymede's magnetic structure, *JUICE* will make measurements of plasma density, velocity, and composition in the magnetosphere. These measurements allow for density profiles, and thus ionospheric scale heights to be determined, as well as flow and circulation patterns, all of which are essential pieces of the global magnetospheric configuration.

5.2 Magnetospheric Dynamics

The configuration of Ganymede's magnetosphere may appear to be in a quasi-steady state, as described in Sect. 5.1, on time scales comparable with the typical time for the plasma to flow from the upstream to the downstream (of the order of a few minutes). However, there

are a variety of phenomena occurring in Ganymede's magnetosphere that are not steady on time scales shorter than that reference time, such as magnetic reconnection, boundary processes, and generation and propagation of plasma and MHD waves (see reviews by Jia and Kivelson 2021 and Kivelson et al. 2025). Here we briefly review the key aspects of Ganymede's magnetospheric dynamics as inferred from previous *Galileo* observations as well as modelling work, and highlight outstanding open questions that will be addressed by the *JUICE* mission.

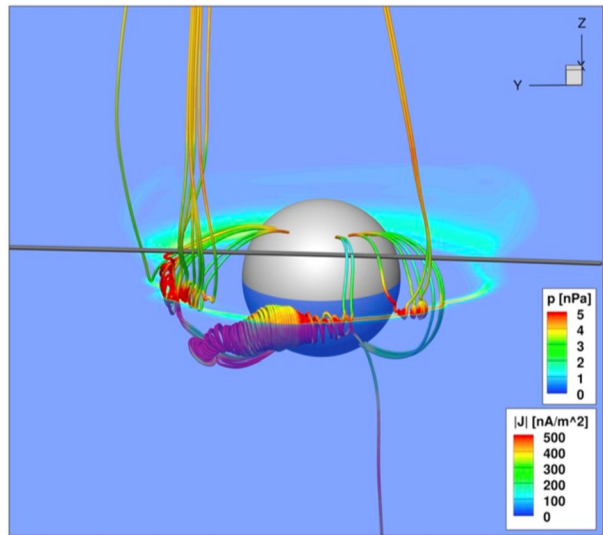
- Reconnection-driven processes

At Ganymede's orbit, Jupiter's magnetospheric field always remains largely anti-parallel to Ganymede's internal field at the equator (Khurana 1997; Kivelson et al. 2002). Combined with the relatively low plasma β of the ambient plasma (e.g., Kivelson et al. 2004b, 2025), the environment around Ganymede's upstream magnetopause is very conducive to magnetic reconnection. As a result, Ganymede's global plasma convection and magnetospheric dynamics are dominated by the so-called "Dungey cycle" driven by magnetic reconnection occurring on the upstream magnetopause and in the downstream magnetotail. Indeed, *Galileo* measurements indicate highly efficient reconnection producing significant cross-magnetopause plasma transport (Kivelson et al. 1998). Subsequent numerical simulations predict the presence of widespread flux transfer events as a result of multiple X-line reconnection despite relatively steady upstream conditions (Jia et al. 2010b; Tóth et al. 2016; Zhou et al. 2019, 2020), and the simulated magnetic signatures appear to be consistent with the large-amplitude magnetic field fluctuations observed by *Galileo* during crossings of the magnetopause (Kivelson et al. 1998). Figure 16 shows an example of magnetic topologies that could arise from magnetopause reconnection, based on numerical modelling (Tóth et al. 2016).

A recent analytical assessment of reconnection onset conditions confirms that the plasma and magnetic field conditions near Ganymede's magnetopause are indeed favourable for reconnection throughout the closed-field equatorial region (Kaweeyanun et al. 2020). The associated reconnection electric field is estimated to range between $2 - 20 \text{ mV m}^{-1}$, suggesting widespread reconnection over an extended region on the magnetopause although their global structure remains poorly constrained (Kaweeyanun et al. 2020; Zhou et al. 2020). Moreover, it is found that the average reconnection electric field exhibits a periodic variation resulting from periodic changes in the upstream plasma and magnetic conditions governed by Jupiter's rotation. Re-analysis of the *Galileo* plasma data shows evidence of moon-ward plasma movement in the downstream region, consistent with magnetotail reconnection in a Dungey-like convection cycle (Collinson et al. 2018). The downstream reconnection rate is also likely to be significant, given the long-term stability of the location and shape of the observed aurora oval, which is strongly correlated to the open-closed field line boundary (McGrath et al. 2013; Saur et al. 2015).

While the *Galileo* observations and modelling work have provided valuable insight, our knowledge on the reconnection process at Ganymede and its global impact remains quite limited. Additional crossings of the upstream magnetopause and the downstream magnetotail are needed to resolve global reconnection structures, improve estimates of reconnection rate and efficiency, and characterise temporal variations in reconnection-driven dynamics. *JUICE* with its modern instrumentation, such as high-resolution magnetometer and particle instruments, will provide an unprecedented opportunity to establish a significantly completer and more detailed picture of Ganymede's reconnection. During its orbital phase, especially the GEO elliptical phase, the trajectories of *JUICE* will allow the spacecraft to probe a wide variety of regions of the moon's magnetosphere where reconnection could potentially occur. In-situ measurements to be acquired over the moon's polar caps together with remote

Fig. 16 3-D visualization of magnetic field lines in a snapshot of a high-resolution simulation that combines an MHD approach with embedded domains that solve the equation of motion for individual particles. Ganymede is shown as viewed from the upstream region, along the direction of incoming plasma flow, at slightly positive GPhiO z-coordinate. The almost straight grey tube indicates the trajectory of a Galileo flyby. The coloured tubes show selected magnetic field lines coloured by the local plasma pressure. The translucent equatorial plane is coloured with the current density. Ganymede's surface is shown by the grey sphere. From Tóth et al. (2016)



sensing observations of Ganymede's aurora would provide key datasets to constrain the role of reconnection in plasma energisation and transport of magnetic flux, thereby providing further insights into the global magnetospheric dynamics.

Recent observations from Juno during its flyby of Ganymede on 7 June 2021 (e.g., Allegri et al. 2022; Clark et al. 2022) and MHD simulations of the encounter (Duling et al. 2022) suggest that the spacecraft remained in the moon's open field line region throughout the entire flyby. However, accelerated, field-aligned electrons observed near Ganymede's upstream magnetopause provide evidence that magnetic reconnection is indeed occurring (Ebert et al. 2022). This is consistent with previous scenarios proposing that reconnection is a driver of magnetosphere dynamics for the satellite (e.g., Jia et al. 2010a,b). JUICE will allow the detailed investigation of the reconnection processes occurring at Ganymede through multiple particle and field observations enabling the refinement of numerical models and offering essential feedback for testing and enhancing current theoretical scenarios.

- Viscous-like interactions

We define a “viscous-like” interaction as one where a tenuous plasma flow around a magnetised obstacle exerts an effective viscous drag on the obstacle, despite the low frequency of inter-particle collisions and often achieved via MHD waves. Such interactions have long been recognised to also play an important role in coupling the external plasma flow with planetary magnetospheres, especially at the magnetopause boundary in the form of Kelvin-Helmholtz (K-H) waves. Potential evidence of K-H waves was first speculated based on *Galileo* observations near Ganymede's magnetopause (Kivelson et al. 1998), although this was later suggested to be more likely associated with magnetic structures arising from unsteady magnetopause reconnection (e.g., Jia et al. 2010b; Volwerk et al. 2013; Tóth et al. 2016). In a recent effort to analytically assess the stability conditions of Ganymede's upstream magnetopause, Kaweeyanun et al. (2021) found that the onset condition for linear K-H waves is satisfied along both magnetopause flank regions at all latitudes. When Ganymede is at the centre of the Jovian plasma sheet, the threshold for K-H instability is lowered due to (1) weaker magnetic fields adjacent to the magnetopause that are (2) more strongly orthogonal to the perturbation wave vector. Estimated phase speeds of the K-H waves are roughly

half that of the external Jovian plasma bulk flow speed, which are consistent with previous estimates based on in-situ measurements (Kivelson et al. 1998; Kaweeyanun et al. 2021).

Heavy ions (O and S species) that dominate Jupiter's magnetospheric plasma at Ganymede's orbit possess non-negligible gyroradii compared to the typical thickness of the magnetopause boundary. Consequently, kinetic phenomena, particularly finite-gyroradius effects, must be considered when evaluating K-H instability on Ganymede's magnetopause. These fine-gyroradius effects are expected to induce a small but notable inter-flank asymmetry in instability growth, slightly favouring the sub-Jovian flank where local ion flow shear adds to the bulk flow shear (Kaweeyanun et al. 2021). Nonlinear K-H vortices hence should be more prevalent on the sub-Jovian flank, where those vortices, if formed, could potentially facilitate plasma and energy transport across Ganymede's magnetopause.

Like magnetic reconnection, verification of any K-H instability predictions currently is limited by the rather sparse in-situ measurements. Nevertheless, Stahl et al. (2023) used a hybrid model (kinetic ions, fluid electrons) to provide context for plasma and magnetic field observations during *Juno*'s flyby of Ganymede on 7 June 2021. They found that Ganymede's sub-Jovian magnetopause is susceptible to K-H instabilities, causing the location of the boundary layer to oscillate. The JUICE mission will greatly contribute in the study of these phenomena by conducting a large number of magnetopause crossings during its orbital phase, where signatures of linear and non-linear K-H structures could be measured. Data from JUICE magnetopause crossings will help answer many open questions concerning the nature of viscous-like interaction at Ganymede's magnetopause, such as prevalence and growth rate of K-H instability, transition of linear K-H waves toward nonlinear K-H vortices, and the overall contribution of viscous-like interactions to the plasma and energy transport across the magnetopause.

- Waves

As a source of energetic and anisotropic charged particle distributions (e.g., loss cones because of particle absorption by Ganymede's surface), Ganymede's magnetosphere is a natural environment for the generation, growth, and propagation of radio and plasma waves (Gurnett et al. 1996). During its multiple close encounters with Ganymede, *Galileo*'s Plasma Wave Subsystem (PWS) (Gurnett et al. 1992) measured electrostatic and electromagnetic plasma wave emissions covering a large range of frequencies from <10 to 10^5 Hz. From the lower band, whistler-mode in the form of 'chorus' and 'hiss' were detected. This mode remains trapped within Ganymede's magnetosphere and is an indicator of electron loss-cone anisotropies and beam-plasma instabilities. It is not understood how the whistler-mode waves that pervade Ganymede's magnetosphere interact with its electrons as well as where the source regions are. Addressing these issues will be achievable by utilising *JUICE*'s fields and particles instruments sampling the various regions of Ganymede's magnetosphere in depth. The outcome will be critical to understanding Ganymede's auroral and radiation belt dynamics.

The UHR emission is typically pronounced during flybys through Ganymede's magnetosphere. Near the UHR frequency, electrostatic electron cyclotron waves can mode-convert into electromagnetic non-thermal radio waves, which are capable of escaping Ganymede's magnetosphere (Kurth et al. 1997). Although not surprising for a magnetosphere, Ganymede as a radio source is unusual in that the cyclotron maser emission (such as Earth's auroral kilometric radiation and Jupiter's decametric and hectometric radiation) is not present due to the relatively large plasma densities in its aurora regions. *JUICE*, during its Ganymede orbital phase, will be able to map the radio sources and directly relate the observed emissions to non-thermal particle distributions to shed light on the underlying generation mechanisms.

Furthermore, the dependence of the UHR emission on the electron plasma frequency allows for accurate inference of the electron density and scale height of Ganymede's ionosphere (e.g., Eviatar et al. 2001a). Through such measurements, a complete profile of the properties of Ganymede's ionosphere will be enabled by *JUICE*'s largely enhanced coverage, thus providing essential constraints for the modelling of Ganymede's ionosphere and magnetosphere (e.g., Carnielli et al. 2019, 2020a, 2020b; Galand et al. 2025).

In addition to high frequency plasma waves, Ganymede's magnetosphere also generates low frequency MHD waves, which can give insight into the local plasma environment. As demonstrated through *Galileo* observations, the closed magnetic field lines in Ganymede's magnetosphere are prone to field line resonances (Volwerk et al. 1999, 2013). These waves usually show a spectrum with the base frequency and several harmonics. The wave frequencies are dependent on the length of the field line (or the L-shell) and the Alfvén speed along the field line, for which it is usually assumed that the lowest speed is found at the equator where the plasma density is highest and the field strength is smallest. Through comparing the spectrum with models (e.g. Cummings, O'Sullivan and Coleman 1969) a value for the local plasma density at the equator can be obtained. Indeed, the densities inferred from the only two *Galileo* flybys that penetrated the closed field line region (G8 and G28) delivered an ionospheric scale height of ~ 465 km (Volwerk et al. 1999, 2013), not too far off from the estimate by Eviatar et al. (2001a) of 600 km based on the PWS measurements. For *JUICE*, during its Ganymede orbital phase, these waves can be used to sound the magnetosphere and to probe how the equatorial plasma density distributions vary as a function of Jovian latitude, e.g., when Ganymede is located inside and outside of Jupiter's plasma sheet.

The interaction of the Jovian plasma with Ganymede's surface and exosphere leads to sputtering and impact ionisation, which may subsequently result in pick-up of the freshly created ions. This creates a ring(-beam) distribution in velocity space, which is unstable to the generation of ion cyclotron waves. A first indication of O^+ or H_2O^+ ion cyclotron waves at Ganymede was found by Volwerk and Khurana (2010) in the *Galileo* magnetometer data. As the cyclotron wave frequencies are closely related to the ion gyrofrequency determined by its mass and charge and the local magnetic field strength, magnetic field measurements of ion cyclotron waves can be used as an ion identification tool. This can be achieved during flybys, as was done with past missions, such as *Galileo* at Europa (Volwerk et al. 2001) and *Cassini* at Titan (Russell et al. 2016). Furthermore, the handedness of cyclotron waves can be used to deduce whether the ion involved is positively or negatively charged. As such, *JUICE* observations of ion cyclotron waves during both the flyby phase and the orbital phase can give valuable information about the ions created around Ganymede and be used as a tool to get an estimate of the exospheric neutral density (e.g., Delva et al. 2009; Schmid et al. 2022).

5.3 Auroral Processes

Ganymede auroral emission were first observed by Hall et al. (1998) with the Goddard High Resolution Spectrograph on board of the *HST* and subsequently imaged with the Space Telescope Imaging Spectrograph (Feldman et al. 2000). Ganymede's aurorae offer insights into its magnetic environment, atmosphere, and the potential existence of a subsurface ocean. At Earth, aurorae are generated by the interaction between accelerated, charged particles that follow the magnetic field and the components of the atmosphere. The situation at Ganymede, however, is markedly more complex due to its location within Jupiter's magnetosphere. Due to the interaction of Ganymede's internal dynamo field (~ 750 nT at the equator) and Jupiter's magnetospheric flow, Ganymede possesses a distinctive mini-magnetosphere

within Jupiter's overarching magnetosphere. The variation of Jupiter's magnetospheric field at Ganymede (~ 100 nT) periodically tilts the OCFB. The damped oscillation amplitude of the aurorae oval tilt angles has been used as evidence to support the existence of a subsurface ocean on Ganymede (Saur et al. 2015; Van Hoolst 2024, this journal).

Ganymede's unique auroral processes are linked to its thin, tenuous atmosphere. The atmospheres of the Galilean satellites Europa, Ganymede, and Callisto are composed of a combination of O_2 , O, H_2O , and CO_2 and are ultimately sourced from their surfaces. The interaction of charged particles with this atmosphere results in distinct auroral emissions. Recently, Roth (2021) and Roth et al. (2021) used auroral data sets to independently constrain the atomic O abundance in the atmospheres of Europa and Ganymede by measuring the resonant scattering component of the 1304 \AA emission as the satellites passed through Jupiter's shadow. These data sets placed a tight upper limit on the O abundance, which then requires a new mechanism to explain the low $1356/1304 \text{ \AA}$ (e.g., Roth 2021) on the trailing hemispheres of these satellites.

The proposed mechanism is a consistently present H_2O atmosphere centred on the trailing hemisphere for Europa and on both hemispheres (but six times denser on the trailing) for Ganymede, which can be produced by sublimation in the case of Ganymede (as is also predicted on Callisto (Carberry Mogan et al. 2021)) and by sputtering combined with sublimation of the fresh deposits of sputtered H_2O in the case of Europa (Teolis et al. 2017; Roth 2021). The derived mixing ratios of H_2O / O_2 over the trailing hemisphere are in the 10–30 range for both satellites. The UV lines are significantly more sensitive to O_2 than to H_2O , and observations of H in addition to O, and/or observations of lines with higher intrinsic emission rates following electron impact on H_2O , would strengthen the constraints on the presence and abundance of H_2O . Using observations at optical wavelengths during Jupiter eclipses, de Kleer et al. (2023) could place an upper bound on the H_2O content in Ganymede's bulk atmosphere of $H_2O/O_2 < 0.6$. Monte Carlo models have shown that the spatial distribution of H_2O and O_2 in the atmosphere is modulated on an orbital time scale due to influences from Jupiter's gravitational field as well as source processes on the surface (Leblanc et al. 2017, 2023). Thus, temporal variations in auroral emissions may be a product of both temporal variation in electron acceleration processes and in the atmosphere.

Eviatar et al. (2001b) used a model for the neutral atmosphere to study the behaviour of charged particles interacting with Ganymede's atmosphere. They demonstrate that the brightness of Ganymede's aurora, either arcs or diffuse emission, cannot be matched by models assuming the electron energies and densities at Ganymede's orbit, so the electrons of Jupiter's magnetosphere do not have sufficient energy to excite the auroral emissions, in contrast to the aurorae generated at Io and Europa (e.g., Saur et al. 1998, 2000; Retherford et al. 2000; Roth et al. 2011, 2014a,b). Thus, at Ganymede, local particle acceleration is necessary to explain the observed UV fluxes. Such a conclusion was also reached by Lavrukhin and Alexeev (2015) who analysed Ganymede's magnetospheric interaction and estimated that the required current of ~ 500 kA could not be carried by the surrounding plasma, thus requiring energisation. Eviatar et al. (2001b) suggest two possible energisation mechanisms: 1) stochastic heating by Landau damping of electron plasma oscillations, and 2) acceleration by electric fields associated with field-aligned currents and which they considered the more likely option.

The generally sub-Alfvénic flow upstream of Ganymede suggests magnetic reconnection can proceed very efficiently and quickly (e.g., Kivelson et al. 1998; Neubauer 1998) (see Sect. 2.6 and 5.2) thus providing acceleration that can generate the required energy flux into the atmosphere. The acceleration of charged particles by reconnection has been studied in MHD simulations (Paty and Winglee 2004; Jia et al. 2008; Dorelli et al. 2015; Payan et al.

2015) and coupled kinetic-MHD simulations (Zhou et al. 2019). These models demonstrate that reconnection can drive energy fluxes at a level comparable to the observed emissions, although in the coupled kinetic-MHD simulations around 40% or less of the emission could be attributed to reconnection-related acceleration suggesting other mechanisms would be involved.

As a lower threshold, the excitation of aurora at Ganymede via dissociative impacts of electrons on O_2 requires energies beyond 14.3 eV. Payan et al. (2015) report that hot Jovian plasma species have modelled energies well above this threshold and thus, a large majority of the hot Jovian plasma precipitating into Ganymede's neutral atmosphere through the cusps is able to excite the aurora. Related recent work based on Juno/JADE data has been done by Pelcener et al. (2024), characterising the temporal and spatial variability of the electron environment upstream of Ganymede (see Sect. 2.6).

Simulations therefore seem to suggest that on the flow-facing hemisphere of Ganymede the bright auroral emissions should map to the cusp, containing recently reconnected flux and thus containing Jovian plasma that has been accelerated in magnetopause reconnection sites, and on the anti-flow-facing hemisphere the emissions at lower latitudes should map to dipolarisation regions in the magnetotail and thus contain accelerated plasma from Ganymede's magnetosphere (e.g., Paty and Winglee 2004; Payan et al. 2015). In the simulations of Payan et al. (2015) strong parallel electric fields are associated with the brightest auroral emissions. Marzok et al. (2022) found that brightness maxima on the flow-facing and anti-flow-facing hemispheres were rotated slightly towards the Jovian-facing side. Such a rotation is reproduced in Hall MHD simulations where the Hall effect slightly distorts field-aligned currents and convection patterns (e.g., Dorelli et al. 2015) but it has been suggested that a slight tilt in the magnetic moment of Ganymede may also produce a similar effect (Marzok et al. 2022). The origin of auroral emissions on the flanks could also be the result of reconnection (e.g., Jia et al. 2008), or field-aligned currents associated with shear flow, or pitch-angle scattering of Jovian energetic particles may be responsible (Marzok et al. 2022). Despite all these predictions, the most recent observations suggest that Ganymede's brightest auroral emissions could correspond to closed-field regions (Greathouse et al. 2022), highlighting that we have much to learn concerning these emissions with *JUICE*.

The brightness of the aurora depends on whether a hemisphere is facing the Jovian plasma sheet. When the northern (southern) hemisphere faces the plasma sheet then the northern (southern) hemisphere has the brighter aurora suggesting that the plasma sheet and its magnetic coupling to Ganymede are involved in applying asymmetrical stress to Ganymede causing asymmetrical Poynting fluxes that feed auroral processes (Saur et al. 2022). Figure 17 shows example *HST* images in the UV that show Ganymede's auroras, where each image corresponds to a different location of Ganymede with respect to the plasma sheet.

The processes underlying diffuse auroral emissions are subjected to a similar issue of the lack of thermal energy (Eviatar et al. 2001b) and require some process to scatter particles into the loss cone. Pitch angle scattering by whistler waves is a potential candidate but modelled based on *Galileo* observations by Tripathi et al. (2017) suggested this wasn't sufficient leading Singhal et al. (2016) to suggest that additional acceleration by electrostatic electron cyclotron harmonic waves would be readily sufficient to produce the diffuse aurora. However, Li et al. (2023) re-examined this question using in-situ *Juno* observations of whistler waves and found much larger pitch angle diffusion rates, possibly because the *Galileo* wave amplitudes were smaller and Tripathi et al. (2017) only considered quasi-parallel whistlers. Li et al. (2023) were able to show that quasi-parallel whistler-mode waves play a dominant role in accelerating particles above about 1 keV whereas highly oblique waves are important below 1 keV. Acceleration above tens of keV is cannot be fully explained by whistler

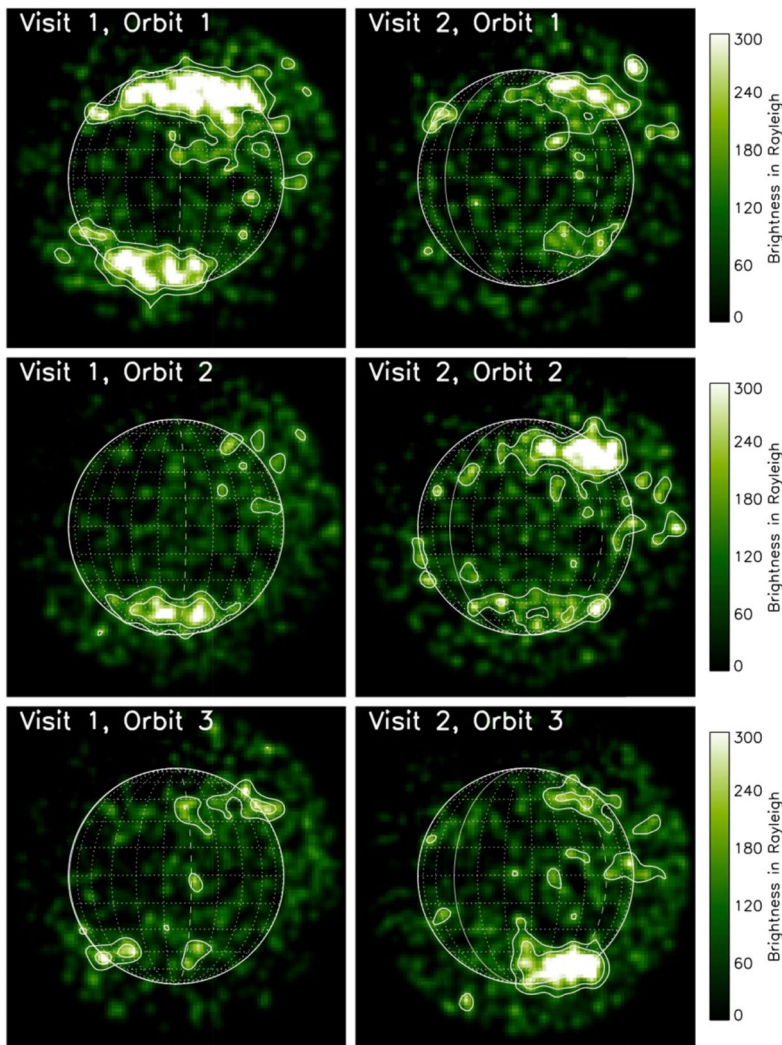


Fig. 17 HST/STIS images of Ganymede's auroral brightness in Rayleigh at OI 1, 356 Å. Visit 1 occurred before and visit 2 after the Juno flyby on 7 June 2021. Observations show mostly Ganymede's trailing, that is, plasma flow upstream, hemisphere. The dashed line indicates the 90° meridian. From Saur et al. (2022)

waves and requires additional wave modes, turbulence, or waves in the non-linear regime. Li et al. (2023) report about *Juno* measurements of whistler-mode waves that could drive precipitating electrons.

The electron acceleration in relation to the Ganymede aurora were studied by Payan et al. (2015) employing a 3D multifluid model and an auroral brightness model. They assume an oxygen column density of $3.75 \times 10^{14} \text{ cm}^{-2}$ and find that electron acceleration regions coincide with brightest auroral emission regions and that electrons generating the aurora are sourced in Jovian plasma and in magnetotail, despite earlier conjecture from Eviatar et al. (2001b). The aurora on the orbital trailing hemisphere is generated by electrons sourced in the Jovian plasma and penetrating into Ganymede's neutral atmosphere through the cusps.

As for the aurora on the orbital leading hemisphere, it is generated by electrons originating from Ganymede's ionospheric and magnetospheric flow. These electrons are accelerated by parallel electric fields along newly closed magnetic field lines created by magnetic reconnection in Ganymede's magnetotail, and precipitate into Ganymede's neutral atmosphere at much lower latitudes. The work by Payan et al. (2015) illustrates that the regions of brightest auroral emissions coincide well with regions of strongest acceleration due to parallel electric fields.

The high energy part of precipitating electrons was investigated by Liuzzo et al. (2020). They discuss how energetic electron bombardment on Ganymede varies over different timescales and locations on the moon. The study used data from the Energetic Particle Detector instrument on board the *Galileo* spacecraft, which measured the flux and spectra of electrons in a wide range of energies. These observations were compared to the modelled outcome of energetic particle tracing. For this, the relativistic electrons were modelled using a combination between hybrid modelling of electromagnetic fields and a special energetic particle tracer. The electron bombardment was found to be highly variable, with peak electron fluxes at some locations being orders of magnitude higher than at others. The variability had a strong dependence on the location on the moon and on the timescale considered and affects the properties of the moon's atmosphere, such as its density, temperature, and composition. Note that even though precipitation is enhanced along the open-closed field line boundary, energetic electrons do not significantly contribute to the generation of auroral signatures at Ganymede. They rather affect the surface materials by space weathering.

Note that recent ground-based observations succeeded in detecting Ganymede auroral emissions due to oxygen and hydrogen in the visible spectral range during eclipses of the satellite (de Kleer et al. 2023). Although not spectrally resolved, such emission for Ganymede may offer the possibility for *JUICE* to remotely trace emissions in vertical and nocturnal limb scans at different latitudes, with particularly high spatial resolution during low-altitude circular orbits. Additional searches for auroral signatures and their mapping for all three relevant Galilean moons could be performed during several satellites' eclipses observable from the position of *JUICE*, provide further insights into their tenuous atmospheres.

5.4 Ionosphere

Ganymede hosts a tenuous atmosphere, primarily produced through sublimation of water ice and irradiation of the moon's surface by energetic particles (H_2O , O_2 , H_2) (Marconi 2007; Plainaki et al. 2015; Leblanc et al. 2017, 2023; Vorburger et al. 2022). This envelope of neutral gas gets partially ionised, which formed the ionosphere. This plasma layer dominates over the Jovian plasma inside Ganymede's magnetosphere (except in part of the Alfvén wings) (Carnielli et al. 2020a).

The ionosphere plays a critical role in the coupling of the magnetized moon with the Jovian environment and with the moon's subsurface ocean (Saur et al. 2015). The ionosphere provides a conductive medium that acts as a closure region for electric currents generated in the magnetosphere, with closure occurring across the magnetic field near Ganymede's surface. Magnetically field-aligned currents should close in the ionosphere in the form of auroral electrojets around the auroral ovals, and through the Alfvén wings of Ganymede into the polar cap ionosphere. Alfvén waves in these regions may also become inertial when propagating toward the ionospheric shore and dump their energy and momentum there.

Isolating magnetic fields arising from electromagnetic induction occurring in Ganymede's ionosphere is essential to distinguish it from the inductive response of the

sub-surface ocean (see Van Hoolst 2024, this collection). The ionosphere is a source of dense and cold-oxygen rich plasma to both Ganymede and Jupiter magnetospheres, and a source for Ganymede's neutral atmosphere through particle irradiation on the moon's surface. In fact, this contribution may significantly dominate that by Jovian ions (Carnielli et al. 2020b).

However, little is known about Ganymede's ionosphere due to limited in-situ observations, reduced mainly to the two close flybys by *Galileo* (G1 and G2) (Gurnett et al. 1996; Eviatar et al. 2001a) and one by *Juno* (PJ34) (Hansen et al. 2022). As a result, we must currently rely heavily on modelling to characterise the ionosphere (Galand et al. 2025). Such ionospheric modelling is limited, in part, by the large uncertainty in the density and composition of the atmosphere. *JUICE* will offer the first opportunity to probe comprehensively and assess in detail the ionospheric density, composition, dynamics, and energy budget of Ganymede's critical plasma layer.

We review here the open problems related to Ganymede's ionosphere to be targeted by *JUICE*. Relevant key open questions are listed below.

- *What is the main source of ionization of Ganymede's tenuous atmosphere?*
- *What is the role played by collisions in Ganymede's ionosphere?*
- *Is transport of ionospheric species well quantified?*
- *What are the key drivers of Ganymede's ionospheric densities?*
- *Is Ganymede's ionosphere affected by dust?*
- *How is the ionosphere contributing to auroral, magnetosphere-ionosphere coupling?*
- *What are the drivers of the ionospheric energy budget?*
- *What are the waves present in Ganymede's ionosphere?*
- *How significant are the ionospheric ions, that are directed back to the surface and induce secondary sputtering, as a source of the exosphere?*

Ionizing sources of Ganymede's atmosphere include solar extreme ultraviolet radiation on the dayside and energetic (~ 15 eV to a few 100 eV) electrons everywhere. Electron-impact frequencies for the major neutral species derived from energy spectra at Ganymede's orbit were found to be a factor 4 to 5 higher than photo-ionization frequencies (Carnielli et al. 2019). However, the electron population is significantly affected within Ganymede's magnetosphere, as attested by the few *Galileo* and *Juno* close flybys of the moon (Williams et al. 1998; Allegrini et al. 2022; Kurth et al. 2022). In the absence of a more comprehensive set of observations, the spatial distribution of electron-impact ionization frequency around the moon remains poorly known, though energetic electrons may be the main source of Ganymede's ionosphere. The electron distribution will be measured from *JUICE* over the 1 eV to 50 keV range. As most of electrons responsible for ionisation are also responsible for dissociative excitation yielding auroral emissions, UV spectra from atomic oxygen can be used to constrain the spatial distribution of the ionising electrons. Quantitative information on the electrons can also be derived by combining UV auroral observations with other atmospheric observations.

The ionospheric collision frequency is a critical parameter because it not only gives the level of electrical conductivity, but also limitations for ion plasma convection and thermal conditions near the surface. Typical atmospheric peak number densities near the surface are in the range 10^8 – 10^9 cm $^{-3}$ (e.g., Marconi 2007), giving ion-neutral momentum transfer collision frequencies (e.g., Schunk and Nagy 1980) in the range 10^{-3} – 10^{-1} s $^{-1}$ for O $_2$ and H $_2$ O below an altitude of 100 km. This can be compared to the magnetic gyrofrequency of a few s $^{-1}$ near the surface. There is therefore no highly collisional ionospheric layer, meaning, no "typical" ionosphere on Ganymede. However, the Hall and Pedersen conductivities rise

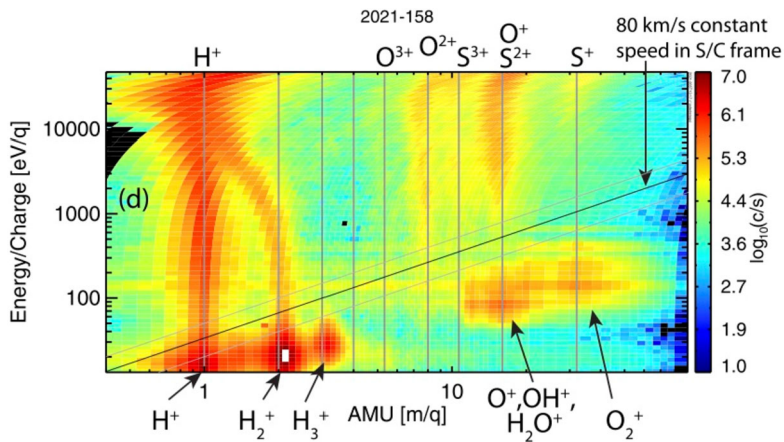


Fig. 18 On counts-per-second energy-time spectrograms and energy-per-charge (E/q) versus mass-per-charge (m/q) during the close Ganymede flyby by Juno on 7 June 2021. Adapted From Allegrini et al. (2022)

exponentially toward the surface and reach 10^{-5} – 10^{-3} S m^{-1} and can be large enough to support cross-magnetic field currents, while the field-aligned conductivity is around 50 S m^{-1} and can easily support field-aligned currents. What seems to be present is a very dense and cold (a few eV to 10 eV) (Frank et al. 1997; Collinson et al. 2018; Allegrini et al. 2022) “topside like” ionospheric plasma which is dominantly magnetized even close to the surface. Magnetospheric “E cross B” drift convection fields, mapped from the magnetosphere down to the ionosphere, primarily in the auroral zones, would not only be reduced by ion-neutral collisions, but also heat the local ion population. The magnetosphere-ionosphere coupling is therefore in a domain not yet encountered before in the Solar System with a limited but finite conductivity near the surface.

Ion composition is a marker of neutral composition and provides evidence of ion-neutral chemistry. The interpretation of *Galileo*/PLS has demonstrated the presence of light (e.g., H^+ , H_2^+) and heavier (e.g., O^+ , O_2^+) ions (Carnielli et al. 2020a). This finding was confirmed by observations from *Juno*/JADE ion spectrograms (Allegrini et al. 2022; Valek et al. 2022). Though water and atomic oxygen ions could not be distinguished due to the limited mass resolution, the detection of H_3^+ by *Juno*/JADE during PJ34 attests of ion-neutral chemistry (see Fig. 18). *JUICE* will be capable of measuring ion composition, distinguishing between H_2O^+ and H_3O^+ , though for energies below 5 eV (Föhn et al. 2021). This will be complemented by measurements of the 3D ion velocity distribution (1 eV to 50 keV). Detected ENAs will be sensitive to both energetic molecular and atomic neutrals produced through ion-neutral charge-exchange (Carnielli et al. 2020a).

Due to the presence of intense electric fields, newly born ions in Ganymede’s ionosphere can be accelerated up to 10 s of keV (Carnielli et al. 2019). It is hence critical to assess ionospheric dynamics in order to interpret ionospheric densities and temperatures. 3D test-particle simulations of the ionospheric ions, driven by electric and magnetic fields from an MHD model (Jia et al. 2009), have been applied to the *Galileo* G2 flyby. The simulated shape of the ion energy spectra agrees well with that from *Galileo*/PLS measurements, validating the 3D configuration of the fields in which the ions evolve (Carnielli et al. 2020a). However, this comparison can only be extended to a handful of flybys from *Galileo* and one from *Juno*. Little is known on how ionospheric dynamics is affected by Jovian magnetospheric

and Ganymede's orbital conditions. *JUICE* will quantify ion transport through concurrent measurements of ion distribution, ion bulk velocity, and electric and magnetic fields.

In terms of peak ionospheric densities, *Galileo*'s Plasma Wave Subsystem detected peak electron densities of $\sim 200 \text{ cm}^{-3}$ during the G2 flyby, at an altitude of $\sim 260 \text{ km}$, and $\sim 40 \text{ cm}^{-3}$ during the G1 flyby, at an altitude of about 790 km (Eviatar et al. 2001a). Only one of *Galileo*'s eight Ganymede radio occultations resulted in a strong detection of an ionosphere (Kliore et al. 2001; McGrath et al. 2004). This was from the G8 flyby (Kliore 1998) which yielded a peak electron density of $\sim 5000 \pm 1500 (1-\sigma) \text{ cm}^{-3}$ near the surface. Radio occultation data from the *Juno*'s Ganymede flyby PJ34 resulted in the detection of a peak electron density of $2000 \pm 500 (1-\sigma) \text{ cm}^{-3}$ near the surface during ingress, and no statistically significant ionosphere during egress (Buccino et al. 2022). Electron densities from plasma wave measurements gave a peak density on the dayside of 30 cm^{-3} near closest approach around 1000 km (Kurth et al. 2022). The total ion density from the mass spectrometer was found to be ~ 2.5 times larger at closest approach (Valek et al. 2022). The very limited available dataset highlights inconsistencies in the observed plasma density profiles and peak densities. Furthermore, *Galileo* multi-instrument analysis has highlighted inconsistencies between exospheric simulations and plasma observations (Carnielli et al. 2020a). *JUICE* radio occultations and *in situ* measurements over a range of orbits will make an invaluable contribution in this area. We will also take advantage of occultations of Jupiter's auroral radio emissions by Ganymede's ionosphere (Cecconi et al. 2021).

Galileo detected tenuous dust clouds surrounding Ganymede (Krüger et al. 1999, 2000, 2003). The observed μm sized dust grains are gravitationally captured by the moon within $\sim 5 R_G$. Near Ganymede, grain dynamics is affected by Jupiter's gravity, and the continuous dust ejection from the surface is needed for dust clouds to form, possibly resulting from hypervelocity impacts of interplanetary dust. Such surface impacts could also be a source of plasma. Alternatively, electromagnetic forces can alter the charged grain motion into non-Keplerian. *JUICE* will investigate the dust environment and origin of the dust cloud, as well as dust impact on the surface, atmosphere, and plasma around Ganymede. This will include assessment of the potential effect of dust on the plasma through the presence of negatively charged ions, as seen at Enceladus (Coates et al. 2010).

As introduced in Sect. 5.3., Ganymede's ionosphere is electrodynamically coupled to the surrounding magnetosphere. We expect electrostatic acceleration structures, Alfvén waves and other plasma waves to both accelerate and heat charged particles along the auroral field lines above the ionosphere. The ions are expected to be transversely heated and be expelled by the magnetic mirror force out toward the magnetosphere (e.g., Winsor et al. 1989; Wahlund et al. 1992), leading to plasma cavities in the topside ionosphere that in turn allow for more intense electric field structures that accelerate electrons to higher energies (so called "inverted V's"). Alfvén waves generated in the magnetosphere propagate down the field lines and hit the sharp density gradients within the cavities, becoming dispersive, and through smaller scale broadband plasma waves transfer their energy to field-aligned electron beams and transverse ion acceleration (Louarn et al. 1994; Wahlund et al. 1994, 1998; André et al. 1998; Stasiewicz et al. 2000; Strangeway et al. 2005; Zheng et al. 2005; Chaston et al. 2007). These processes mediate the field-aligned currents that couple to the transverse currents in the ionosphere (part of the auroral electrojet). A similar set of processes occurs in the Alfvén wings connected to Ganymede, where strong gradients also play a role in the generation of Alfvén wave activity on magnetic flux tubes that connect to Jupiter's ionosphere. In this area, limited insight has been provided by *Galileo* and *Juno* (Gurnett et al. 1996; Kurth et al. 2022), but complementary plasma, particle, field & UV measurements by *JUICE* are expected to dramatically change our view.

Transport is driving ionospheric plasma. In a given region, ions can originate from different parts of Ganymede's ionosphere, e.g., produced locally or transported into this region. Hence, they have undergone different levels of acceleration and ion temperature can be large, as high as a few 100 s eV in the equatorial regions for heavy ions (Carnielli et al. 2019). Dynamics is playing a key role in driving ion temperature though the details of it remain to be confirmed. Ion heating is also expected in the auroral zone through, e.g., reconnection and due to waves. Little is known concerning electron temperature, which has never been measured or simulated. It will however be a critical for determining the frequency of electron collisions with neutral particles, a key source of cooling, while heating sources include electron-electron Coulomb collisions, acceleration through the field, and wave-particle interactions. Heat flow from the magnetosphere could also affect the ionospheric energy budget. *JUICE* will offer the first opportunity to assess the plasma energy budget over a large range of latitudes, longitudes, and magnetospheric conditions.

Ionospheric ions impact Ganymede's surface and contribute as a source of the moon's atmosphere. So far only sublimation of water ice and irradiation of Ganymede's surface by Jovian ions have been considered as a primary source of neutrals in exospheric models of Ganymede (Marconi 2007; Plainaki et al. 2015; Leblanc et al. 2017; Vorburger et al. 2022). While the former generates a localised H₂O-dominated exosphere around the sub-solar point, the latter leads to the release of O₂ and H₂ through radiolysis and induces an O₂-dominated global exosphere. Irradiation of Ganymede's surface by ionospheric ions particularly affects equatorial regions; its contribution to the neutral release rates was found to dominate by a factor of 5–10 compared to the Jovian ion contribution (Carnielli et al. 2020b). However, large uncertainties in these rates remain due to poorly constrained exospheric densities. There is also an inconsistency between the total release rate assumed in exospheric models and that estimated from kinetic, ion simulations of ionospheric and Jovian ions. Assessment of ionospheric vs Jovian particle contributions as a source of the exosphere will be made by *JUICE* using particle measurements as a basis (Plainaki et al. 2022). The identification of open and closed field line regions, surface composition, and atmospheric densities will all factor into this important assessment.

6 High-Level Operations Strategy

The *JUICE* mission has a wide range of science investigations, extending well beyond those listed in Table 1 that are relevant for the magnetosphere and plasma science that we have reviewed. Spacecraft operations, both during the cruise and after we arrive at the Jupiter system are carefully planned to ensure that all objectives are met, spanning all four of the mission's science working groups, often requiring non-trivial technical and scheduling problems to be solved (Fletcher et al. 2023; Boutonnet et al. 2024; Tosi et al. 2024; Van Hoolst 2024; Witasse et al. 2025, all in this collection). To guide this critical exercise, recommendations for operations necessary to achieve all magnetosphere and plasma science objectives (see Table 1) have been made. This operational strategy is described at a high level here. Actual spacecraft operations represent the result of a careful assessment of a wider range of recommendations.

The primary issue for magnetosphere and plasma science with *JUICE* is the importance of continuous operation of *in situ* instruments, namely PEP, J-MAG, and RPWI (see Table 2). This includes during communication windows, short eclipses, etc. As we have seen, all the space plasma environments of interest (and space plasma environments in general) display significant variability in both space and time. Present understanding of these systems

is nowhere near sufficient to allow us to accurately predict dynamics, one of the ultimate goals of research in this broad field. Observing these dynamics, including extreme, transient events that are infrequent, is central to all of *JUICE*'s magnetosphere and science investigations. This leads to the strong recommendation for continuous operation of the instruments that monitor the plasma and electromagnetic fields. The synergy of PEP, J-MAG, and RPWI measurements is required for a comprehensive view of the magnetised plasma around the spacecraft. Note that the cadence of measurements providing continuous operation need not be the highest possible with each instrument, compared to measurements during specific science events when higher cadences are required. Continuous operation of the three *in situ* instruments at relatively low measurement cadence will underpin a large fraction of *JUICE*'s promised magnetosphere and plasma science. Wherever possible, spacecraft attitude will allow sensors fields-of-view that are needed to observe particle flows, for example.

On top of continuous operation, higher cadence measurements by the three *in situ* instruments will be needed during specific events that will occur following Jupiter orbit insertion, in order to allow the necessary science. While in Jupiter orbit, this includes during intervals when we pass through the region of corotation breakdown, intervals during the high-latitude orbits that provide favourable viewing for ENA imaging, for example, and surrounding planned moon flybys when *in situ* instruments need appropriate spacecraft attitude for instrument pointing. While in Ganymede orbit, higher data cadences will be needed when crossing the thin current sheets and the OCFB in Ganymede's magnetosphere. High quality UVS observations of Ganymede's auroral emissions at these crossing points will likewise be needed.

There will be important opportunities for remote sensing that is also central to ensuring science return in this area of magnetosphere and plasma science. Multi-wavelength observations of both Jupiter's auroral emissions (Fletcher et al. 2023) and Ganymede's auroral emissions by the JANUS, MAJIS, RPWI, and UVS instruments will provide important information about the space plasma physics that is responsible, providing a diagnostic of the physics at work on larger scales. As we have seen, radio occultations have proved to be a powerful tool for understanding ionospheres and plasma structures like moon tori in the Jupiter system in the past, and *JUICE* will enable a significant expansion to the existing volume of such measurements. Instruments such as 3GM, PRIDE, and the instruments mentioned above will make new measurements possible. Numerous UVS stellar occultation measurements of the neutral atmospheric structure will be needed to analyse these ionospheres and plasma structures. A particularly exciting opportunity provided by *JUICE* will be remote sensing of the global space plasma environment via ENA imaging. This has never been done at Jupiter before, and will address a key challenge when trying to understand these tenuous magnetised plasmas: Our limited ability to image them. In synergy with *in situ* measurements, *JUICE*'s ENA imaging will reveal dynamic magnetospheres in ways we have not been able to previously. Across all this relevant remote sensing, operations will satisfy pointing requirements and be conducted during identified intervals with favourable geometry.

Solar wind measurements by the *in situ* instruments during approach to Jupiter will be particularly important for *JUICE*-era understanding of Jupiter's magnetosphere and the environment around each Galilean moon. The state of the solar wind is unpredictable, but large-scale structures show some repeatability with solar rotation over ~ 27 days. Given that the spacecraft will not sample the solar wind after the opening orbits around Jupiter, this initial characterisation of the solar wind is therefore particularly important to support science return in this area. Upstream measurements spanning multiple solar rotations is desirable, to allow a valuable assessment of the predictability of the large-scale solar wind state.

In parallel with the new observations that will be made by *JUICE* instruments, theory and numerical models will remain essential for progress in this field. Such models will provide the context needed for new information obtained *in situ*, and provide a broader, physics-based picture of complex space plasma systems. Models will range from global models of Jupiter's magnetosphere and its interaction with the solar wind, down to local models of the environment immediately surrounding each Galilean moon. Because of this, the *JUICE* modelling community will employ a range of approaches, from fluid descriptions of the magnetised plasma to solving the equation of motion for individual charged particles.

7 Summary & Outlook

At the time of writing the *JUICE* spacecraft is en route to the Jupiter system. As we have reviewed in this article, *JUICE* is designed to enable significant advances in the field of magnetosphere and space plasma science. While the science return in this area will be broad, two areas in particular are worthy of special mention. Firstly, *JUICE*'s measurement capabilities mean that throughout Jupiter's equatorial magnetosphere, including within the region of corotation breakdown, the mission will allow a step change in understanding this important region. Highly relevant for this area is ENA imaging, which will be carried out at Jupiter for the first time. Secondly, Ganymede's magnetosphere is a distinct system within a system, barely explored and utterly unlike the surrounding Jovian magnetosphere. *JUICE*'s orbits around Ganymede will lead to a surge forward in the boundary of our understanding of the Solar System's only known moon magnetosphere.

In the coming years leading up to arrival at Jupiter in 2031 a number of critical activities must run, from the magnetospheric science perspective of this paper. A modelling framework comprised of many individual models and which carefully considers the coupling between them must be in place by Jupiter orbit insertion in order to avoid a delay in full magnetospheric science return. While not considered here, the combination of the *JUICE* and Europa Clipper missions offers unique opportunities for multi-point measurements that will allow unique magnetosphere and plasma science; for example, measurements by both spacecraft inside Jupiter's magnetosphere would provide a powerful tool for separating spatial and temporal effects when studying magnetospheric dynamics. We strongly support interaction between these two projects to take advantage of such opportunities. At the time of writing, *JUICE* is carrying out its interplanetary cruise to Jupiter. In addition to operations required to calibrate different instruments before arrival, measurements during cruise will provide additional heliospheric science, such as the study of coronal mass ejections from Earth to Jupiter's orbit.

Acknowledgements We would like to sincerely thank the entire ESA *JUICE* project, Airbus partners, and many members of the international scientific community. In particular, we are grateful to both the project and Airbus for designing and building such an electromagnetically clean spacecraft. AMA was supported by a Royal Society University Research Fellowship. MH acknowledges support from the Science Foundation Ireland (Grant: 18/FRL/6199) and the Discovery programme of the European Space Agency (Contract No: 4000137683/22/NL/GLC/my). HH's work at DIAS was supported by a DIAS Research Fellowship in Astrophysics and by Taighde Éireann - Research Ireland award 22/FFP-P/11545. HH gratefully acknowledges financial support from Khalifa University's Space and Planetary Science Center (Abu Dhabi, UAE) under Grant no. KU-SPSC- 8474000336. We thank Stephenie Brophy Lee for designing the schematic illustrating Europa's interaction with the surrounding Jovian magnetosphere, (Fig. 11). AC and GJ acknowledge support from UK STFC consolidated grant ST/W001004/1 to UCL-MSSL. AG and PW were supported by the AV Swiss National Science Foundation under grant 200020_207409. DH was supported by the German Aerospace Center (Deutsches Zentrum für Luft- und Raumfahrt, DLR) through grant number 50QJ1501. LB, LI, AM, PT, MZ and AMo are grateful to the Italian Space Agency (ASI) for financial support through

ASI-INAF agreements No. 2018-25-HH.0 and 2023-6-HH.0 in the context of ESA's *JUICE* mission. YK is supported by JSPS KAKENHI Grants JP18H03727, JP21H04520, JP23H01229 and JP23H05429. French authors acknowledge support from CNES and CNRS/INSU national programs of planetology (PNP) and heliophysics (PNST, also funded by CEA). JS received funding from the European Research Council (ERC) under the European Union's Horizon 2020 research and innovation programme (grant agreement No. 884711).

Declarations

Competing Interests The authors have no relevant financial or non-financial interests to disclose.

Open Access This article is licensed under a Creative Commons Attribution 4.0 International License, which permits use, sharing, adaptation, distribution and reproduction in any medium or format, as long as you give appropriate credit to the original author(s) and the source, provide a link to the Creative Commons licence, and indicate if changes were made. The images or other third party material in this article are included in the article's Creative Commons licence, unless indicated otherwise in a credit line to the material. If material is not included in the article's Creative Commons licence and your intended use is not permitted by statutory regulation or exceeds the permitted use, you will need to obtain permission directly from the copyright holder. To view a copy of this licence, visit <http://creativecommons.org/licenses/by/4.0/>.

References

- Achilleos N, André N, Blanco-Cano X, et al (2015) Transport of mass, momentum and energy in planetary magnetodisc regions. *Space Sci Rev* 187:229–299. <https://doi.org/10.1007/s11214-014-0086-y>
- Addison P, Liuzzo L, Arnold H, Simon S (2021) Influence of Europa's time-varying electromagnetic environment on magnetospheric ion precipitation and surface weathering. *JGR Space Phys* 126:e2020JA029087. <https://doi.org/10.1029/2020JA029087>
- Addison P, Liuzzo L, Simon S (2022) Effect of the magnetospheric plasma interaction and solar illumination on ion sputtering of Europa's surface ice. *JGR Space Phys* 127:e2021JA030136. <https://doi.org/10.1029/2021JA030136>
- Addison P, Haynes CM, Stahl AM, Liuzzo L, Simon S (2024) Magnetic signatures of the interaction between Europa and Jupiter's magnetosphere during the Juno flyby. *Geophys Res Lett* 51:e2023GL106810. <https://doi.org/10.1029/2023GL106810>
- Allegrini F, Gladstone GR, Hue V, et al (2020) First report of electron measurements during a Europa footprint tail crossing by Juno. *Geophys Res Lett* 47:e2020GL089732. <https://doi.org/10.1029/2020GL089732>
- Allegrini F, Bagenal F, Ebert RW, et al (2022) Plasma observations during the 7 June 2021 Ganymede flyby from the Jovian auroral distributions experiment (JADE) on Juno. *Geophys Res Lett* 49:e2022GL098682. <https://doi.org/10.1029/2022GL098682>
- Allegrini F, Saur J, Szalay JR, Ebert RW, Kurth WS, Cervantes S, et al (2024) Electron beams at Europa. *Geophys Res Lett* 51:e2024GL108422. <https://doi.org/10.1029/2024GL108422>
- Allen RC, Paranicas CP, Bagenal F, et al (2019) Energetic oxygen and sulfur charge states in the outer Jovian magnetosphere: insights from the Cassini Jupiter flyby. *Geophys Res Lett* 46:11709–11717. <https://doi.org/10.1029/2019GL085185>
- André M, Norqvist P, Andersson L, et al (1998) Ion energization mechanisms at 1700 km in the auroral region. *J Geophys Res* 103:4199–4222. <https://doi.org/10.1029/97JA00855>
- André N, Dougherty MK, Russell CT, et al (2005) Dynamics of the saturnian inner magnetosphere: first inferences from the Cassini magnetometers about small-scale plasma transport in the magnetosphere. *Geophys Res Lett* 32:2005GL022643. <https://doi.org/10.1029/2005GL022643>
- Arnold H, Liuzzo L, Simon S (2019) Magnetic signatures of a plume at Europa during the Galileo E26 flyby. *Geophys Res Lett* 46:1149–1157. <https://doi.org/10.1029/2018GL081544>
- Bagenal F (1994) Empirical model of the Io plasma torus: Voyager measurements. *J Geophys Res* 99:11043–11062. <https://doi.org/10.1029/93JA02908>
- Bagenal F, Delamere PA (2011) Flow of mass and energy in the magnetospheres of Jupiter and Saturn: mass and energy. *J Geophys Res* 116. <https://doi.org/10.1029/2010JA016294>
- Bagenal F, Dols V (2020) The space environment of Io and Europa. *JGR Space Phys* 125:e2019JA027485. <https://doi.org/10.1029/2019JA027485>
- Bagenal F, Sullivan JD (1981) Direct plasma measurements in the Io torus and inner magnetosphere of Jupiter. *J Geophys Res* 86:8447–8466. <https://doi.org/10.1029/JA086iA10p08447>

- Bagenal F, Crary FJ, Stewart AIF, et al (1997) Galileo measurements of plasma density in the Io torus. *Geophys Res Lett* 24:2119–2122. <https://doi.org/10.1029/97GL01254>
- Bagenal F, Dowling TE, McKinnon WB (2004) Jupiter: the planet, satellites and magnetosphere. Cambridge university Press, Cambridge
- Bagenal F, Sidrow E, Wilson RJ, et al (2015) Plasma conditions at Europa's orbit. *Icarus* 261:1–13. <https://doi.org/10.1016/j.icarus.2015.07.036>
- Bagenal F, Wilson RJ, Siler S, et al (2016) Survey of Galileo plasma observations in Jupiter's plasma sheet. *JGR Planets* 121:871–894. <https://doi.org/10.1002/2016JE005009>
- Bagenal F, Adriani A, Allegrini F, et al (2017a) Magnetospheric science objectives of the Juno mission. *Space Sci Rev* 213:219–287. <https://doi.org/10.1007/s11214-014-0036-8>
- Bagenal F, Dougherty LP, Bodisch KM, et al (2017b) Survey of Voyager plasma science ions at Jupiter: 1. Analysis method. *JGR Space Phys* 122:8241–8256. <https://doi.org/10.1002/2016JA023797>
- Barabash S, Bhardwaj A, Wieser M, et al (2009) Investigation of the solar wind–Moon interaction onboard Chandrayaan-1 mission with the SARA experiment. *Curr Sci* 96:526–532
- Barbosa DD (1994) Neutral cloud theory of the Jovian nebula: anomalous ionization effect of superthermal electrons. *Astrophys J* 430:376. <https://doi.org/10.1086/174413>
- Barbosa DD, Kivelson MG (1983) Dawn-dusk electric field asymmetry of the Io plasma torus. *Geophys Res Lett* 10:210–213. <https://doi.org/10.1029/GL010i003p00210>
- Belcher JW, Goertz CK, Bridge HS (1980) The low energy plasma in the Jovian magnetosphere. *Geophys Res Lett* 7:17–20. <https://doi.org/10.1029/GL007i001p00017>
- Bigg EK (1964) Influence of the satellite Io on Jupiter's decametric emission. *Nature* 203:1008–1010. <https://doi.org/10.1038/2031008a0>
- Bird MK, Asmar SW, Brenkle JP, et al (1992) Ulysses radio occultation observations of the Io plasma torus during the Jupiter encounter. *Science* 257:1531–1535. <https://doi.org/10.1126/science.257.5076.1531>
- Birmingham TJ (1982) Charged particle motions in the distended magnetospheres of Jupiter and Saturn. *J Geophys Res* 87:7421–7430. <https://doi.org/10.1029/JA087iA09p07421>
- Blöcker A, Saur J, Roth L (2016) Europa's plasma interaction with an inhomogeneous atmosphere: development of Alfvén winglets within the Alfvén wings. *JGR Space Phys* 121:9794–9828. <https://doi.org/10.1002/2016JA022479>
- Bodisch KM, Dougherty LP, Bagenal F (2017) Survey of Voyager plasma science ions at Jupiter: 3. Protons and minor ions. *JGR Space Phys* 122:8277–8294. <https://doi.org/10.1002/2017JA024148>
- Bolton SJ, Lunine J, Stevenson D, et al (2017) The Juno mission. *Space Sci Rev* 213:5–37. <https://doi.org/10.1007/s11214-017-0429-6>
- Bonfond B, Hess S, Bagenal F, Gérard JC, Grodent D, Radioti A, et al (2013) The multiple spots of the Ganymede auroral footprint. *Geophys Res Lett* 40:4977–4981. <https://doi.org/10.1002/grl.50989>
- Bonfond B, Yao Z, Grodent D (2020) Six pieces of evidence against the corotation enforcement theory to explain the main aurora at Jupiter. *JGR Space Phys* 125:e2020JA028152. <https://doi.org/10.1029/2020JA028152>
- Bonfond B, Yao ZH, Gladstone GR, et al (2021) Are dawn storms Jupiter's auroral substorms?. *AGU Adv* 2:e2020AV000275. <https://doi.org/10.1029/2020AV000275>
- Boutonnet A, Langevin Y, Erd C, et al (2024) Designing the JUICE trajectory. *Space Sci Rev* 220:67. <https://doi.org/10.1007/s11214-024-01093-y>
- Brandt PC, Paranicas CP, Carbary JF, et al (2008) Understanding the global evolution of Saturn's ring current. *Geophys Res Lett* 35:2008GL034969. <https://doi.org/10.1029/2008GL034969>
- Brandt PC, Khurana KK, Mitchell DG, et al (2010) Saturn's periodic magnetic field perturbations caused by a rotating partial ring current. *Geophys Res Lett* 37:2010GL045285. <https://doi.org/10.1029/2010GL045285>
- Brandt PC (2021) Global energetic neutral atom (ENA) imaging of magnetospheres. In: Maggiolo R, André N, Hasegawa H, et al (eds) *Geophysical monograph series*, 1st edn. Wiley, New York, pp 673–698
- Breer BR, Liuzzo L, Arnold H, et al (2019) Energetic ion dynamics in the perturbed electromagnetic fields near Europa. *JGR Space Phys* 124:7592–7613. <https://doi.org/10.1029/2019JA027147>
- Broadfoot AL, Belton MJS, Takacs PZ, et al (1979) Extreme ultraviolet observations from Voyager 1 encounter with Jupiter. *Science* 204:979–982. <https://doi.org/10.1126/science.204.4396.979>
- Buccino DR, Parisi M, Gramigna E, et al (2022) Ganymede's ionosphere observed by a dual-frequency radio occultation with Juno. *Geophys Res Lett* 49:e2022GL098420. <https://doi.org/10.1029/2022GL098420>
- Burke BF, Franklin KL (1955) Observations of a variable radio source associated with the planet Jupiter. *J Geophys Res* 60:213–217. <https://doi.org/10.1029/JZ060i002p00213>
- Carberry Mogan SR, (2022) *Advancing the State-of-the-Art of Modeling Callisto's Atmosphere*. ProQuest Dissertations and Thesis; Thesis (Ph.D.)—New York University Tandon School of Engineering, 2022.; Publication Number: AAT 29208163; ISBN: 9798802702734; Source: Dissertations Abstracts International, Volume: 83-12, Section: B.; 190 p

- Carberry Mogan SR, Tucker OJ, Johnson RE, et al (2021) A tenuous, collisional atmosphere on Callisto. *Icarus* 368:114597. <https://doi.org/10.1016/j.icarus.2021.114597>
- Carberry Mogan SR, Liuzzo L, Poppe AR, et al (2023) Callisto's atmosphere: the oxygen enigma. *JGR Planets* 128:e2023JE007894. <https://doi.org/10.1029/2023JE007894>
- Carlson RW (1999) A tenuous carbon dioxide atmosphere on Jupiter's Moon Callisto. *Science* 283:820–821. <https://doi.org/10.1126/science.283.5403.820>
- Carnielli G, Galand M, Leblanc F, et al (2019) First 3D test particle model of Ganymede's ionosphere. *Icarus* 330:42–59. <https://doi.org/10.1016/j.icarus.2019.04.016>
- Carnielli G, Galand M, Leblanc F, et al (2020a) Constraining Ganymede's neutral and plasma environments through simulations of its ionosphere and Galileo observations. *Icarus* 343:113691. <https://doi.org/10.1016/j.icarus.2020.113691>
- Carnielli G, Galand M, Leblanc F, et al (2020b) Simulations of ion sputtering at Ganymede. *Icarus* 351:113918. <https://doi.org/10.1016/j.icarus.2020.113918>
- Cassidy TA, Paranicas CP, Shirley JH, et al (2013) Magnetospheric ion sputtering and water ice grain size at Europa. *Planet Space Sci* 77:64–73. <https://doi.org/10.1016/j.pss.2012.07.008>
- Cecconi B, Zarka P (2005) Direction finding and antenna calibration through analytical inversion of radio measurements performed using a system of two or three electric dipole antennas on a three-axis stabilized spacecraft. *Radio Sci* 40:2004RS003070. <https://doi.org/10.1029/2004RS003070>
- Cecconi B, Louis CK, Muñoz Crego C, Vallat C (2021) Jovian auroral radio source occultation modelling and application to the JUICE science mission planning. *Planet Space Sci* 209:105344. <https://doi.org/10.1016/j.pss.2021.105344>
- Cervantes S, Saur J (2022) Constraining Europa's subsolar atmosphere with a joint analysis of HST spectral images and Galileo magnetic field data. *JGR Space Phys* 127:e2022JA030472. <https://doi.org/10.1029/2022JA030472>
- Chaston CC, Carlson CW, McFadden JP, et al (2007) How important are dispersive Alfvén waves for auroral particle acceleration? *Geophys Res Lett* 34:2006GL029144. <https://doi.org/10.1029/2006GL029144>
- Cheng AF (1980) Effects of Io's volcanos on the plasma torus and Jupiter's magnetosphere. *Astrophys J* 242:812–827. <https://doi.org/10.1086/158516>
- Clark G, Mauk BH, Paranicas C, et al (2016) Charge states of energetic oxygen and sulfur ions in Jupiter's magnetosphere. *JGR Space Phys* 121:2264–2273. <https://doi.org/10.1002/2015JA022257>
- Clark G, Mauk BH, Haggerty D, et al (2017) Energetic particle signatures of magnetic field-aligned potentials over Jupiter's polar regions. *Geophys Res Lett* 44:8703–8711. <https://doi.org/10.1002/2017GL074366>
- Clark G, Tao C, Mauk BH, et al (2018) Precipitating electron energy flux and characteristic energies in Jupiter's main auroral region as measured by Juno/JEDI. *JGR Space Phys* 123:7554–7567. <https://doi.org/10.1029/2018JA025639>
- Clark G, Mauk BH, Kollmann P, et al (2020) Heavy ion charge states in Jupiter's polar magnetosphere inferred from auroral megavolt electric potentials. *JGR Space Phys* 125:e2020JA028052. <https://doi.org/10.1029/2020JA028052>
- Clark G, Kollmann P, Mauk BH, et al (2022) Energetic charged particle observations during Juno's close flyby of Ganymede. *Geophys Res Lett* 49:e2022GL098572. <https://doi.org/10.1029/2022GL098572>
- Clarke JT, Ballester G, Trauger J, et al (1998) Hubble Space Telescope imaging of Jupiter's UV aurora during the Galileo orbiter mission. *J Geophys Res* 103:20217–20236. <https://doi.org/10.1029/98JE01130>
- Clarke JT, Ajello J, Ballester G, et al (2002) Ultraviolet emissions from the magnetic footprints of Io, Ganymede and Europa on Jupiter. *Nature* 415:997–1000
- Clarke JT, Grodent D, Cowley SWH, et al (2004) Jupiter's aurora. In: Bagenal F, Dowling TE, McKinnon WB (eds) *Jupiter: the planet, satellites and magnetosphere*. Cambridge University Press, Cambridge
- Coates AJ, Jones GH, Lewis GR, et al (2010) Negative ions in the Enceladus plume. *Icarus* 206:618–622. <https://doi.org/10.1016/j.icarus.2009.07.013>
- Cohen CMS, Stone EC, Selesnick RS (2001) Energetic ion observations in the middle Jovian magnetosphere. *J Geophys Res* 106:29871–29881. <https://doi.org/10.1029/2001JA000008>
- Collett B, Lamy L, Louis CK, et al (2023) Characterization of Jovian hectometric sources with Juno: statistical position and generation by shell-type electrons. In: Louis CK, Jackman CM, Fischer G, Sulaiman AH, Zucca P (eds) *Planetary, solar and heliospheric radio emissions IX*. Dublin Institute for Advanced Studies, Trinity College Dublin, Dublin
- Collinson G, Paterson WR, Bard C, et al (2018) New results from Galileo's first flyby of Ganymede: reconnection-driven flows at the low-latitude magnetopause boundary, crossing the cusp, and icy ionospheric escape. *Geophys Res Lett* 45:3382–3392. <https://doi.org/10.1002/2017GL075487>
- Connerney JEP, Kotsiaros S, Oliverson RJ, et al (2018) A new model of Jupiter's magnetic field from Juno's first nine orbits. *Geophys Res Lett* 45:2590–2596. <https://doi.org/10.1002/2018GL077312>
- Connerney JEP, Timmins S, Hecceg M, Joergensen JL (2020) A Jovian magnetodisc model for the Juno era. *JGR Space Phys* 125:e2020JA028138. <https://doi.org/10.1029/2020JA028138>

- Connerney JEP, Timmins S, Oliverson RJ, et al (2022) A new model of Jupiter's magnetic field at the completion of Juno's prime mission. *JGR Planets* 127:e2021JE007055. <https://doi.org/10.1029/2021JE007055>
- Cooper J (2001) Energetic ion and electron irradiation of the icy Galilean satellites. *Icarus* 149:133–159. <https://doi.org/10.1006/icar.2000.6498>
- Cowley SWH, Bunce EJ (2001) Origin of the main auroral oval in Jupiter's coupled magnetosphere–ionosphere system. *Planet Space Sci* 49:1067–1088. [https://doi.org/10.1016/S0032-0633\(00\)00167-7](https://doi.org/10.1016/S0032-0633(00)00167-7)
- Cummings WD O'Sullivan RJ Coleman PJ (1969) Standing Alfvén waves in the magnetosphere. *J Geophys Res* 74:778–793. <https://doi.org/10.1029/JA074i003p00778>
- Cunningham NJ, Spencer JR, Feldman PD, et al (2015) Detection of Callisto's oxygen atmosphere with the Hubble Space Telescope. *Icarus* 254:178–189. <https://doi.org/10.1016/j.icarus.2015.03.021>
- Damiano PA, Delamere PA, Stauffer B, et al (2019) Kinetic simulations of electron acceleration by dispersive scale Alfvén waves in Jupiter's magnetosphere. *Geophys Res Lett* 46:3043–3051. <https://doi.org/10.1029/2018GL081219>
- Davis MR, Meier RM, Cooper JF, Loeffler MJ (2021) The contribution of electrons to the sputter-produced O₂ exosphere on Europa. *Astrophys J Lett* 908:L53
- Dayton-Oxland R, Huybrighs HLF, Winterhalder TO, et al (2023) In-situ detection of Europa's water plumes is Harder than previously thought. *Icarus* 395:115488. <https://doi.org/10.1016/j.icarus.2023.115488>
- De Becker A, Head LA, Bonfond B, et al (2023) A study of Io's sodium jets with the TRAPPIST telescopes. *Astron Astrophys* 680:A3. <https://doi.org/10.1051/0004-6361/202347447>
- De Kleer K, Nimmo F, Kite E (2019) Variability in Io's volcanism on timescales of periodic orbital changes. *Geophys Res Lett* 46:6327–6332. <https://doi.org/10.1029/2019GL082691>
- Delamere PA, Bagenal F (2003) Modeling variability of plasma conditions in the Io torus. *J Geophys Res* 108:2002JA009706. <https://doi.org/10.1029/2002JA009706>
- Delamere PA, Steffl A, Bagenal F (2004) Modeling temporal variability of plasma conditions in the Io torus during the Cassini era. *J Geophys Res* 109:2003JA010354. <https://doi.org/10.1029/2003JA010354>
- Delamere PA, Bagenal F, Steffl A (2005) Radial variations in the Io plasma torus during the Cassini era. *J Geophys Res* 110:2005JA011251. <https://doi.org/10.1029/2005JA011251>
- Delva M, Volwerk M, Mazelle C, et al (2009) Hydrogen in the extended Venus exosphere. *Geophys Res Lett* 36:2008GL036164. <https://doi.org/10.1029/2008GL036164>
- Desai RT, Cowee MM, Wei H, et al (2017) Hybrid simulations of positively and negatively charged pickup ions and cyclotron wave generation at Europa. *J Geophys Res* 122:10,408–10,420. <https://doi.org/10.1002/2017JA024479>
- Dessler AJ (1983) *Physics of the Jovian magnetosphere*. Cambridge University Press, Cambridge
- Dessler AJ, Sandel BR (1992) System III variations in apparent distance of Io plasma torus from Jupiter. *Geophys Res Lett* 19:2099–2102. <https://doi.org/10.1029/92GL02380>
- Dessler AJ, Sandel BR (1993) Reply [to “Comment on ‘System III variations in apparent distance of Io plasma torus from Jupiter’”]. *Geophys Res Lett* 20:2489–2490. <https://doi.org/10.1029/93GL02429>
- Dols VJ, Bagenal F, Cassidy TA, et al (2016) Europa's atmospheric neutral escape: importance of symmetrical O₂ charge exchange. *Icarus* 264:387–397. <https://doi.org/10.1016/j.icarus.2015.09.026>
- Dorelli JC, Gloer A, Collinson G, Tóth G (2015) The role of the Hall effect in the global structure and dynamics of planetary magnetospheres: Ganymede as a case study. *JGR Space Phys* 120:5377–5392. <https://doi.org/10.1002/2014JA020951>
- Dougherty LP, Bodisch KM, Bagenal F (2017) Survey of Voyager plasma science ions at Jupiter: 2. Heavy ions. *JGR Space Phys* 122:8257–8276. <https://doi.org/10.1002/2017JA024053>
- Duling S, Saur J, Clark G, Allegrini F, Greathouse T, Gladstone R, et al (2022) Ganymede MHD model: magnetospheric context for Juno's PJ34 flyby. *Geophys Res Lett* 49:e2022GL101688. <https://doi.org/10.1029/2022GL101688>
- Dumont M, Grodent D, Radioti A, et al (2014) Jupiter's equatorward auroral features: Possible signatures of magnetospheric injections. *JGR Space Phys* 119. <https://doi.org/10.1002/2014JA020527>
- Dunn WR, Branduardi-Raymont G, Ray LC, et al (2017) The independent pulsations of Jupiter's northern and southern X-ray auroras. *Nat Astron* 1:758–764. <https://doi.org/10.1038/s41550-017-0262-6>
- Ebert RW, Allegrini F, Bagenal F, et al (2017) Accelerated flows at Jupiter's magnetopause: evidence for magnetic reconnection along the dawn flank. *Geophys Res Lett* 44:4401–4409. <https://doi.org/10.1002/2016GL072187>
- Ebert RW, Fuselier SA, Allegrini F, Bagenal F, Bolton SJ, Clark G, et al (2022) Evidence for magnetic reconnection at Ganymede's upstream magnetopause during the PJ34 Juno flyby. *Geophys Res Lett* 49:e2022GL099775. <https://doi.org/10.1029/2022GL099775>
- Evans DS (1968) The observations of a near monoenergetic flux of auroral electrons. *J Geophys Res* 73:2315–2323. <https://doi.org/10.1029/JA073i007p02315>
- Eviatar A, Paranicas C (2005) The plasma plumes of Europa and Callisto. *Icarus* 178:360–366. <https://doi.org/10.1016/j.icarus.2005.06.007>

- Eviatar A, Strobel DF, Wolven BC, et al (2001b) Excitation of the Ganymede ultraviolet aurora. *Astrophys J* 555:1013. <https://doi.org/10.1086/321510>
- Eviatar A, Vasyliūnas VM, Gurnett DA (2001a) The ionosphere of Ganymede. *Planet Space Sci* 49:327–336. [https://doi.org/10.1016/S0032-0633\(00\)00154-9](https://doi.org/10.1016/S0032-0633(00)00154-9)
- Feldman PD, McGrath MA, Strobel DF, et al (2000) HST /STIS ultraviolet imaging of polar aurora on Ganymede. *Astrophys J* 535:1085–1090. <https://doi.org/10.1086/308889>
- Fletcher LN, Cavalié T, Grassi D, et al (2023) Jupiter science enabled by ESA's Jupiter Icy Moons Explorer. *Space Sci Rev* 219:53. <https://doi.org/10.1007/s11214-023-00996-6>
- Föhn M, Tulej M, Galli A, et al (2021) Initial calibration results of the NIM flight spare mass spectrometer for exploration of Jupiter's Icy Moons Exospheres. EGU General Assembly 2021, EGU21-3821. <https://doi.org/10.5194/egusphere-egu21-382>
- Frank LA, Paterson WR, Ackerson KL, Bolton SJ (1997) Low-energy electron measurements at Ganymede with the Galileo spacecraft: probes of the magnetic topology. *Geophys Res Lett* 24:2159–2162. <https://doi.org/10.1029/97GL01632>
- Futaana Y, Chaufray J-Y, Smith HT, et al (2011) Exospheres and energetic neutral atoms of Mars, Venus and Titan. *Space Sci Rev* 162:213–266. <https://doi.org/10.1007/s11214-011-9834-4>
- Futaana Y, Barabash S, Wieser M, et al (2012) Empirical energy spectra of neutralized solar wind protons from the lunar regolith. *J Geophys Res* 117:2011JE004019. <https://doi.org/10.1029/2011JE004019>
- Futaana Y, Barabash S, Wang X-D, et al (2015) Low-energy energetic neutral atom imaging of Io plasma and neutral tori. *Planet Space Sci* 108:41–53. <https://doi.org/10.1016/j.pss.2014.12.022>
- Galand M, Carnielli G, Jia X (2025) The ionosphere of Ganymede. In: Volwerk M, Jia X, McGrath M, Spohn T (eds) *Ganymede*. Cambridge University Press, Cambridge, pp 269–289. <https://doi.org/10.1017/9781108966474.018>
- Galli A, Vorburger A, Carberry Mogan SR, et al (2022) Callisto's atmosphere and its space environment: prospects for the particle environment package on board JUICE. *Earth Space Sci* 9:e2021EA002172. <https://doi.org/10.1029/2021EA002172>
- Galoiseau PHM, Boudjada MY (2016) An oblate beaming cone for Io-controlled Jovian decameter emission. *JGR Space Phys* 121:3120–3138. <https://doi.org/10.1002/2015JA021038>
- Garrett HB, Kim W, Evans RW (2016) Updating the Jovian plasma and radiation environments: the latest results for 2015. *J Spacecr Rockets* 53:693–707. <https://doi.org/10.2514/1.A33510>
- Geiss J, Gloeckler G, Balsiger H, et al (1992) Plasma composition in Jupiter's magnetosphere: initial results from the solar wind ion composition spectrometer. *Science* 257:1535–1539. <https://doi.org/10.1126/science.257.5076.1535>
- Gérard J-C, Gustin J, Grodent D, et al (2003) Spectral observations of transient features in the FUV Jovian polar aurora. *J Geophys Res* 108:2003JA009901. <https://doi.org/10.1029/2003JA009901>
- Gérard J-C, Bonfond B, Grodent D, et al (2014) Mapping the electron energy in Jupiter's aurora: Hubble spectral observations. *JGR Space Phys* 119:9072–9088. <https://doi.org/10.1002/2014JA020514>
- Gladstone GR, Waite JH, Grodent D, et al (2002) A pulsating auroral X-ray hot spot on Jupiter. *Nature* 415:1000–1003. <https://doi.org/10.1038/4151000a>
- Goertz CK (1974) Polarization of Jovian decametric radiation. *Planet Space Sci* 22:1491–1500. [https://doi.org/10.1016/0032-0633\(74\)90014-2](https://doi.org/10.1016/0032-0633(74)90014-2)
- Goertz CK (1980) Io's interaction with the plasma torus. *J Geophys Res* 85:2949–2956. <https://doi.org/10.1029/JA085iA06p02949>
- Goertz CK, Ip W-H (1984) A dawn-to-dusk electric field in the Jovian magnetosphere. *Planet Space Sci* 32:179–185. [https://doi.org/10.1016/0032-0633\(84\)90152-1](https://doi.org/10.1016/0032-0633(84)90152-1)
- Grasset O, Dougherty MK, Coustenis A, et al (2013) Jupiter ICy Moons Explorer (JUICE): an ESA mission to orbit Ganymede and to characterise the Jupiter system. *Planet Space Sci* 78:1–21. <https://doi.org/10.1016/j.pss.2012.12.002>
- Greathouse TK, Gladstone GR, Molyneux PM, et al (2022) UVS observations of Ganymede's aurora during Juno orbits 34 and 35. *Geophys Res Lett* 49:e2022GL099794. <https://doi.org/10.1029/2022GL099794>
- Grodent D, Gérard J-C, Gustin J, et al (2006) Europa's FUV auroral tail on Jupiter. *Geophys Res Lett* 33:2005GL025487. <https://doi.org/10.1029/2005GL025487>
- Gruntman M (1997) Energetic neutral atom imaging of space plasmas. *Rev Sci Instrum* 68:3617–3656. <https://doi.org/10.1063/1.1148389>
- Guo RL, Yao ZH, Sergis N, et al (2018) Reconnection acceleration in Saturn's dayside magnetodisk: a multi-case study with Cassini. *Astrophys J Lett* 868:L23. <https://doi.org/10.3847/2041-8213/aadedab>
- Guo RL, Yao ZH, Grodent D, et al (2021) Jupiter's double-arc aurora as a signature of magnetic reconnection: simultaneous observations from HST and Juno. *Geophys Res Lett* 48:e2021GL093964. <https://doi.org/10.1029/2021GL093964>
- Gurnett DA, Kurth WS, Shaw RR, et al (1992) The Galileo plasma wave investigation. *Space Sci Rev* 60:341–355. <https://doi.org/10.1007/BF00216861>

- Gurnett DA, Kurth WS, Roux A, et al (1996) Evidence for a magnetosphere at Ganymede from plasma-wave observations by the Galileo spacecraft. *Nature* 384:535–537. <https://doi.org/10.1038/384535a0>
- Gurnett DA, Kurth WS, Roux A, Bolton SJ (1997) Absence of a magnetic-field signature in plasma-wave observations at Callisto. *Nature* 387:261–262. <https://doi.org/10.1038/387261a0>
- Gurnett DA, Persoon AM, Kurth WS, et al (2000) Plasma densities in the vicinity of Callisto from Galileo plasma wave observations. *Geophys Res Lett* 27:1867–1870. <https://doi.org/10.1029/2000GL003751>
- Gurnett DA, Kurth WS, Hospodarsky GB, et al (2002) Control of Jupiter's radio emission and aurorae by the solar wind. *Nature* 415:985–987. <https://doi.org/10.1038/415985a>
- Gurnett DA, Kurth WS, Kirchner DL, et al (2004) The Cassini Radio and Plasma Wave Investigation. *Space Sci Rev* 114:395–463. <https://doi.org/10.1007/s11214-004-1434-0>
- Gurnett DA, Kurth WS, Hospodarsky GB, et al (2005) Radio and plasma wave observations at Saturn from Cassini's approach and first orbit. *Science* 307:1255–1259. <https://doi.org/10.1126/science.1105356>
- Gurvits LI, CIMÒ G, Dirkx D, et al (2023) Planetary Radio Interferometry and Doppler Experiment (PRIDE) of the JUICE mission. *Space Sci Rev* 219:79. <https://doi.org/10.1007/s11214-023-01026-1>
- Hajdas W, Gonçalves P, Pinto M, et al (2025) The JUICE radiation environment monitor, RADEM. *Space Sci Rev* 221
- Hall DT, Gladstone GR, Herbert F, et al (1995) Io torus EUV emissions during the comet Shoemaker-Levy/9 impacts. *Geophys Res Lett* 22:3441–3444. <https://doi.org/10.1029/95GL03011>
- Hall DT, Feldman PD, McGrath MA, Strobel DF (1998) The far-ultraviolet oxygen airglow of Europa and Ganymede. *Astrophys J* 499:475. <https://doi.org/10.1086/305604>
- Hallinan G, Littlefair SP, Cotter G, et al (2015) Magnetospherically driven optical and radio aurorae at the end of the stellar main sequence. *Nature* 523:568–571. <https://doi.org/10.1038/nature14619>
- Han S, Murakami G, Kita H, et al (2018) Investigating solar wind-driven electric field influence on long-term dynamics of Jovian synchrotron radiation. *JGR Space Phys* 123:9508–9516. <https://doi.org/10.1029/2018JA025849>
- Hansen CJ, Bolton S, Sulaiman AH, et al (2022) Juno's close encounter with Ganymede—an overview. *Geophys Res Lett* 49:e2022GL099285. <https://doi.org/10.1029/2022GL099285>
- Hao Y-X, Sun Y-X, Roussos E, et al (2020) The formation of Saturn's and Jupiter's electron radiation belts by magnetospheric electric fields. *Astrophys J Lett* 905:L10. <https://doi.org/10.3847/2041-8213/abca3f>
- Harris CDK, Jia X, Slavin JA, et al (2021) Multi-fluid MHD simulations of Europa's plasma interaction under different magnetospheric conditions. *JGR Space Phys* 126:e2020JA028888. <https://doi.org/10.1029/2020JA028888>
- Harris CDK, Jia X, Slavin JA (2022) Multi-fluid MHD simulations of Europa's plasma interaction: effects of variation in Europa's atmosphere. *JGR Space Phys* 127:e2022JA030569. <https://doi.org/10.1029/2022JA030569>
- Hartkorn O, Saur J (2017) Induction signals from Callisto's ionosphere and their implications on a possible subsurface ocean. *JGR Space Phys* 122. <https://doi.org/10.1002/2017JA024269>
- Hartkorn O, Saur J, Strobel DF (2017) Structure and density of Callisto's atmosphere from a fluid-kinetic model of its ionosphere: comparison with Hubble Space Telescope and Galileo observations. *Icarus* 282:237–259. <https://doi.org/10.1016/j.icarus.2016.09.020>
- Heber B, Potgieter MS, Ferreira SES, et al (2007) An overview of Jovian electrons during the distant Ulysses Jupiter flyby. *Planet Space Sci* 55:1–11. <https://doi.org/10.1016/j.pss.2006.06.018>
- Herbert F, Sandel BR (2000) Azimuthal variation of ion density and electron temperature in the Io plasma torus. *J Geophys Res* 105:16035–16052. <https://doi.org/10.1029/1998JA000259>
- Hess S, Zarka P, Mottez F (2007) Io–Jupiter interaction, millisecond bursts and field-aligned potentials. *Planet Space Sci* 55:89–99. <https://doi.org/10.1016/j.pss.2006.05.016>
- Hess S, Cecconi B, Zarka P (2008) Modeling of Io-Jupiter decameter arcs, emission beaming and energy source. *Geophys Res Lett* 35:2008GL033656. <https://doi.org/10.1029/2008GL033656>
- Hess SLG, Echer E, Zarka P, et al (2014) Multi-instrument study of the Jovian radio emissions triggered by solar wind shocks and inferred magnetospheric subcorotation rates. *Planet Space Sci* 99:136–148. <https://doi.org/10.1016/j.pss.2014.05.015>
- Hill TW (1976) Interchange stability of a rapidly rotating magnetosphere. *Planet Space Sci* 24:1151–1154. [https://doi.org/10.1016/0032-0633\(76\)90152-5](https://doi.org/10.1016/0032-0633(76)90152-5)
- Hill TW (1979) Inertial limit on corotation. *J Geophys Res* 84:6554–6558. <https://doi.org/10.1029/JA084iA11p06554>
- Hill TW (1983) Longitudinal asymmetry of the Io plasma torus. *Geophys Res Lett* 10:969–972. <https://doi.org/10.1029/GL010i010p00969>
- Hill TW, Dessler AJ, Michel FC (1974) Configuration of the Jovian magnetosphere. *Geophys Res Lett* 1:3–6. <https://doi.org/10.1029/GL001i001p00003>
- Horne RB, Thorne RM, Shprits YY, et al (2005) Wave acceleration of electrons in the Van Allen radiation belts. *Nature* 437:227–230. <https://doi.org/10.1038/nature03939>

- Hospodarsky GB, et al (2017) Jovian bow shock and magnetopause encounters by the Juno spacecraft. *Geophys Res Lett* 44:4506–4512. <https://doi.org/10.1002/2017GL073177>
- Huang TS, Hill TW (1989) Corotation lag of the Jovian atmosphere, ionosphere, and magnetosphere. *J Geophys Res* 94:3761–3765. <https://doi.org/10.1029/JA094iA04p03761>
- Huscher E, Bagenal F, Wilson RJ, et al (2021) Survey of Juno observations in Jupiter's plasma disk: density. *JGR Space Phys* 126:e2021JA029446. <https://doi.org/10.1029/2021JA029446>
- Huybrighs HLF, Futaana Y, Barabash S, et al (2017) On the in-situ detectability of Europa's water vapour plumes from a flyby mission. *Icarus* 289:270–280. <https://doi.org/10.1016/j.icarus.2016.10.026>
- Huybrighs HLF, Roussos E, Blöcker A, et al (2020) An active plume eruption on Europa during Galileo flyby E26 as indicated by energetic proton depletions. *Geophys Res Lett* 47:e2020GL087806. <https://doi.org/10.1029/2020GL087806>
- Huybrighs HLF, Roussos E, Blöcker A, et al (2021) Reply to comment on “An active plume eruption on Europa during Galileo flyby E26 as indicated by energetic proton depletions.”. *Geophys Res Lett* 48:e2021GL095240. <https://doi.org/10.1029/2021GL095240>
- Huybrighs HLF, Blöcker A, Roussos E, et al (2023) Europa's perturbed fields and induced dipole affect energetic proton depletions during distant Alfvén wing flybys. *J Geophys Res Space Phys* 128:e2023JA031420
- Iess L, et al (2025) *Space Sci Rev* 221
- Imai M, Imai K, Higgins CA, Thieman JR (2008) Angular beaming model of Jupiter's decametric radio emissions based on Cassini RPWS data analysis. *Geophys Res Lett* 35:2008GL034987. <https://doi.org/10.1029/2008GL034987>
- Imai M, Greathouse TK, Kurth WS, et al (2019) Probing Jovian broadband kilometric radio sources tied to the ultraviolet main auroral oval with Juno. *Geophys Res Lett* 46:571–579. <https://doi.org/10.1029/2018GL081227>
- Intriligator DS, Miller WD (1982) First evidence for a Europa plasma torus. *J Geophys Res* 87:8081–8090. <https://doi.org/10.1029/JA087iA10p08081>
- Jia X, Walker RJ, Kivelson MG, et al (2008) Three-dimensional MHD simulations of Ganymede's magnetosphere. *J Geophys Res* 113:2007JA012748. <https://doi.org/10.1029/2007JA012748>
- Jia X, Walker RJ, Kivelson MG, et al (2009) Properties of Ganymede's magnetosphere inferred from improved three-dimensional MHD simulations. *J Geophys Res* 114:2009JA014375. <https://doi.org/10.1029/2009JA014375>
- Jia X, Kivelson MG, Khurana KK, Walker RJ (2010a) Magnetic fields of the satellites of Jupiter and Saturn. *Space Sci Rev* 152:271–305. <https://doi.org/10.1007/s11214-009-9507-8>
- Jia X, Walker RJ, Kivelson MG, et al (2010b) Dynamics of Ganymede's magnetopause: intermittent reconnection under steady external conditions. *J Geophys Res* 115:2010JA015771. <https://doi.org/10.1029/2010JA015771>
- Jia X, Kivelson MG, Khurana KK, Kurth WS (2018) Evidence of a plume on Europa from Galileo magnetic and plasma wave signatures. *Nat Astron* 2:459–464. <https://doi.org/10.1038/s41550-018-0450-z>
- Jia X, Kivelson MG (2021) The magnetosphere of Ganymede. In: Maggiolo R, André N, Hasegawa H, et al (eds) *Geophysical monograph series*, 1st edn. Wiley, New York, pp 557–573
- Jia X, Kivelson MG, Paranicas C (2021) Comment on “An active plume eruption on Europa during Galileo flyby E26 as indicated by energetic proton depletions”. by Huybrighs et al. *Geophys Res Lett* 48:e2020GL091550. <https://doi.org/10.1029/2020GL091550>
- Johnson RE (2004) The magnetospheric plasma-driven evolution of satellite atmospheres. *Astrophys J* 609:L99. <https://doi.org/10.1086/422912>
- Joy SP, Kivelson MG, Walker RJ, et al (2002) Probabilistic models of the Jovian magnetopause and bow shock locations. *J Geophys Res* 107. <https://doi.org/10.1029/2001JA009146>
- Kabin K, Combi MR, Gombosi TI, et al (1999) On Europa's magnetospheric interaction: a MHD simulation of the E4 flyby. *J Geophys Res* 104:19983–19992. <https://doi.org/10.1029/1999JA900263>
- Kane M, Mauk BH, Keath EP, Krimigis SM (1995) Hot ions in Jupiter's magnetodisc: a model for Voyager 2 low-energy charged particle measurements. *J Geophys Res* 100:19473–19486. <https://doi.org/10.1029/95JA00793>
- Katoh Y, Tsuchiya F, Miyoshi Y, et al (2011) Whistler mode chorus enhancements in association with energetic electron signatures in the Jovian magnetosphere. *J Geophys Res* 116:A02215. <https://doi.org/10.1029/2010JA016183>
- Katoh Y, Kojima H, Asamura K, et al (2018) Software-type Wave-Particle Interaction Analyzer (S-WPIA) by RPWI for JUICE: Science objectives and implementation. Verlag der Österreichischen Akademie der Wissenschaften
- Kaweeyanun N, Masters A, Jia X (2020) Favorable conditions for magnetic reconnection at Ganymede's upstream magnetopause. *Geophys Res Lett* 47:e2019GL086228. <https://doi.org/10.1029/2019GL086228>

- Kaweeyanun N, Masters A, Jia X (2021) Analytical assessment of Kelvin-Helmholtz instability growth at Ganymede's upstream magnetopause. *JGR Space Phys* 126:e2021JA029338. <https://doi.org/10.1029/2021JA029338>
- Khurana KK (1997) Euler potential models of Jupiter's magnetospheric field. *J Geophys Res* 102:11295–11306. <https://doi.org/10.1029/97JA00563>
- Khurana KK, Schwarzl HK (2005) Global structure of Jupiter's magnetospheric current sheet. *J Geophys Res* 110:2004JA010757. <https://doi.org/10.1029/2004JA010757>
- Khurana KK, Kivelson MG, Russell CT, et al (1997) Absence of an internal magnetic field at Callisto. *Nature* 387:262–264. <https://doi.org/10.1038/387262a0>
- Khurana KK, Kivelson MG, Stevenson DJ, et al (1998) Induced magnetic fields as evidence for subsurface oceans in Europa and Callisto. *Nature* 395:777–780. <https://doi.org/10.1038/27394>
- Khurana KK, Kivelson MG, Vasyliūnas VM, et al (2004) The configuration of Jupiter's magnetosphere. In: Bagenal F, Dowling TE, McKinnon WB (eds) *Jupiter: the planet, satellites and magnetosphere*. Cambridge University Press, Cambridge
- Kim TK, Ebert RW, Valek PW, et al (2020) Survey of ion properties in Jupiter's plasma sheet: Juno JADE-I observations. *JGR Space Phys* 125:e2019JA027696. <https://doi.org/10.1029/2019JA027696>
- Kimura T, Tsuchiya F, Misawa H, et al (2008a) Occurrence and source characteristics of the high-latitude components of Jovian broadband kilometric radiation. *Planet Space Sci* 56:1155–1168. <https://doi.org/10.1016/j.pss.2008.03.001>
- Kimura T, Tsuchiya F, Misawa H, et al (2008b) Radiation characteristics of quasi-periodic radio bursts in the Jovian high-latitude region. *Planet Space Sci* 56:1967–1976. <https://doi.org/10.1016/j.pss.2008.09.021>
- Kimura T, Cecconi B, Zarka P, et al (2012) Polarization and direction of arrival of Jovian quasiperiodic bursts observed by Cassini. *J Geophys Res* 117:2012JA017506. <https://doi.org/10.1029/2012JA017506>
- Kimura T, Badman SV, Tao C, et al (2015) Transient internally driven aurora at Jupiter discovered by Hisaki and the Hubble Space Telescope. *Geophys Res Lett* 42:1662–1668. <https://doi.org/10.1002/2015GL063272>
- Kimura T, Nichols JD, Gray RL, et al (2017) Transient brightening of Jupiter's aurora observed by the Hisaki satellite and Hubble Space Telescope during approach phase of the Juno spacecraft. *Geophys Res Lett* 44:4523–4531. <https://doi.org/10.1002/2017GL072912>
- Kimura T, Hiraki Y, Tao C, et al (2018) Response of Jupiter's aurora to plasma mass loading rate monitored by the Hisaki satellite during volcanic eruptions at Io. *JGR Space Phys* 123:1885–1899. <https://doi.org/10.1002/2017JA025029>
- Kirsch E, Krimigis SM, Kohl JW, Keath EP (1981) Upper limits for X - ray and energetic neutral particle emission from Jupiter: Voyager-1 results. *Geophys Res Lett* 8:169–172. <https://doi.org/10.1029/GL008i002p00169>
- Kita H, Kimura T, Tao C, et al (2019) Jovian UV aurora's response to the solar wind: Hisaki EXCEED and Juno observations. *JGR Space Phys* 124:10209–10218. <https://doi.org/10.1029/2019JA026997>
- Kivelson MG (2004b) Moon–magnetosphere interactions: a tutorial. *Adv Space Res* 33:2061–2077. <https://doi.org/10.1016/j.asr.2003.08.042>
- Kivelson MG, Khurana KK, Russell CT, et al (1996) Discovery of Ganymede's magnetic field by the Galileo spacecraft. *Nature* 384:537–541. <https://doi.org/10.1038/384537a0>
- Kivelson MG, Khurana KK, Russell CT, Walker RJ (1997) Intermittent short-duration magnetic field anomalies in the Io torus: evidence for plasma interchange? *Geophys Res Lett* 24:2127–2130. <https://doi.org/10.1029/97GL02202>
- Kivelson MG, Warnecke J, Bennett L, et al (1998) Ganymede's magnetosphere: magnetometer overview. *J Geophys Res* 103:19963–19972. <https://doi.org/10.1029/98JE00227>
- Kivelson MG, Khurana KK, Stevenson DJ, et al (1999) Europa and Callisto: induced or intrinsic fields in a periodically varying plasma environment. *J Geophys Res* 104:4609–4625. <https://doi.org/10.1029/1998JA900095>
- Kivelson MG, Khurana KK, Volwerk M (2002) The permanent and inductive magnetic moments of Ganymede. *Icarus* 157:507–522. <https://doi.org/10.1006/icar.2002.6834>
- Kivelson MG, Bagenal F, Kurth WS, et al (2004a) Magnetospheric interactions with satellites. In: Bagenal F, Dowling TE, McKinnon WB (eds) *Jupiter: the planet, satellites and magnetosphere*. Cambridge University Press, Cambridge
- Kivelson MG, Khurana KK, Volwerk M (2009) Europa's interaction with the Jovian magnetosphere. In: Pappalardo RT, McKinnon WB, Khurana KK (eds) *Europa*. University of Arizona Press, Tucson, pp 545–570
- Kivelson MG, Bagenal F, Jia X, et al (2025) Ganymede: its magnetosphere and its interaction with the Jovian magnetosphere. In: Volwerk M, Jia X, McGrath M, Spohn T (eds) *Ganymede*. Cambridge University Press, Cambridge, pp 215–236. <https://doi.org/10.1017/9781108966474.015>

- Kleer K, Milby Z, Schmidt C, et al (2023) The optical aurorae of Europa, Ganymede, and Callisto. *Planet Sci J* 4:37. <https://doi.org/10.3847/PSJ/acb53c>
- Kliore AJ (1998) atellite atmospheres and magnetospheres. Highlights of Astronomy, Volume 11, Issue 2: Highlights of Astronomy. As presented at the XXIIIrd General Assembly of the IAU (Part B), 1997, 1998, pp. 1065–1069. <https://doi.org/10.1017/S1539299600019602>
- Kliore AJ, Hinson DP, Flasar FM, et al (1997) The ionosphere of Europa from Galileo radio occultations. *Science* 277:355–358. <https://doi.org/10.1126/science.277.5324.355>
- Kliore AJ, Anabtawi A, Nagy AF, et al (2001) The ionospheres of Ganymede and Callisto from Galileo radio occultations. American Astronomical Society, DPS Meeting #33, id.24.10; Bulletin of the American Astronomical Society, Vol. 33, p. 1084
- Kliore AJ, Anabtawi A, Herrera RG, et al (2002) Ionosphere of Callisto from Galileo radio occultation observations. *J Geophys Res* 107. <https://doi.org/10.1029/2002JA009365>
- Knight S (1973) Parallel electric fields. *Planet Space Sci* 21:741–750. [https://doi.org/10.1016/0032-0633\(73\)90093-7](https://doi.org/10.1016/0032-0633(73)90093-7)
- Koga R, Tsuchiya F, Kagitani M, et al (2019) Transient change of Io's neutral oxygen cloud and plasma torus observed by Hisaki. *JGR Space Phys* 124:10318–10331. <https://doi.org/10.1029/2019JA026877>
- Kollmann P, Paranicas C, Clark G, et al (2016) The vertical thickness of Jupiter's Europa gas torus from charged particle measurements. *Geophys Res Lett* 43:9425–9433. <https://doi.org/10.1002/2016GL070326>
- Kollmann P, Roussos E, Paranicas C, et al (2018) Electron acceleration to MeV energies at Jupiter and Saturn. *JGR Space Phys* 123:9110–9129. <https://doi.org/10.1029/2018JA025665>
- Krimigis SM, Mitchell DG, Hamilton DC, et al (2002) A nebula of gases from Io surrounding Jupiter. *Nature* 415:994–996. <https://doi.org/10.1038/415994a>
- Krimigis SM, Mitchell DG, Hamilton DC, et al (2004) Magnetosphere imaging instrument (MIMI) on the Cassini mission to Saturn/Titan. *Space Sci Rev* 114:233–329. <https://doi.org/10.1007/s11214-004-1410-8>
- Kronberg EA, Glassmeier K-H, Woch J, et al (2007) A possible intrinsic mechanism for the quasi-periodic dynamics of the Jovian magnetosphere. *J Geophys Res* 112:2006JA011994. <https://doi.org/10.1029/2006JA011994>
- Krüger H, Krivov AV, Hamilton DP, Grün E (1999) Detection of an impact-generated dust cloud around Ganymede. *Nature* 399:558–560. <https://doi.org/10.1038/21136>
- Krüger H, Krivov AV, Grün E (2000) A dust cloud of Ganymede maintained by hypervelocity impacts of interplanetary micrometeoroids. *Planet Space Sci* 48:1457–1471. [https://doi.org/10.1016/S0032-0633\(00\)00092-1](https://doi.org/10.1016/S0032-0633(00)00092-1)
- Krüger H, Krivov AV, Sremčević M, Grün E (2003) Impact-generated dust clouds surrounding the Galilean moons. *Icarus* 164:170–187. [https://doi.org/10.1016/S0019-1035\(03\)00127-1](https://doi.org/10.1016/S0019-1035(03)00127-1)
- Krupp N, Woch J, Lagg A, et al (1998) Energetic particle bursts in the predawn Jovian magnetotail. *Geophys Res Lett* 25:1249–1252. <https://doi.org/10.1029/98GL00863>
- Krupp N, Lagg A, Livi S, et al (2001a) Global flows of energetic ions in Jupiter's equatorial plane: first-order approximation. *J Geophys Res* 106:26017–26032. <https://doi.org/10.1029/2000JA900138>
- Krupp N, Woch J, Lagg A, et al (2001b) Local time asymmetry of energetic ion anisotropies in the Jovian magnetosphere. *Planet Space Sci* 49:283–289. [https://doi.org/10.1016/S0032-0633\(00\)00149-5](https://doi.org/10.1016/S0032-0633(00)00149-5)
- Krupp N, Woch J, Lagg A, et al (2002) Leakage of energetic particles from Jupiter's dusk magnetosphere: Dual spacecraft observations. *Geophys Res Lett* 29. <https://doi.org/10.1029/2001GL014290>
- Krupp N, Vasyliūnas VM, Woch J, et al (2004a) Dynamics of the Jovian magnetosphere. In: Bagenal F, Dowling TE, McKinnon WB (eds) *Jupiter: the planet, satellites and magnetosphere*. Cambridge University Press, Cambridge
- Krupp N, Woch J, Lagg A, et al (2004b) Energetic particle observations in the vicinity of Jupiter: Cassini MIMI/LEMMS results. *J Geophys Res* 109:2003JA010111. <https://doi.org/10.1029/2003JA010111>
- Kurth WS, Gunnelt DA, Roux A, Bolton SJ (1997) Ganymede: a new radio source. *Geophys Res Lett* 24:2167–2170. <https://doi.org/10.1029/97GL02249>
- Kurth WS, Hospodarsky GB, Kirchner DL, et al (2017) The Juno waves investigation. *Space Sci Rev* 213:347–392. <https://doi.org/10.1007/s11214-017-0396-y>
- Kurth WS, Sulaiman AH, Hospodarsky GB, et al (2022) Juno plasma wave observations at Ganymede. *Geophys Res Lett* 49:e2022GL098591. <https://doi.org/10.1029/2022GL098591>
- Kurth WS, Wilkinson DR, Hospodarsky GB, et al (2023) Juno plasma wave observations at Europa. *Geophys Res Lett* 50:e2023GL105775. <https://doi.org/10.1029/2023GL105775>
- Ladreiter HP, Zarka P, Lecacheux A (1994) Direction finding study of Jovian hectometric and broadband kilometric radio emissions: evidence for their auroral origin. *Planet Space Sci* 42:919–931. [https://doi.org/10.1016/0032-0633\(94\)90052-3](https://doi.org/10.1016/0032-0633(94)90052-3)

- Lagg A, Krupp N, Woch J, Williams DJ (2003) In-situ observations of a neutral gas torus at Europa. *Geophys Res Lett* 30:2003GL017214. <https://doi.org/10.1029/2003GL017214>
- Lamy L, Colombari L, Zarka P, et al (2022) Determining the beaming of Io decametric emissions: a remote diagnostic to probe the Io-Jupiter interaction. *JGR Space Phys* 127:e2021JA030160. <https://doi.org/10.1029/2021JA030160>
- Lavrukhin AS, Alexeev II (2015) Aurora at high latitudes of Ganymede. *Astron Lett* 41:687–692. <https://doi.org/10.1134/S1063773715110043>
- Leblanc F, Oza AV, Leclercq L, et al (2017) On the orbital variability of Ganymede's atmosphere. *Icarus* 293:185–198. <https://doi.org/10.1016/j.icarus.2017.04.025>
- Leblanc F, Roth L, Chaufray JY, et al (2023) Ganymede's atmosphere as constrained by HST/STIS observations. *Icarus* 399:115557. <https://doi.org/10.1016/j.icarus.2023.115557>
- Lecacheux A, Boischoat A, Boudjada MY, Dulk GA (1991) Spectra and complete polarization state of two, Io-related, radio storms from Jupiter. *Astron Astrophys* 251:339–348
- Li W, Shen X-C, Menietti JD, et al (2020) Global distribution of whistler mode waves in Jovian inner magnetosphere. *Geophys Res Lett* 47:e2020GL088198. <https://doi.org/10.1029/2020GL088198>
- Li W, Ma Q, Shen X-C, et al (2023) Driver of energetic electron precipitation in the vicinity of Ganymede. *Geophys Res Lett* 50:e2022GL101555. <https://doi.org/10.1029/2022GL101555>
- Lindkvist J, Holmström M, Khurana KK, et al (2015) Callisto plasma interactions: hybrid modeling including induction by a subsurface ocean. *JGR Space Phys* 120:4877–4889. <https://doi.org/10.1002/2015JA021212>
- Liou K, Meng C-I, Lui ATY, et al (2000) Auroral kilometric radiation at substorm onset. *J Geophys Res* 105:25325–25331. <https://doi.org/10.1029/2000JA000038>
- Liuzzo L, Feyerabend M, Simon S, Motschmann U (2015) The impact of Callisto's atmosphere on its plasma interaction with the Jovian magnetosphere. *JGR Space Phys* 120:9401–9427. <https://doi.org/10.1002/2015JA021792>
- Liuzzo L, Simon S, Feyerabend M, Motschmann U (2016) Disentangling plasma interaction and induction signatures at Callisto: the Galileo C10 flyby. *JGR Space Phys* 121:8677–8694. <https://doi.org/10.1002/2016JA023236>
- Liuzzo L, Simon S, Feyerabend M (2018) Observability of Callisto's inductive signature during the Jupiter icy Moons Explorer mission. *JGR Space Phys* 123:9045–9054. <https://doi.org/10.1029/2018JA025951>
- Liuzzo L, Simon S, Regoli L (2019) Energetic ion dynamics near Callisto. *Planet Space Sci* 166:23–53. <https://doi.org/10.1016/j.pss.2018.07.014>
- Liuzzo L, Poppe AR, Paranicas C, et al (2020) Variability in the energetic electron bombardment of Ganymede. *JGR Space Phys* 125:e2020JA028347. <https://doi.org/10.1029/2020JA028347>
- Louarn P, Wahlund JE, Chust T, et al (1994) Observation of kinetic Alfvén waves by the FREJA spacecraft. *Geophys Res Lett* 21:1847–1850. <https://doi.org/10.1029/94GL00882>
- Louarn P, Kurth WS, Gurnett DA, et al (2007) Observation of similar radio signatures at Saturn and Jupiter: implications for the magnetospheric dynamics. *Geophys Res Lett* 34:2007GL030368. <https://doi.org/10.1029/2007GL030368>
- Louarn P, Paranicas CP, Kurth WS (2014) Global magnetodisk disturbances and energetic particle injections at Jupiter. *JGR Space Phys* 119:4495–4511. <https://doi.org/10.1002/2014JA019846>
- Louarn P, Andre N, Jackman CM, et al (2015) Magnetic reconnection and associated transient phenomena within the magnetospheres of Jupiter and Saturn. *Space Sci Rev* 187:181–227. <https://doi.org/10.1007/s11214-014-0047-5>
- Louarn P, Allegrini F, McComas DJ, et al (2017) Generation of the Jovian hectometric radiation: first lessons from Juno. *Geophys Res Lett* 44:4439–4446. <https://doi.org/10.1002/2017GL072923>
- Louis CK, Lamy L, Zarka P, et al (2017) Detection of Jupiter decametric emissions controlled by Europa and Ganymede with Voyager/PRA and Cassini/RPWS. *JGR Space Phys* 122:9228–9247. <https://doi.org/10.1002/2016JA023779>
- Louis CK, Prangé R, Lamy L, et al (2019) Jovian auroral radio sources detected in situ by Juno/waves: comparisons with model auroral ovals and simultaneous HST FUV images. *Geophys Res Lett* 46:11606–11614. <https://doi.org/10.1029/2019GL084799>
- Louis CK, Louarn P, Allegrini F, et al (2020) Ganymede-induced decametric radio emission: in situ observations and measurements by Juno. *Geophys Res Lett* 47:e2020GL090021. <https://doi.org/10.1029/2020GL090021>
- Louis CK, Zarka P, Dabidin K, et al (2021) Latitudinal beaming of Jupiter's radio emissions from Juno/waves flux density measurements. *JGR Space Phys* 126:e2021JA029435. <https://doi.org/10.1029/2021JA029435>
- Lysak RL (1990) Electrodynamical coupling of the magnetosphere and ionosphere. *Space Sci Rev* 52:33–87. <https://doi.org/10.1007/BF00704239>

- Lysak RL, Song Y (2020) Field line resonances in Jupiter's magnetosphere. *Geophys Res Lett* 47:e2020GL089473. <https://doi.org/10.1029/2020GL089473>
- Ma Q, Li W, Zhang X-J, et al (2021) Energetic electron distributions near the magnetic equator in the Jovian plasma sheet and outer radiation belt using Juno observations. *Geophys Res Lett* 48:e2021GL095833. <https://doi.org/10.1029/2021GL095833>
- Manners H, Masters A (2020) The global distribution of ultralow-frequency waves in Jupiter's magnetosphere. *JGR Space Phys* 125:e2020JA028345. <https://doi.org/10.1029/2020JA028345>
- Marconi ML (2007) A kinetic model of Ganymede's atmosphere. *Icarus* 190:155–174. <https://doi.org/10.1016/j.icarus.2007.02.016>
- Marhavilas PK, Anagnostopoulos GC, Sarris ET (2001) Periodic signals in Ulysses' energetic particle events upstream and downstream from the Jovian bow shock. *Planet Space Sci* 49:1031–1047. [https://doi.org/10.1016/S0032-0633\(01\)00018-6](https://doi.org/10.1016/S0032-0633(01)00018-6)
- Marques MS, Zarka P, Echer E, et al (2017) Statistical analysis of 26 yr of observations of decametric radio emissions from Jupiter. *Astron Astrophys* 604:A17. <https://doi.org/10.1051/0004-6361/201630025>
- Martin CJ, Ray LC, Constable DA, et al (2020) Evaluating the ionospheric mass source for Jupiter's magnetosphere: an ionospheric outflow model for the auroral regions. *J Geophys Res* 125:e2019JA027727. <https://doi.org/10.1029/2019JA027727>
- Marzok A, Schlegel S, Saur J, et al (2022) Mapping the brightness of Ganymede's ultraviolet aurora using Hubble Space Telescope observations. *JGR Planets* 127:e2022JE007256. <https://doi.org/10.1029/2022JE007256>
- Masters A (2017) Model-Based Assessments of Magnetic Reconnection and Kelvin-Helmholtz Instability at Jupiter's Magnetopause. *JGR Space Phys* 122. <https://doi.org/10.1002/2017JA024736>
- Mauk BH (2014) Comparative investigation of the energetic ion spectra comprising the magnetospheric ring currents of the Solar System. *JGR Space Phys* 119:9729–9746. <https://doi.org/10.1002/2014JA020392>
- Mauk BH, Williams DJ, McEntire RW, et al (1999) Storm-like dynamics of Jupiter's inner and middle magnetosphere. *J Geophys Res* 104:22759–22778. <https://doi.org/10.1029/1999JA900097>
- Mauk BH, Clarke JT, Grodent D, et al (2002) Transient aurora on Jupiter from injections of magnetospheric electrons. *Nature* 415:1003–1005. <https://doi.org/10.1038/4151003a>
- Mauk BH, Mitchell DG, Krimigis SM, et al (2003) Energetic neutral atoms from a trans-Europa gas torus at Jupiter. *Nature* 421:920–922. <https://doi.org/10.1038/nature01431>
- Mauk BH, Mitchell DG, McEntire RW, et al (2004) Energetic ion characteristics and neutral gas interactions in Jupiter's magnetosphere. *J Geophys Res* 109:2003JA010270. <https://doi.org/10.1029/2003JA010270>
- Mauk BH, Haggerty DK, Paranicas C, et al (2017) Juno observations of energetic charged particles over Jupiter's polar regions: analysis of monodirectional and bidirectional electron beams. *Geophys Res Lett* 44:4410–4418. <https://doi.org/10.1002/2016GL072286>
- Mauk BH, Haggerty DK, Paranicas C, et al (2018) Diverse electron and ion acceleration characteristics observed over Jupiter's main aurora. *Geophys Res Lett* 45:1277–1285. <https://doi.org/10.1002/2017GL076901>
- Mauk BH, Clark G, Allegrini F, et al (2020b) Juno energetic neutral atom (ENA) remote measurements of magnetospheric injection dynamics in Jupiter's Io torus regions. *JGR Space Phys* 125:e2020JA027964. <https://doi.org/10.1029/2020JA027964>
- Mauk BH, Clark G, Gladstone GR, Kotsiaros S, Adriani A, Allegrini F, et al (2020a) Energetic particles and acceleration regions over Jupiter's polar cap and main aurora; a broad overview. *J Geophys Res Space Phys* 125(3):e2019JA027699. <https://doi.org/10.1029/2019JA027699>
- Mauk BH, Allegrini F, Bagenal F, et al (2022) Loss of energetic ions comprising the ring current populations of Jupiter's middle and inner magnetosphere. *JGR Space Phys* 127:e2022JA030293. <https://doi.org/10.1029/2022JA030293>
- McComas DJ, et al (2017) Plasma environment at the dawn flank of Jupiter's magnetosphere: Juno arrives at Jupiter. *Geophys Res Lett* 44. <https://doi.org/10.1002/2017GL072831>
- McGrath MA, Sparks WB (2017) Galileo ionosphere profile coincident with repeat plume detection location at Europa. *Res Notes AAS* 1:14. <https://doi.org/10.3847/2515-5172/aa988e>
- McGrath MA, Lellouch E, Strobel DF, et al (2004) Satellite atmospheres. In: Bagenal F, Dowling TE, McKinnon WB (eds) *Jupiter: the planet, satellites and magnetosphere*. Cambridge University Press, Cambridge
- McGrath MA, Hansen CJ, Hendrix AR (2009) Observations of Europa's tenuous atmosphere. In: Pappalardo RT, McKinnon WB, Khurana KK (eds) *Europa*. University of Arizona Press, Tucson, pp 485–506
- McGrath MA, Jia X, Retherford K, et al (2013) Aurora on Ganymede. *JGR Space Phys* 118:2043–2054. <https://doi.org/10.1002/jgra.50122>
- McIlwain CE (1960) Direct measurement of particles producing visible auroras. *J Geophys Res* 65:2727–2747. <https://doi.org/10.1029/JZ065i009p02727>
- Mendillo M, Baumgardner J, Flynn B, Hughes WJ (1990) The extended sodium nebula of Jupiter. *Nature* 348:312–314. <https://doi.org/10.1038/348312a0>

- Menietti JD, Horne RB, Gurnett DA, et al (2008) A survey of Galileo plasma wave instrument observations of Jovian whistler-mode chorus. *Ann Geophys* 26:1819–1828. <https://doi.org/10.5194/angeo-26-1819-2008>
- Menietti JD, Groene JB, Averkamp TF, et al (2016) Survey of whistler mode chorus intensity at Jupiter. *JGR Space Phys* 121:9758–9770. <https://doi.org/10.1002/2016JA022969>
- Menietti JD, Averkamp TF, Imai M, et al (2021a) Low-latitude whistler-mode and higher-latitude Z-mode emission at Jupiter observed by Juno. *JGR Space Phys* 126:e2020JA028742. <https://doi.org/10.1029/2020JA028742>
- Menietti JD, Averkamp TF, Kurth WS, et al (2021b) Analysis of whistler-mode and Z-mode emission in the Juno primary mission. *JGR Space Phys* 126:e2021JA029885. <https://doi.org/10.1029/2021JA029885>
- Mitchell DG, Jaskulek SE, Schlemm CE, et al (2000) High energy neutral atom (HENA) imager for the IMAGE mission. *Space Sci Rev* 91:67–112. <https://doi.org/10.1023/A:1005207308094>
- Mitchell DG, Brandt PC, Roelof EC, et al (2005) Energetic ion acceleration in Saturn's magnetotail: substorms at Saturn? *Geophys Res Lett* 32:2005GL022647. <https://doi.org/10.1029/2005GL022647>
- Mitchell DG, Krimigis SM, Paranicas C, et al (2009) Recurrent energization of plasma in the midnight-to-dawn quadrant of Saturn's magnetosphere, and its relationship to auroral UV and radio emissions. *Planet Space Sci* 57:1732–1742. <https://doi.org/10.1016/j.pss.2009.04.002>
- Mitchell DG, Brandt PC, Carbary JF, et al (2015) Injection, interchange, and reconnection: energetic particle observations in Saturn's magnetosphere. In: Keiling A, Jackman CM, Delamere PA (eds) *Geophysical monograph series*, vol 1. Wiley, New York, pp 327–343
- Moirano A, Gomez Casajus L, Zannoni M, et al (2021) Morphology of the Io plasma torus from Juno radio occultations. *JGR Space Phys* 126:e2021JA029190. <https://doi.org/10.1029/2021JA029190>
- Montgomery J, Ebert RW, Clark G, Fuselier SA, Allegrini F, Bagenal F, et al (2022) Investigating the occurrence of magnetic reconnection at Jupiter's dawn magnetopause during the Juno era. *Geophys Res Lett* 49:e2022GL099141. <https://doi.org/10.1029/2022GL099141>
- Morioka A, Tsuchiya F (1996) Solar wind control of Jovian electron flux: Pioneer 11 analysis. *Geophys Res Lett* 23:2963–2966. <https://doi.org/10.1029/96GL02774>
- Murakami G, Yoshioka K, Yamazaki A, et al (2016) Response of Jupiter's inner magnetosphere to the solar wind derived from extreme ultraviolet monitoring of the Io plasma torus. *Geophys Res Lett* 43. <https://doi.org/10.1002/2016GL071675>
- Néron Q, André N (2019) Evidence of Europa neutral gas torii from energetic sulfur ion measurements. *Geophys Res Lett* 46:3599–3606. <https://doi.org/10.1029/2019GL082200>
- Néron Q, Sicard A, Kollmann P, et al (2018) A physical model of the proton radiation belts of Jupiter inside Europa's orbit. *JGR Space Phys* 123:3512–3532. <https://doi.org/10.1029/2018JA025216>
- Nerney EG (2023) PhD thesis, University of Colorado, USA
- Nerney EG, Bagenal F (2020) Combining UV spectra and physical chemistry to constrain the hot electron fraction in the Io plasma torus. *JGR Space Phys* 125:e2019JA027458. <https://doi.org/10.1029/2019JA027458>
- Nerney EG, Bagenal F, Steffl AJ (2017) Io plasma torus ion composition: Voyager, Galileo, and Cassini. *JGR Space Phys* 122:727–744. <https://doi.org/10.1002/2016JA023306>
- Neubauer FM (1980) Nonlinear standing Alfvén wave current system at Io. *Theory J Geophys Res* 85:1171–1178. <https://doi.org/10.1029/JA085iA03p01171>
- Neubauer FM (1998) The sub-Alfvénic interaction of the Galilean satellites with the Jovian magnetosphere. *J Geophys Res* 103:19843–19866. <https://doi.org/10.1029/97JE03370>
- Neubauer FM (1999) Alfvén wings and electromagnetic induction in the interiors: Europa and Callisto. *J Geophys Res* 104:28671–28684. <https://doi.org/10.1029/1999JA000217>
- Ng CS, Delamere PA, Kaminker V, Damiano PA (2018) Radial transport and plasma heating in Jupiter's magnetodisc. *JGR Space Phys* 123:6611–6620. <https://doi.org/10.1029/2018JA025345>
- Ng CS, Neupane BR, Delamere PA, Damiano PA (2022) A turbulent heating model combining diffusion and advection effects for giant planet magnetospheres. *Geophys Res Lett* 49:e2021GL096662. <https://doi.org/10.1029/2021GL096662>
- Nichols JD, Cowley SWH (2003) Magnetosphere-ionosphere coupling currents in Jupiter's middle magnetosphere: dependence on the effective ionospheric Pedersen conductivity and iogenic plasma mass outflow rate. *Ann Geophys* 21:1419–1441. <https://doi.org/10.5194/angeo-21-1419-2003>
- Nichols JD, Cowley SWH (2004) Magnetosphere-ionosphere coupling currents in Jupiter's middle magnetosphere: effect of precipitation-induced enhancement of the ionospheric Pedersen conductivity. *Ann Geophys* 22:1799–1827. <https://doi.org/10.5194/angeo-22-1799-2004>
- Nichols JD, Cowley SWH (2022) Relation of Jupiter's dawnside main emission intensity to magnetospheric currents during the Juno mission. *JGR Space Phys* 127:e2021JA030040. <https://doi.org/10.1029/2021JA030040>

- Nordheim TA, Regoli LH, Harris CDK, et al (2022) Magnetospheric ion bombardment of Europa's surface. *Planet Sci J* 3:5. <https://doi.org/10.3847/PSJ/ac382a>
- Oza AV, Leblanc F, Johnson RE, Schmidt C, Leclercq L, Cassidy TA, Chaufray JY (2019) Dusk over dawn O₂ asymmetry in Europa's near-surface atmosphere. *Planet Space Sci* 167:23–32
- Paganini L, Villanueva GL, Roth L, et al (2020) A measurement of water vapour amid a largely quiescent environment on Europa. *Nat Astron* 4:266–272. <https://doi.org/10.1038/s41550-019-0933-6>
- Paranicas C, Paterson WR, Cheng AF, et al (1999) Energetic particle observations near Ganymede. *J Geophys Res* 104:17459–17469. <https://doi.org/10.1029/1999JA900199>
- Paranicas C, McEntire RW, Cheng AF, et al (2000) Energetic charged particles near Europa. *J Geophys Res* 105:16005–16015. <https://doi.org/10.1029/1999JA000350>
- Paranicas C, Carlson RW, Johnson RE (2001) Electron bombardment of Europa. *Geophys Res Lett* 28:673–676. <https://doi.org/10.1029/2000GL012320>
- Paranicas C, Mitchell DG, Roelof EC, et al (2005) Periodic intensity variations in global ENA images of Saturn. *Geophys Res Lett* 32:2005GL023656. <https://doi.org/10.1029/2005GL023656>
- Paranicas C, Mauk BH, Khurana K, et al (2007) Europa's near-surface radiation environment. *Geophys Res Lett* 34:2007GL030834. <https://doi.org/10.1029/2007GL030834>
- Paranicas C, Szalay JR, Mauk BH, et al (2021) Energy spectra near Ganymede from Juno data. *Geophys Res Lett* 48:e2021GL093021. <https://doi.org/10.1029/2021GL093021>
- Paranicas C, Mauk BH, Kollmann P, et al (2022) Energetic charged particle fluxes relevant to Ganymede's polar region. *Geophys Res Lett* 49:e2022GL098077. <https://doi.org/10.1029/2022GL098077>
- Parisi M, Caruso A, Buccino DR, et al (2023) Radio occultation measurements of Europa's ionosphere from Juno's close flyby. *Geophys Res Lett* 50(22):e2023GL106637
- Parkinson CD, Stewart AIF, Wong AS, et al (2006) Enhanced transport in the polar mesosphere of Jupiter: evidence from Cassini UVIS helium 584 Å airglow. *J Geophys Res* 111:2005JE002539. <https://doi.org/10.1029/2005JE002539>
- Paterson WR, Frank LA, Ackerson KL (1999) Galileo plasma observations at Europa: ion energy spectra and moments. *J Geophys Res* 104:22779–22791. <https://doi.org/10.1029/1999JA900191>
- Paty C, Winglee R (2004) Multi-fluid simulations of Ganymede's magnetosphere. *Geophys Res Lett* 31:2004GL021220. <https://doi.org/10.1029/2004GL021220>
- Payan AP, Paty CS, Retherford KD (2015) Uncovering local magnetospheric processes governing the morphology and variability of Ganymede's aurora using three-dimensional multifluid simulations of Ganymede's magnetosphere. *JGR Space Phys* 120:401–413. <https://doi.org/10.1002/2014JA020301>
- Pelcener S, André N, Nénon Q, et al (2024) Temporal and spatial variability of the electron environment at the orbit of Ganymede as observed by Juno. *J Geophys Res Space Phys* 129:e2023JA032043. <https://doi.org/10.1029/2023JA032043>
- Phipps P, Bagenal F (2021) Centrifugal equator in Jupiter's plasma sheet. *JGR Space Phys* 126:e2020JA028713. <https://doi.org/10.1029/2020JA028713>
- Phipps PH, Withers P (2017) Radio occultations of the Io plasma torus by Juno are feasible. *JGR Space Phys* 122:1731–1750. <https://doi.org/10.1002/2016JA023447>
- Phipps PH, Withers P, Buccino DR, Yang Y (2018) Distribution of plasma in the Io plasma torus as seen by radio occultation during Juno perijove 1. *JGR Space Phys* 123:6207–6222. <https://doi.org/10.1029/2017JA025113>
- Phipps PH, Withers P, Buccino DR, et al (2019) Variations in the density distribution of the Io plasma torus as seen by radio occultations on Juno perijoves 3, 6, and 8. *JGR Space Phys* 124:5200–5221. <https://doi.org/10.1029/2018JA026297>
- Phipps PH, Withers P, Vogt MF, et al (2020) Where is the Io plasma torus? A comparison of observations by Juno radio occultations to predictions from Jovian magnetic field models. *JGR Space Phys* 125:e2019JA027633. <https://doi.org/10.1029/2019JA027633>
- Phipps PH, Withers P, Buccino DR, et al (2021) Two years of observations of the Io plasma torus by Juno radio occultations: results from perijoves 1 to 15. *JGR Space Phys* 126:e2020JA028710. <https://doi.org/10.1029/2020JA028710>
- Plainaki C, Milillo A, Mura A, et al (2013) Exospheric O₂ densities at Europa during different orbital phases. *Planet Space Sci* 88:42–52. <https://doi.org/10.1016/j.pss.2013.08.011>
- Plainaki C, Milillo A, Massetti S, et al (2015) The H₂O and O₂ exospheres of Ganymede: the result of a complex interaction between the Jovian magnetospheric ions and the icy moon. *Icarus* 245:306–319. <https://doi.org/10.1016/j.icarus.2014.09.018>
- Plainaki C, Cassidy TA, Shematovich VI, et al (2018) Towards a global unified model of Europa's tenuous atmosphere. *Space Sci Rev* 214:40. <https://doi.org/10.1007/s11214-018-0469-6>
- Plainaki C, Massetti S, Jia X, et al (2020) Kinetic simulations of the Jovian energetic ion circulation around Ganymede. *Astrophys J* 900:74

- Plainaki C, Massetti S, Jia X, et al (2022) The Jovian energetic ion environment of Ganymede: planetary space weather considerations in view of the JUICE mission. *Astrophys J* 940:186. <https://doi.org/10.3847/1538-4357/ac9c54>
- Pontoni A, Shimoyama M, Futaana Y, Fatemi S, Poppe AR, Wieser M, Barabash S (2022) Simulations of energetic neutral atom sputtering from Ganymede in preparation for the JUICE mission. *J Geophys Res Space Phys* 127(1):e2021JA029439
- Ranquist DA, Bagenal F, Wilson RJ (2020) Polar flattening of Jupiter's magnetosphere. *Geophys Res Lett* 47:e2020GL089818. <https://doi.org/10.1029/2020GL089818>
- Ray LC, Su Y-J, Ergun RE, et al (2009) Current-voltage relation of a centrifugally confined plasma. *J Geophys Res* 114:2008JA013969. <https://doi.org/10.1029/2008JA013969>
- Ray LC, Ergun RE, Delamere PA, Bagenal F (2010) Magnetosphere-ionosphere coupling at Jupiter: effect of field-aligned potentials on angular momentum transport. *J Geophys Res* 115:2010JA015423. <https://doi.org/10.1029/2010JA015423>
- Reiner MJ, Fainberg J, Stone RG, et al (1993) Source characteristics of Jovian narrow-band kilometric radio emissions. *J Geophys Res* 98:13163–13176. <https://doi.org/10.1029/93JE00536>
- Retherford KD, Moos HW, Strobel DF (2003) Io's auroral limb glow: Hubble Space Telescope FUV observations. *J Geophys Res* 108:2002JA009710. <https://doi.org/10.1029/2002JA009710>
- Retherford KD, et al (2025) *Space Sci Rev* 221
- Roelof EC, Mitchell DG, Williams DJ (1985) Energetic neutral atoms ($E \sim 50$ keV) from the ring current: IMP 7/8 and ISEE 1. *J Geophys Res* 90:10991–11008. <https://doi.org/10.1029/JA090iA11p10991>
- Roth L (2021) A stable H_2 O atmosphere on Europa's trailing hemisphere from HST images. *Geophys Res Lett* 48:e2021GL094289. <https://doi.org/10.1029/2021GL094289>
- Roth L, Saur J, Retherford KD, et al (2011) Simulation of Io's auroral emission: constraints on the atmosphere in eclipse. *Icarus* 214:495–509. <https://doi.org/10.1016/j.icarus.2011.05.014>
- Roth L, Saur J, Retherford KD, et al (2014a) Transient water vapor at Europa's south pole. *Science* 343:171–174. <https://doi.org/10.1126/science.1247051>
- Roth L, Saur J, Retherford KD, et al (2014b) A phenomenological model of Io's UV aurora based on HST/STIS observations. *Icarus* 228:386–406. <https://doi.org/10.1016/j.icarus.2013.10.009>
- Roth L, Saur J, Retherford KD, et al (2016) Europa's far ultraviolet oxygen aurora from a comprehensive set of HST observations. *JGR Space Phys* 121:2143–2170. <https://doi.org/10.1002/2015JA022073>
- Roth L, Ivchenko N, Gladstone GR, et al (2021) A sublimated water atmosphere on Ganymede detected from Hubble Space Telescope observations. *Nat Astron* 5:1043–1051. <https://doi.org/10.1038/s41550-021-01426-9>
- Roth L, Smith HT, Yoshioka K, et al (2023) Constraints on Europa's water group torus from HST/COS observations. *Planet Sci J* 4:87. <https://doi.org/10.3847/PSJ/acdddd>
- Roth L, Blöcker A, de Kleer K, et al (2025) Mass supply from Io to Jupiter's magnetosphere. *Space Sci Rev* 221:13. [arXiv:2403.13970](https://arxiv.org/abs/2403.13970). <https://doi.org/10.1007/s11214-025-01137-x>
- Roussos E, Krupp N, Mitchell DG, et al (2016) Quasi-periodic injections of relativistic electrons in Saturn's outer magnetosphere. *Icarus* 263:101–116. <https://doi.org/10.1016/j.icarus.2015.04.017>
- Roussos E, Kollmann P, Krupp N, et al (2018) Drift-resonant, relativistic electron acceleration at the outer planets: insights from the response of Saturn's radiation belts to magnetospheric storms. *Icarus* 305:160–173. <https://doi.org/10.1016/j.icarus.2018.01.016>
- Roussos E, Allanson O, André N, et al (2022) The in-situ exploration of Jupiter's radiation belts. *Exp Astron* 54:745–789
- Rubin M, Jia X, Altwegg K, et al (2015) Self-consistent multifluid MHD simulations of Europa's exospheric interaction with Jupiter's magnetosphere. *JGR Space Phys* 120:3503–3524. <https://doi.org/10.1002/2015JA021149>
- Russell CT, Huddleston DE, Khurana KK, Kivelson MG (1998) The fluctuating magnetic field in the middle Jovian magnetosphere: initial Galileo observations. *Planet Space Sci* 47:133–142. [https://doi.org/10.1016/S0032-0633\(98\)00092-0](https://doi.org/10.1016/S0032-0633(98)00092-0)
- Russell CT, Wei HY, Cowee MM, et al (2016) Ion cyclotron waves at Titan. *JGR Space Phys* 121:2095–2103. <https://doi.org/10.1002/2015JA022293>
- Salveter A, Saur J, Clark G, Mauk BH (2022) Jovian auroral electron precipitation budget—a statistical analysis of diffuse, mono-energetic, and broadband auroral electron distributions. *JGR Space Phys* 127:e2021JA030224. <https://doi.org/10.1029/2021JA030224>
- Sandel BR, Shemansky DE, Broadfoot AL, et al (1979) Extreme ultraviolet observations from Voyager 2 encounter with Jupiter. *Science* 206:962–966. <https://doi.org/10.1126/science.206.4421.962>
- Satoh S, Tsuchiya F, Sakai S, et al (2024) Changes in the plasma sheet conditions at Europa's orbit retrieved from lead angle of the satellite auroral footprints. *Geophys Res Lett* 51(15):e2024GL110079
- Saur J, Strobel DF, Neubauer FM (1998) Interaction of the Jovian magnetosphere with Europa: constraints on the neutral atmosphere. *J Geophys Res* 103:19947–19962. <https://doi.org/10.1029/97JE03556>

- Saur J, Neubauer FM, Strobel DF, Summers ME (2000) Io's ultraviolet aurora: remote sensing of Io's interaction. *Geophys Res Lett* 27:2893–2896. <https://doi.org/10.1029/2000GL003824>
- Saur J, Pouquet A, Matthaeus WH (2003) An acceleration mechanism for the generation of the main auroral oval on Jupiter. *Geophys Res Lett* 30:2002GL015761. <https://doi.org/10.1029/2002GL015761>
- Saur J, Neubauer FM, Connerney JEP, et al (2004) Plasma interactions of Io with its plasma torus. In: Bagenal F, Dowling TE, McKinnon WB (eds) *Jupiter: the planet, satellites and magnetosphere*. Cambridge University Press, Cambridge
- Saur J, Grambusch T, Duling S, et al (2013) Magnetic energy fluxes in sub-Alfvénic planet star and moon planet interactions. *Astron Astrophys* 552:A119. <https://doi.org/10.1051/0004-6361/201118179>
- Saur J, Duling S, Roth L, et al (2015) The search for a subsurface ocean in Ganymede with Hubble Space Telescope observations of its auroral ovals. *J Geophys Res Space Phys* 120:1715–1737. <https://doi.org/10.1002/2014JA020778>
- Saur J, Janser S, Schreiner A, et al (2018) Wave-particle interaction of Alfvén waves in Jupiter's magnetosphere: auroral and magnetospheric particle acceleration. *JGR Space Phys* 123:9560–9573. <https://doi.org/10.1029/2018JA025948>
- Saur J, Duling S, Wennmacher A, et al (2022) Alternating North-south brightness ratio of Ganymede's auroral ovals: Hubble Space Telescope observations around the Juno PJ34 flyby. *Geophys Res Lett* 49:e2022GL098600. <https://doi.org/10.1029/2022GL098600>
- Schilling N, Neubauer FM, Saur J (2007) Time-varying interaction of Europa with the Jovian magnetosphere: constraints on the conductivity of Europa's subsurface ocean. *Icarus* 192:41–55. <https://doi.org/10.1016/j.icarus.2007.06.024>
- Schilling N, Neubauer FM, Saur J (2008) Influence of the internally induced magnetic field on the plasma interaction of Europa. *J Geophys Res* 113:2007JA012842. <https://doi.org/10.1029/2007JA012842>
- Schmid D, Lammer H, Plaschke F, et al (2022) Magnetic evidence for an extended hydrogen exosphere at Mercury. *JGR Planets* 127:e2022JE007462. <https://doi.org/10.1029/2022JE007462>
- Schreier R, Eviatar A, Vasyliūnas VM, Richardson JD (1993) Modeling the Europa plasma torus. *J Geophys Res* 98:21231–21243. <https://doi.org/10.1029/93JA02585>
- Schunk RW, Nagy AF (1980) Ionospheres of the terrestrial planets. *Rev Geophys* 18:813–852. <https://doi.org/10.1029/RG018i004p00813>
- Scudder JD, Sittler EC, Bridge HS (1981) A survey of the plasma electron environment of Jupiter: a view from Voyager. *J Geophys Res* 86:8157–8179. <https://doi.org/10.1029/JA086iA10p08157>
- Selesnick RS, Cohen CMS, Stone EC (2001) Mapping Jupiter's outer radiation belt. *J Geophys Res* 106:29859–29869. <https://doi.org/10.1029/2001JA000061>
- Shemansky DE (1980) Mass-loading and diffusion-loss rates of the Io plasma torus. *Astrophys J* 242:1266–1277. <https://doi.org/10.1086/158557>
- Shemansky DE (1988) Energy branching in the Io plasma torus: the failure of neutral cloud theory. *J Geophys Res* 93:1773–1784. <https://doi.org/10.1029/JA093iA03p01773>
- Shen X-C, Li W, Ma Q, Nishimura Y, Daly A, Kollmann P, et al (2022) Energetic proton distributions in the inner and middle magnetosphere of Jupiter using Juno observations. *Geophys Res Lett* 49:e2022GL099832. <https://doi.org/10.1029/2022GL099832>
- Shprits YY, Menietti JD, Gu X, et al (2012) Gyroresonant interactions between the radiation belt electrons and whistler mode chorus waves in the radiation environments of Earth, Jupiter, and Saturn: a comparative study. *J Geophys Res* 117:2012JA018031. <https://doi.org/10.1029/2012JA018031>
- Sicard A, Bourdarie S, Krupp N, et al (2004) Long-term dynamics of the inner Jovian electron radiation belts. *Adv Space Res* 33:2039–2044. <https://doi.org/10.1016/j.asr.2003.04.053>
- Simpson JA, Anglin JD, Balogh A, et al (1992) Energetic charged-particle phenomena in the Jovian magnetosphere: first results from the Ulysses COSPIN collaboration. *Science* 257:1543–1550. <https://doi.org/10.1126/science.257.5076.1543>
- Simpson JA, Smith DA, Zhang M, Balogh A (1993) Jovian electron propagation in three dimensions of the heliosphere: the Ulysses investigations. *J Geophys Res* 98:21129–21144. <https://doi.org/10.1029/93JA02674>
- Singhal RP, Tripathi AK, Halder S, Ii ONS (2016) Diffuse aurora on Ganymede driven by electrostatic waves. *Astrophys J* 832:172. <https://doi.org/10.3847/0004-637X/832/2/172>
- Sittler EC, Strobel DF (1987) Io plasma torus electrons: Voyager 1. *J Geophys Res* 92:5741–5762. <https://doi.org/10.1029/JA092iA06p05741>
- Smith RA, Bagenal F, Cheng AF, Strobel DF (1988) On the energy crisis in the Io plasma torus. *Geophys Res Lett* 15:545–548. <https://doi.org/10.1029/GL015i006p00545>
- Smith HT, Mitchell DG, Johnson RE, et al (2019) Europa neutral torus confirmation and characterization based on observations and modeling. *Astrophys J* 871:69. <https://doi.org/10.3847/1538-4357/aaed38>
- Smyth WH, Marconi ML (2006) Europa's atmosphere, gas tori, and magnetospheric implications. *Icarus* 181:510–526. <https://doi.org/10.1016/j.icarus.2005.10.019>

- Southwood DJ, Kivelson MG (1987) Magnetospheric interchange instability. *J Geophys Res* 92:109–116. <https://doi.org/10.1029/JA092iA01p00109>
- Southwood DJ, Kivelson MG (1989) Magnetospheric interchange motions. *J Geophys Res* 94:299–308. <https://doi.org/10.1029/JA094iA01p00299>
- Sparks WB, Hand KP, McGrath MA, et al (2016) Probing for evidence of plumes on Europa with HST/STIS. *Astrophys J* 829:121 <https://doi.org/10.3847/0004-637X/829/2/121>
- Sparks WB, Schmidt BE, McGrath MA, et al (2017) Active cryovolcanism on Europa?. *Astrophys J Lett* 839:L18. <https://doi.org/10.3847/2041-8213/aa67f8>
- Stahl A, Addison P, Simon S, Liuzzo L (2023) A model of Ganymede's magnetic and plasma environment during the Juno PJ34 flyby. *J Geophys Res Space Phys* 128(12):e2023JA032113
- Stasiewicz K, Bellan P, Chaston C, et al (2000) Small scale Alfvénic structure in the aurora. *Space Sci Rev* 92:423–533
- Steffl A (2004a) Cassini UVIS observations of the Io plasma torus.I. Initial results. *Icarus* 172:78–90. <https://doi.org/10.1016/j.icarus.2003.12.027>
- Steffl A (2004b) Cassini UVIS observations of the Io plasma torus.II. Radial variations. *Icarus* 172:91–103. <https://doi.org/10.1016/j.icarus.2004.04.016>
- Steffl A, Delamere P, Bagenal F (2006) Cassini UVIS observations of the Io plasma torusIII. Observations of temporal and azimuthal variability. *Icarus* 180:124–140. <https://doi.org/10.1016/j.icarus.2005.07.013>
- Steffl AJ, Delamere PA, Bagenal F (2008) Cassini UVIS observations of the Io plasma torus. *Icarus* 194:153–165. <https://doi.org/10.1016/j.icarus.2007.09.019>
- Strangeway RJ, Ergun RE, Su Y-J, et al (2005) Factors controlling ionospheric outflows as observed at intermediate altitudes. *J Geophys Res* 110:2004JA010829. <https://doi.org/10.1029/2004JA010829>
- Strobel DF (1983) Photochemistry of the reducing atmospheres of Jupiter, Saturn and Titan. *Int Rev Phys Chem* 3:145–176. <https://doi.org/10.1080/01442358309353342>
- Strobel DF, Saur J, Feldman PD, McGrath MA (2002) Hubble Space Telescope space telescope imaging spectrograph search for an atmosphere on Callisto: a Jovian unipolar inductor. *Astrophys J* 581:L51. <https://doi.org/10.1086/345803>
- Szabo PS, Poppe AR, Mutzke A, Liuzzo L, Mogan SRC (2024) Backscattering of ions impacting Ganymede's surface as a source for energetic neutral atoms. *Astrophys J Lett* 963(1):L32. <https://doi.org/10.3847/2041-8213/ad2701>
- Szalay JR, Smith HT, Nirstein EJ, McComas DJ, Begley LJ, Bagenal F, et al (2022) Water-group pickup ions from Europa-genic neutrals orbiting Jupiter. *Geophys Res Lett* 49:e2022GL098111. <https://doi.org/10.1029/2022GL098111>
- Szalay JR, Allegrini F, Ebert RW, Bagenal F, Bolton SJ, Fatemi S, et al (2024a) Oxygen production from dissociation of Europa's water-ice surface. *Nat Astron*. <https://doi.org/10.1038/s41550-024-02206-x>
- Szalay JR, Saur J, McComas DJ, Allegrini F, Bagenal F, Bolton SJ, et al (2024b) Europa modifies Jupiter's plasma sheet. *Geophys Res Lett* 51:e2023GL105809. <https://doi.org/10.1029/2023GL105809>
- Tao C, Kimura T, Kronberg EA, et al (2021) Variation of Jupiter's aurora observed by Hisaki/EXCEED: 4. Quasi-periodic variation. *JGR Space Phys* 126:e2020JA028575. <https://doi.org/10.1029/2020JA028575>
- Teegarden BJ, McDonald FB, Trainor JH, et al (1974) Interplanetary Mev electrons of Jovian origin. *J Geophys Res* 79:3615–3622. <https://doi.org/10.1029/JA079i025p03615>
- Teolis BD, Wyrick DY, Bouquet A, et al (2017) Plume and surface feature structure and compositional effects on Europa's global exosphere: preliminary Europa mission predictions. *Icarus* 284:18–29. <https://doi.org/10.1016/j.icarus.2016.10.027>
- Thomas N, Bagenal F, Hill TW, Wilson JK (2004) The Io neutral clouds and plasma torus. In: Bagenal F, Dowling TE, McKinnon WB (eds) *Jupiter: the planet, satellites and magnetosphere*. Cambridge University Press, Cambridge
- Tosi F, Roatsch T, Galli A, et al (2024) Characterization of the surfaces and near-surface atmospheres of Ganymede, Europa and Callisto by JUICE. *Space Sci Rev* 220:59. <https://doi.org/10.1007/s11214-024-01089-8>
- Tóth G, Jia X, Markidis S, et al (2016) Extended magnetohydrodynamics with embedded particle-in-cell simulation of Ganymede's magnetosphere. *JGR Space Phys* 121:1273–1293. <https://doi.org/10.1002/2015JA021997>
- Treumann RA (2006) The electron-cyclotron maser for astrophysical application. *Astron Astrophys Rev* 13:229–315. <https://doi.org/10.1007/s00159-006-0001-y>
- Tripathi AK, Singhal RP, Singh Ii O (2017) The generation of Ganymede's diffuse aurora through pitch angle scattering. *Ann Geophys* 35:239–252. <https://doi.org/10.5194/angeo-35-239-2017>
- Tsuchiya F, Morioka A, Misawa H (1999) Jovian electron modulations by the solar wind interaction with the magnetosphere. *Earth Planets Space* 51:987–996. <https://doi.org/10.1186/BF03351569>
- Tsuchiya F, Morioka A, Misawa H (2014) Jovian electron modulations by the solar wind interaction with the magnetosphere. *Earth Planets Space* 51:987–996. <https://doi.org/10.1186/BF03351569>



- Tsuchiya F, Yoshioka K, Kimura T, et al (2018) Enhancement of the Jovian magnetospheric plasma circulation caused by the change in plasma supply from the satellite Io. *JGR Space Phys* 123:6514–6532. <https://doi.org/10.1029/2018JA025316>
- Tsuchiya F, Arakawa R, Misawa H, et al (2019) Azimuthal variation in the Io plasma torus observed by the Hisaki satellite from 2013 to 2016. *JGR Space Phys* 124:3236–3254. <https://doi.org/10.1029/2018JA026038>
- Valek PW, Thomsen MF, Allegrini F, et al (2017) Hot flow anomaly observed at Jupiter's bow shock. *Geophys Res Lett* 44:8107–8112. <https://doi.org/10.1002/2017GL073175>
- Valek PW, Waite JH, Allegrini F, et al (2022) In situ ion composition observations of Ganymede's outflowing ionosphere. *Geophys Res Lett* 49:e2022GL100281 <https://doi.org/10.1029/2022GL100281>
- Van Hoolst T, Tobie G, Vallat C, et al (2024) Geophysical characterization of the interiors of Ganymede, Callisto and Europa by ESA's Jupiter ICy moons Explorer. *Space Sci Rev* 220:54. <https://doi.org/10.1007/s11214-024-01085-y>
- Vasyliūnas VM (1983) Plasma distribution and flow. In: Dessler AJ (ed) *Physics of the Jovian magnetosphere*. Cambridge University Press, Cambridge
- Vogt MF, Jackman CM, Slavin JA, et al (2014) Structure and statistical properties of plasmoids in Jupiter's magnetotail. *JGR Space Phys* 119:821–843. <https://doi.org/10.1002/2013JA019393>
- Vogt MF, Gyalay S, Kronberg EA, et al (2019) Solar wind interaction with Jupiter's magnetosphere: a statistical study of Galileo in situ data and modeled upstream solar wind conditions. *JGR Space Phys* 124:10170–10199. <https://doi.org/10.1029/2019JA026950>
- Vogt MF, Connerney JEP, DiBraccio GA, et al (2020) Magnetotail reconnection at Jupiter: a survey of Juno magnetic field observations. *JGR Space Phys* 125:e2019JA027486. <https://doi.org/10.1029/2019JA027486>
- Volwerk M (1997) Systems III and IV modulation of the Io phase effect in the Io plasma torus. *J Geophys Res* 102:24403–24410. <https://doi.org/10.1029/97JA02368>
- Volwerk M (2018) On the location of the Io plasma torus: Voyager 1 observations. *Ann Geophys* 36:831–839. <https://doi.org/10.5194/angeo-36-831-2018>
- Volwerk M, Khurana KK (2010) Ion pick-up near the icy Galilean satellites. In: le Roux JA, Florinski V, Zank GP, Coates AJ (eds) *Pickup ions throughout the heliosphere and beyond: proceedings of the 8th annual international astrophysics conference*, pp 263–269
- Volwerk M, Kivelson MG, Khurana KK, McPherron RL (1999) Probing Ganymede's magnetosphere with field line resonances. *J Geophys Res* 104:14729–14738. <https://doi.org/10.1029/1999JA900161>
- Volwerk M, Kivelson MG, Khurana KK (2001) Wave activity in Europa's wake: implications for ion pickup. *J Geophys Res* 106:26033–26048. <https://doi.org/10.1029/2000JA000347>
- Volwerk M, Khurana K, Kivelson M (2007) Europa's Alfvén wing: shrinkage and displacement influenced by an induced magnetic field. *Ann Geophys* 25:905–914. <https://doi.org/10.5194/angeo-25-905-2007>
- Volwerk M, Jia X, Paranicas C, et al (2013) ULF waves in Ganymede's upstream magnetosphere. *Ann Geophys* 31:45–59. <https://doi.org/10.5194/angeo-31-45-2013>
- Vorburger A, Wurz P (2018) Europa's ice-related atmosphere: the sputter contribution. *Icarus* 311:135–145. <https://doi.org/10.1016/j.icarus.2018.03.022>
- Vorburger A, Wurz P (2021) Modeling of possible plume mechanisms on Europa. *JGR Space Phys* 126:e2021JA029690. <https://doi.org/10.1029/2021JA029690>
- Vorburger A, Wurz P, Lammer H, et al (2015) Monte-Carlo simulation of Callisto's exosphere. *Icarus* 262:14–29. <https://doi.org/10.1016/j.icarus.2015.07.035>
- Vorburger A, Fatemi S, Galli A, et al (2022) 3D Monte-Carlo simulation of Ganymede's water exosphere. *Icarus* 375:114810. <https://doi.org/10.1016/j.icarus.2021.114810>
- Vorburger A, Fatemi S, Carberry Mogan SR, et al (2024) 3D Monte-Carlo simulation of Ganymede's atmosphere. *Icarus* 409:115847. <https://doi.org/10.1016/j.icarus.2023.115847>
- Wahlund J-E, Opgenoorth HJ, Häggström I, et al (1992) EISCAT observations of topside ionospheric ion outflows during auroral activity: revisited. *J Geophys Res* 97:3019–3037. <https://doi.org/10.1029/91JA02438>
- Wahlund J-E, Louarn P, Chust T, et al (1994) On ion acoustic turbulence and the nonlinear evolution of kinetic Alfvén waves in aurora. *Geophys Res Lett* 21:1831–1834. <https://doi.org/10.1029/94GL01289>
- Wahlund J-E, Eriksson AI, Holback B, et al (1998) Broadband ELF plasma emission during auroral energization: 1. Slow ion acoustic waves. *J Geophys Res* 103:4343–4375. <https://doi.org/10.1029/97JA02008>
- Wahlund JE, Bergman JES, Åhlén L, et al (2025) The Radio & Plasma Wave Investigation (RPWI) for the Jupiter ICy Moons Explorer (JUICE). *Space Sci Rev* 221:1. <https://doi.org/10.1007/s11214-024-01110-0>
- Waldrop LS, Roelof EC, Fritz TA (2015) Three-dimensional convective flows of energetic ions in Jupiter's equatorial magnetosphere. *JGR Space Phys* 120. <https://doi.org/10.1002/2015JA021103>

- Warwick JW, Pearce JB, Alexander JK, et al (1979b) Planetary radio astronomy observations from Voyager 2 near Jupiter. *Science* 206:991–995. <https://doi.org/10.1126/science.206.4421.991>
- Warwick JW, Pearce JB, Riddle AC, et al (1979a) Voyager 1 planetary radio astronomy observations near Jupiter. *Science* 204:995–998. <https://doi.org/10.1126/science.204.4396.995>
- Wieser M, Barabash S, Futaana Y, et al (2009) Extremely high reflection of solar wind protons as neutral hydrogen atoms from regolith in space. *Planet Space Sci* 57:2132–2134. <https://doi.org/10.1016/j.pss.2009.09.012>
- Wieser M, Barabash S, Wang X-D, et al (2020) The Advanced Small Analyzer for Neutrals (ASAN) on the Chang'E-4 Rover Yutu-2. *Space Sci Rev* 216:73. <https://doi.org/10.1007/s11214-020-00691-w>
- Williams DJ, Mauk B, McEntire RW (1998) Properties of Ganymede's magnetosphere as revealed by energetic particle observations. *J Geophys Res* 103:17523–17534. <https://doi.org/10.1029/98JA01370>
- Wilson RJ, Bagenal F, Valek PW, McComas DJ, Allegrini F, Ebert RW, et al (2018) Solar wind properties during Juno's approach to Jupiter: Data analysis and resulting plasma properties utilizing a 1-D forward model. *J Geophys Res Space Phys* 123. <https://doi.org/10.1002/2017JA024860>
- Wilson RJ, Vogt MF, Provan G, et al (2023) Internal and external Jovian magnetic fields: community code to serve the magnetospheres of the outer planets community. *Space Sci Rev* 219:15. <https://doi.org/10.1007/s11214-023-00961-3>
- Wing S, Brandt PC, Mitchell DG, et al (2020) Periodic narrowband radio wave emissions and inward plasma transport at Saturn's magnetosphere. *Astron J* 159:249. <https://doi.org/10.3847/1538-3881/ab818d>
- Winser KJ, Jones GOL, Williams PJS, Lockwood M (1989) Observations of large field-aligned flows of thermal plasma in the auroral ionosphere. *Adv Space Res* 9:57–63. [https://doi.org/10.1016/0273-1177\(89\)90341-4](https://doi.org/10.1016/0273-1177(89)90341-4)
- Winslow RM, Anderson BJ, Johnson CL, et al (2013) Mercury's magnetopause and bow shock from MESSENGER magnetometer observations. *JGR Space Phys* 118:2213–2227. <https://doi.org/10.1002/jgra.50237>
- Winterhalter TO, Huybrighs HLF (2022) Assessing JUICE's ability of in situ plume detection in Europa's atmosphere. *Planet Space Sci* 210:105375. <https://doi.org/10.1016/j.pss.2021.105375>
- Witasse O, et al (2025) *Space Sci Rev* 221
- Withers P (2020) Revised predictions of uncertainties in atmospheric properties measured by radio occultation experiments. *Adv Space Res* 66:2466–2475. <https://doi.org/10.1016/j.asr.2020.07.049>
- Woodfield EE, Horne RB, Glauert SA, et al (2014) The origin of Jupiter's outer radiation belt. *JGR Space Phys* 119:3490–3502. <https://doi.org/10.1002/2014JA019891>
- Wu CS (1981) The source mechanism of auroral kilometric radiation. In: Akasofu S-I, Kan JR (eds) *Geophysical monograph series*. American Geophysical Union, Washington, pp 418–427
- Wu CS, Lee LC (1979) A theory of the terrestrial kilometric radiation. *Astrophys J* 230:621–626.
- Wurz P, Fuselier SA, Möbius E, et al (2009) IBEX backgrounds and signal-to-noise ratio. *Space Sci Rev* 146:173–206. <https://doi.org/10.1007/s11214-009-9515-8>
- Xu Y, Yao ZH, Zhang B, et al (2023) On the relation between Jupiter's aurora and the dawnside current sheet. *Geophys Res Lett* 50:e2023GL104123. <https://doi.org/10.1029/2023GL104123>
- Yao ZH, Grodent D, Kurth WS, et al (2019) On the relation between Jovian aurorae and the loading/unloading of the magnetic flux: simultaneous measurements from Juno, Hubble Space Telescope, and Hisaki. *Geophys Res Lett* 46:11632–11641. <https://doi.org/10.1029/2019GL084201>
- Yao Z, Dunn WR, Woodfield EE, et al (2021) Revealing the source of Jupiter's X-ray auroral flares. *Sci Adv* 7:eabf0851. <https://doi.org/10.1126/sciadv.abf0851>
- Yoshikawa I, Suzuki F, Hikida R, et al (2017) Volcanic activity on Io and its influence on the dynamics of the Jovian magnetosphere observed by EXCEED/Hisaki in 2015. *Earth Planets Space* 69:110. <https://doi.org/10.1186/s40623-017-0700-9>
- Yoshioka K, Murakami G, Yamazaki A, et al (2014) Evidence for global electron transportation into the Jovian inner magnetosphere. *Science* 345:1581–1584. <https://doi.org/10.1126/science.1256259>
- Yoshioka K, Tsuchiya F, Kimura T, et al (2017) Radial variation of sulfur and oxygen ions in the Io plasma torus as deduced from remote observations by Hisaki. *JGR Space Phys* 122:2999–3012. <https://doi.org/10.1002/2016JA023691>
- Yoshioka K, Tsuchiya F, Kagitani M, et al (2018) The Influence of Io's 2015 Volcanic Activity on Jupiter's Magnetospheric Dynamics. *Geophys Res Lett* 45. <https://doi.org/10.1029/2018GL079264>
- Yuan C, Zuo Y, Roussos E, et al (2021) Large-scale episodic enhancements of relativistic electron intensities in Jupiter's radiation belt. *Earth Planet Phys* 5:314–326. <https://doi.org/10.26464/epp2021037>
- Zarka P (1998) Auroral radio emissions at the outer planets: observations and theories. *J Geophys Res* 103:20159–20194. <https://doi.org/10.1029/98JE01323>
- Zarka P, Kurth WS (2005) Radio wave emission from the outer planets before Cassini. *Space Sci Rev* 116:371–397. <https://doi.org/10.1007/s11214-005-1962-2>

- Zarka P, Marques MS, Louis C, et al (2018) Jupiter radio emission induced by Ganymede and consequences for the radio detection of exoplanets. *Astron Astrophys* 618:A84. <https://doi.org/10.1051/0004-6361/201833586>
- Zhang X-J, Ma Q, Artemyev AV, et al (2020) Plasma sheet boundary layer in Jupiter's magnetodisk as observed by Juno. *JGR Space Phys* 125:e2020JA027957. <https://doi.org/10.1029/2020JA027957>
- Zheng Y, Moore TE, Mozer FS, et al (2005) Polar study of ionospheric ion outflow versus energy input. *J Geophys Res* 110:2004JA010995. <https://doi.org/10.1029/2004JA010995>
- Zhou H, Tóth G, Jia X, et al (2019) Embedded kinetic simulation of Ganymede's magnetosphere: improvements and inferences. *JGR Space Phys* 124:5441–5460. <https://doi.org/10.1029/2019JA026643>
- Zhou H, Tóth G, Jia X, Chen Y (2020) Reconnection-driven dynamics at Ganymede's upstream magnetosphere: 3-D global Hall MHD and MHD-EPIC simulations. *JGR Space Phys* 125:e2020JA028162. <https://doi.org/10.1029/2020JA028162>
- Zimmer C (2000) Subsurface oceans on Europa and Callisto: constraints from Galileo magnetometer observations. *Icarus* 147:329–347. <https://doi.org/10.1006/icar.2000.6456>

Publisher's Note Springer Nature remains neutral with regard to jurisdictional claims in published maps and institutional affiliations.

Authors and Affiliations

A. Masters¹  · R. Modolo² · E. Roussos³ · N. Krupp³ · O. Witasse⁴ · C. Vallat⁵ · B. Cecconi⁶ · N.J.T. Edberg⁷ · Y. Futaana⁸ · M. Galand¹ · D. Heyner⁹ · M. Holmberg¹⁰ · H. Huybrighs^{10,11,12} · X. Jia¹³ · K. Khurana¹⁴ · L. Lamy^{6,15} · L. Roth¹⁶ · A. Sulaiman¹⁷ · P. Tortora¹⁸ · S. Barabash⁸ · L. Bruzzone¹⁹ · M.K. Dougherty¹ · R. Gladstone^{20,21} · L.I. Gurvits^{22,23}  · P. Hartogh³ · H. Hussmann²⁴ · L. Iess²⁵ · F. Poulet²⁶ · J.-E. Wahlund⁷ · D.J. Andrews⁷ · C.S. Arridge²⁷ · F. Bagenal²⁸ · C. Baskevitch^{2,6} · J. Bergman⁷ · T.M. Bocanegra²⁹ · P. Brandt³⁰ · E.J. Bunce³¹ · G. Clark³⁰ · A.J. Coates^{32,33} · E. Galanti³⁴ · A. Galli³⁵ · D. Grodent³⁶ · G. Jones^{32,33} · Y. Kasaba³⁷ · Y. Kaspi³⁴ · Y. Katoh³⁵ · N. Kaweeyanun³⁸ · Y. Khotyaintsev⁷ · T. Kimura³⁹ · P. Kollmann³⁰ · D. Mitchell³⁰ · A. Moirano^{40,36} · G. Molera Calvés⁴¹ · M. Morooka⁷ · I.C.F. Müller-Wodarg¹ · C. Muñoz⁵ · A. Mura⁴⁰ · M. Pätzold⁴² · M. Pinto⁴ · C. Plainaki^{43,40} · K.D. Retherford^{20,21} · A. Retinò⁴⁴ · H. Rothkaehl⁴⁵ · O. Santolík^{46,47} · J. Saur⁴⁸ · G. Stenberg Wieser⁸ · F. Tsuchiya³⁷ · M. Volwerk⁴⁹ · A. Vorburger³⁵ · P. Wurz³⁵ · M. Zannoni¹⁸

✉ A. Masters
a.masters@imperial.ac.uk

- ¹ Blackett Laboratory, Imperial College London, Prince Consort Road, London, SW7 2AZ, UK
- ² LATMOS/IPSL, UVSQ Université, Paris-Saclay, UPMC University Paris CNRS, Guyancourt, France
- ³ Max Planck Institute for Solar System Research, Justus-von-Liebig-Weg 3, 37077, Göttingen, Germany
- ⁴ European Space Agency (ESA), European Space Research and Technology Centre (ESTEC), Noordwijk, The Netherlands
- ⁵ ESAC, European Space Agency (ESA), Camino Bajo del Castillo s/n, Villafranca del Castillo, Villanueva de la Cañada (Madrid), 28692, Spain
- ⁶ Laboratoire d'Etudes Spatiales et Instrumentation en Astrophysique (LESIA), Observatoire de Paris-PSL, CNRS, Sorbonne Université, Université Paris Cité, 5 Place Jules Janssen, 92190, Meudon, France
- ⁷ Swedish Institute of Space Physics (IRF), Box 537, 751 21, Uppsala, Sweden

- 8 Swedish Institute of Space Physics (IRF), Box 812, SE-981 28, Kiruna, Sweden
- 9 Institut für Geophysik und extraterrestrische Physik, Technische Universität Braunschweig, Braunschweig, Germany
- 10 Astronomy & Astrophysics Section, School of Cosmic Physics, Dublin Institute for Advanced Studies, DIAS Dunsink Observatory, Dublin, D15 XR2R, Ireland
- 11 Space and Planetary Science Center, Khalifa University, Abu Dhabi, UAE
- 12 Department of Mathematics, Khalifa University, Abu Dhabi, UAE
- 13 Department of Climate and Space Sciences and Engineering, University of Michigan, Ann Arbor, MI, USA
- 14 Department of Earth, Planetary and Space Sciences, UCLA, Los Angeles, CA, 90095, USA
- 15 Aix Marseille Univ., CNRS, CNES, LAM, Marseille, France
- 16 Royal Institute of Technology (KTH), Space & Plasma Physics, SE-100 44, Stockholm, Sweden
- 17 School of Physics and Astronomy, Minnesota Institute for Astrophysics, University of Minnesota, Minneapolis, MN, USA
- 18 Dipartimento di Ingegneria Industriale, Alma Mater Studiorum - Università di Bologna, Via Fontanelle, 40, 47121 Forlì, Italy
- 19 Department of Information Engineering and Computer Science, University of Trento, Via Sommarive, 5, Povo, 38123, Italy
- 20 Southwest Research Institute, San Antonio, TX, USA
- 21 University of Texas at San Antonio, San Antonio, TX, USA
- 22 Joint Institute for VLBI ERIC, Oude Hoogeveensedijk 4, 7991 PD, Dwingeloo, The Netherlands
- 23 Faculty of Aerospace Engineering, Delft University of Technology, Kluyverweg 1, 2629 HS, Delft, The Netherlands
- 24 German Aerospace Center (DLR), Institute of Planetary Research, Rutherfordstr. 2, 12489, Berlin, Germany
- 25 Dipartimento di Ingegneria Meccanica e Aerospaziale, Università La Sapienza, Rome, Italy
- 26 Institut d'Astrophysique Spatiale, Université Paris-Saclay, 91405, Orsay Cedex, France
- 27 Department of Physics, Lancaster University, Lancaster, LA1 4YB, UK
- 28 Laboratory for Atmospheric and Space Physics, University of Colorado, Boulder, CO, USA
- 29 Jet Propulsion Laboratory, California Institute of Technology, 4800 Oak Grove Dr., Pasadena, 91109, CA, USA
- 30 The Johns Hopkins University Applied Physics Laboratory, 11100 Johns Hopkins Road, Laurel, MD, USA
- 31 Department of Physics and Astronomy, University of Leicester, Leicester, LE1 7R, UK
- 32 Mullard Space Science Laboratory, University College London, Holmbury St Mary, Dorking, RH5 6NT, UK
- 33 The Centre for Planetary Science at UCL-Birkbeck, London, UK
- 34 Weizmann Institute of Science, Rehovot, 76100, Israel
- 35 Space Research and Planetary Sciences, Physics Institute, University of Bern, Sidlerstrasse 5, 3012, Bern, Switzerland

- 36 Laboratoire de Physique Atmosphérique et Planétaire, STAR Institute, Université de Liège, Liège, Belgium
- 37 Graduate School of Science, Tohoku University, 6-3 Aramaki aza Aoba, Aoba-ku, Sendai, 980-8578, Japan
- 38 School of Physics & Astronomy, University of Southampton, Highfield Campus, University Road, Southampton, SO17 1BJ, UK
- 39 Department of Physics, Faculty of Science, Tokyo University of Science, 1-3 Kagurazaka, Shinjuku, Tokyo, 162-8601, Japan
- 40 INAF-Istituto di Astrofisica e Planetologia Spaziali, Via del Fosso del Cavaliere, 100, 00133, Rome, Italy
- 41 School of Natural Sciences, University of Tasmania, Private Bag 37, Hobart, 7015, Tas, Australia
- 42 Rheinisches Institut fuer Umweltforschung, Abteilung Planetforschung, Cologne, Germany
- 43 Agenzia Spaziale Italiana - ASI, Via del Politecnico snc, I-00133, Rome, Italy
- 44 Laboratoire de Physique des Plasmas, CNRS/Ecole Polytechnique/Sorbonne Université/Université Paris-Saclay/Observatoire de Paris, route de Saclay, 91128, Palaiseau cedex, France
- 45 Space Research Centre of the Polish Academy of Sciences, 00-716 Bartycka 18A, Warsaw, Poland
- 46 Department of Space Physics, Institute of Atmospheric Physics of the Czech Academy of Sciences, Bocni II/1401, 14100 Prague, Czechia
- 47 Department of Mathematics and Physics, Charles University, V Holesovickach 2, 18000, Prague, Czechia
- 48 Institute of Geophysics and Meteorology, University of Cologne, Cologne, Germany
- 49 Space Research Institute, Austrian Academy of Sciences, Schmiedlstrasse 6, 8042, Graz, Austria